SOLID STATE NMR AT HIGH MAGNETIC FIELDS USING MULTIPLE PULSE TECHNIQUES

Thesis by

Douglas Glenn Carson

In Partial Fulfillment of the Requirements

for the Degree of

Doctor of Philosophy

California Institute of Technology

Pasadena, California

1981

(Submitted November 5, 1980)

To Isabelle

Acknowledgements

There are many people whom I would like to thank for their guidance and support during my stay at Caltech.

I am grateful to have known and worked with Professor Robert W. Vaughan during my first few years at Caltech. His enthusiasm for science and NMR was truly contagious. He was patient, understanding, and he always was willing to help his students in any way he could. His tragic and untimely death has touched all of us who knew him.

I am indebted to Professor Sunney Chan for the kind support and guidance he has given me for the last year and a half, in helping me to finish my thesis. My discussions with him were invaluable to me.

I wish to thank both past and present members of the Vaughan research group for stimulating discussions about NMR, science, and life in general, and for making the group an interesting place in which to work. I would also like to thank my friends at Caltech for the comaraderie I've experienced over the years.

My parents have always supported me as I pursued my educational goals, for which I'm thankful.

Last but not least, I would like to thank Isabelle for her encouragement and also just for being herself.

ABSTRACT

Part I of this thesis is concerned with measuring the proton chemical shift in solids using a homebuilt high field (6.3 tesla) multiple pulse spectrometer. The distinctive features of the spectrometer are described. The chemical shift tensors for the carboxylic protons in potassium hydrogen malonate, potassium hydrogen oxydiacetate, and potassium hydrogen dicrotonate are reported as determined by multiple pulse experiments. The isotropic part of the chemical shifts relative to a spherical sample of TMS and the anisotropies for the three compounds are -20.5(5), -19.6(7), -18.2(7), and 27.6(6), 28.3(9), 28.9(9) ppm respectively.

Part II of this thesis presents a two pulse double quantum nuclear magnetic resonance (NMR) experiment which is designed to measure the Pake doublet splitting in systems of isolated proton pairs which are inhomogeneously broadened. This experiment is applied to the water molecules in the channels of a single crystal of cordierite as a function of orientation and temperature to obtain structural information about the water molecules. Based on the NMR data, the water molecules are found to exhibit substantial anisotropic motion at room temperature and combined with previously reported infrared absorption data, a two site hopping model

is proposed where the water spends 85% of its time with its proton-proton vector parallel to the channels and 15% of its time perpendicular. The difference in free energy between these two sites is 0.8 kcal/mole.

Average hamiltonian theory is extended to cover the case of strongly coupled proton-pair systems by transforming the hamiltonian to the dipolar pair-toggling reference frame. It is found that the residual dipolar hamiltonian for the Burum-Rhim 24-pulse cycle is governed by a four-body interaction and any other multiple pulse cycle based on phase alternated WAHUHA 4-pulse cycles will do no better than the 24-pulse cycle at reducing the residual dipolar hamiltonian.

Table of Contents:

CHAPTER 1

General Introduction

Solid state NMR encompasses a wide variety of NMR techniques which are applied to many solid state systems and various nuclei. All solid state NMR techniques have a common goal: that is, to elucidate the structure and dynamics of solids. Over the past 10 years or so, great strides have been made in the development of "high resolution" techniques which provide more detailed information about more solid state systems than in the past. This thesis is concerned with developing and using new techniques, namely double quantum NMR and high field multiple pulse NMR to obtain useful information in solid state systems which heretofore were outside the domain of NMR.

One of the characteristics which distinguishes solid state NMR from liquid state NMR is that the many static magnetic interactions present in the solid state, which in general serve to produce broad featureless spectra, are averaged by the rapid molecular motions in the liquid state thus producing narrow absorption peaks which are highly resolved. The magnetic interactions include the Zeeman interaction, homonuclear dipolar interactions, heteronuclear dipolar interactions, quadrupolar interactions, chemical shift interactions, spin-lattice interactions, and applied

radio-frequency fields to name a few (1,2). As an example of the difficulty in obtaining "high resolution" NMR spectra in solids, consider the measurement of the proton chemical shift spectrum in water in a high magnetic field with only homonuclear dipolar interactions and chemical shift interactions. (The measurement of the chemical shift in solids is the problem which is addressed in Part I of this thesis). In the liquid state, the dipolar interaction is completely averaged to zero and the chemical shift interaction, which is a tensoral quantity, is averaged to its isotropic value and we observe a single, narrow absorption peak (< 1 Hz broad), which is used to identify the corresponding proton (i.e. to identify OH groups or CH_3 groups etc.). In the solid state, the dipolar interaction is very large, up to 100 kHz, and completely obscures the chemical shift, which varies over 5 kHz depending on the strength of the external magnetic field. We can use multiple pulse NMR (3,4) to remove the homonuclear dipolar interaction and observe the chemical shift. However, since the chemical shift is a tensoral quantity, in polycrystalline solids, each crystallite contributes to the absorption at its own chemical shift, which results in a broad chemical shift powder pattern, on the order of kHz. If there is more than one inequivalent proton in the sample with a different chemical shift tensor, we have overlapping

powder patterns which are in general very difficult to separate (5). However, we can spatially average the chemical shift tensor to its isotropic value by spinning the sample at the magic angle (2). Thus to obtain a liquid-like spectrum, we must employ both multiple pulse and magic angle spinning techniques (6,7) both of which place stringent requirements on the spectrometer.

On the other hand, in a single crystal, we can use multiple pulse techniques to measure the complete chemical shift tensor by measuring the chemical shift as a function of crystal orientation in the external magnetic field. The chemical shift tensor gives us directional information about the electronic structure around the proton, unlike the isotropic value of the chemical shift tensor in liquids which gives us the spatial average. Thus with the complete tensor, we gain information about the bonding arrangement of the proton ((8) and Chapter 4 of this thesis).

Also, in some cases we can use the lineshape due to the dipolar interactions to provide structural information about the solid, such as in the case of isolated, rigid water molecules ((9) and Chapter 8 of this thesis) where we can obtain the inter-proton distance and orientation of the water molecule. In the liquid state, the dipolar

interactions are averaged to zero.

This example serves to illustrate that by virtue of the greater number of interactions in solids, NMR has the potential for providing much more information than liquid state NMR, but it is more difficult to extract this information. Accordingly, the thrust of new high resolution techniques in solids has been to use spin manipulation to isolate one interaction by nullifying the unwanted interactions, or to use cross-correlation schemes which, for example, measure the chemical shift tensor in polycrystalline samples as a function of the dipolar interaction (1,10).

This example also illustrates the complexity of solid state NMR even in simple systems and that NMR is at present, not a viable technique for all solid state systems. However, new techniques are being developed which extend the domain of solid state NMR.

The investigations in this thesis deal with two NMR techniques: high field multiple pulse NMR and double quantum NMR. Both of these techniques provide data that were not readily attainable before. Part I of this thesis is concerned with removing the dipolar interactions and measuring the proton chemical shift in solids. The

homonuclear dipolar interactions are removed by multiple pulse NMR and the heteronuclear interactions are removed by using a high field (6.3 tesla) spectrometer which is described in Chapter 3. Chapter 4 presents the results of multiple pulse experiments in strongly hydrogen-bonded systems: KH malonate, KH oxidiacetate, and KH dicrotonate. Some limits in resolution of multiple pulse NMR are considered in Chapter 5 which is also concerned with extending average hamiltonian theory to cover the case of strong homonuclear dipolar interactions.

Part II of this thesis is concerned with measuring the Pake doublet splitting due to the homonuclear dipolar interaction in a system of proton pairs (such as water molecules) which is inhomogeneously broadened . Chapter 7 introduces a two pulse, double quantum experiment which is capable of measuring the doublet splittings in such systems. In Chapter 8, this experiment is used to provide the doublet splittings of the water molecules in cordierite. The NMR results are used to characterize the orientation and motional properties of the water molecule.

References

1. R. W. Vaughan, Ann. Rev. Phys. Chem. 29, 397 (1978).

2. M. Mehring, High Resolution NMR Spectroscopy in Solids (Springer-Verlag, Berlin, Heidelberg, New York, 1976).

3. U. Haeberlen, High Resolution NMR in Solids, Selective Averaging (Academic Press, New York 1970).

4. W. K. Rhim, D.D. Elleman, L.B. Schreiber, and R.W. Vaughan, J. Chem. Phys. 60, 4595 (1974).

5. J.A. Reimer, and R.W. Vaughan, Chem. Phys. Lett. 63, 163 (1979).

6. B.C. Gerstein, R.G. Pembleton, R.C. Wilson, and L.M. Ryan, J. Chem. Phys. 66, 361 (1977).

7. R.F. Taylor, R.G. Pembleton, L.M. Ryan, and B.C. Gerstein, J. Chem. Phys. 71, 4541 (1979).

8. B. Berglund and R.W. Vaughan, J. Chem. Phys. 73, 2037 (1980).

9. For a review see Z.M. El Saffar, J. Chem. Phys. 45, 4643 (1966).

10. W.P. Aue, E. Bartholdi, and R.R. Ernst, J. Chem. Phys. 64, 2229 (1976).

PART I

The Determination of Proton Chemical Shift Tensors with Multiple Pulse NMR

CHAPTER 2

Introduction to Part I

Part I of this thesis is concerned with multiple pulse experiments which furnish the proton chemical shift in solids in three respects: 1) the construction of a high field (6.3 tesla) multiple pulse spectrometer (Chapter 3); 2) measuring the chemical shift tensors of the carboxylic protons in KH malonate, KH dicrotonate, and KH oxidiacetate (Chapter 4); and 3) extending average hamiltonain theory to cover the case of very strong homonuclear dipolar coupling, such as in water or CH_2 groups (Chapter5).

Ever since Waugh presented the WAHUHA 4-pulse cycle to measure the chemical shift in solids (1,2), researchers have been trying to find ways to improve the spectral resolution in multiple pulse experiments so that these techniques can be applied to more solid state systems with stronger dipolar interactions.

There are basically three methods to improve the spectral resolution in a multiple pulse line narrowing experiment, depending on the solid state sample. First of all, one can run the multiple pulse cycle with a faster cycle time; that is, to shorten the time between pulses. Typically, the MREV 8-pulse cycle is run with a pulse width of 1 to 1.5 μs and a pulse spacing of 3 to 5 μs for

protons. To shorten the pulse spacing requires an increase in the strength of the radio-frequency pulse and a reduction in the probe ringdown time simultaneously. This is not an easy task since the radio-frequency pulse strength and probe ringdown time are both proportional to the Q (quality factor) of the probe.

Secondly, one can construct new multiple pulse cycles to remove more of the higher order error and homonuclear dipolar hamiltonians in the average hamiltonian, such as the new 24 and 52 pulse cycles (3) which show remarkable improvements over the 8-pulse cycle.

And thirdly, one can construct a high field spectrometer. The effect of the high magnetic field is to increase the chemical shift interaction in absolute frequency while both heteronuclear and homonuclear dipolar interactions are unaffected by the larger field. Thus, we need to remove less of the homonuclear dipolar interaction with multiple pulse at high fields than at relatively low fields to achieve the same resolution. Combined with methods 1 and 2, a high field multiple pulse spectrometer represents the state of the art in multiple pulse NMR spectral resolution. The advantages of a high field multiple pulse spectrometer are demonstrated in Chapters 3

and 4 of this thesis.

In Chapter 3, the distinctive features of the construction of a high field spectrometer are discussed and the resolution is compared with resolution of a low field spectrometer.

In Chapter 4, the chemical shift tensors of the carboxylic protons in KH malonate, KH dicrotonate, and KH oxidiacetate are measured using the high field spectrometer. These data are significant in two respects: 1) Besides the chemical shift tensor of the carboxylic proton in KH maleate observed by Achloma et al.(4), the data in Chapter 4 represent the only high field multiple pulse data to date and demonstrate the superior resolving power of a high field spectrometer in systems with large heteronuclear dipolar coupling. It is not possible to resolve the chemical shift in these systems at lower fields. 2) The observed chemical shift tensors in these systems also represent the only chemical shift data in strongly hydrogen bonded systems ($r_{O-O} < 1.49$ Å). It has long been known that the chemical shift tensor is sensitive to the strength of the hydrogen bond, but it has only been recently that enough chemical shift data have become available to correlate the chemical shift tensor with other parameters in hydrogen-

bonded systems, such as the O--O distance and the quadrupolar coupling constant. Thus the data reported in chapter 4 extend the range of these correlations to include very strong hydrogen bonds (see reference 5 for a review).

As a result of the improved spectral resolution due to the new 24 and 52-pulse cycles, multiple pulse NMR is being applied to systems with very large homonuclear diplolar interactions, on the order of 80 kHz, such as ice and the water molecules in gypsum (6-8). However, the average hamiltonian under which the spins evolve during the multiple pulse experiment has been calculated using average hamiltonian theory which assumes that the dipolar interactions are small compared with the time between pulses. This assumption is not fullfilled with a 80 kHz dipolar interaction. In Chapter 5, average hamiltonian theory is extended to cover the case of strong homonuclear dipolar interactions, by transforming to the dipolar pair-toggling reference frame before applying the Magnus expansion. Of paramount importance in the case of strong homonuclear dipolar interactions is the question of whether or not the pulse imperfection hamiltonians or the dipolar hamiltonians couple with the resonance-offset hamiltonian (i.e. the chemical shift) in such a way that multiple pulse cycles give us a dipolar dependent chemical shift scaling

curve. Also, in the dipolar pair-toggling reference frame, we gain insight into the broadening mechanisms which are coupled with the dipolar hamiltonian during the multiple pulse cycle. This insight will aid us in designing new multiple pulse cycles in the future.

References

1. J.S. Waugh, L.M. Huber, and U. Haeberlen, Phys. Rev. Lett. 20, 180 (1968).
2. U. Haeberlen, High Resolution NMR in Solids, Selective Averaging (Academic Press, New York 1970).
3. D.P. Burum, W.K. Rhim, J. Chem. Phys. 71, 944 (1979).
4. A.M. Achlama, U. Kohlschutter, and U. Haeberlen, Chem. Phys. 7, 287 (1975).
5. B. Berglund and R.W. Vaughan, J. Chem. Phys. 73, 2037 (1980).
6. D.P. Burum, W.K. Rhim, J. Chem. Phys. 70, 3553 (1979).
7. L.M. Ryan, R.C. Wilson, and B.C. Gerstein, Chem. Phys. Lett. 52, 341 (1977).
8. D.P. Burum and W.K. Rhim, J. Mag. Res. 34, 241 (1979).

CHAPTER 3

A High Field (6.3 Tesla) Multiple Pulse Spectrometer

INTRODUCTION

There are two advantages to building a multiple pulse nuclear magnetic resonance (NMR) spectrometer operating with a 6.3 tesla magnet (270 MHz proton resonance) compared with lower field spectrometers. These advantages are: an improved signal to noise ratio (sensitivity) and improved resolution. However, there are some difficulties which are encountered in building a 270 MHz spectrometer due to the high operating frequency that must be overcome. The purpose of this section is to provide the motivation for building a multiple pulse spectrometer at 270 MHz by detailing the advantages of a high field and to describe the modifications we had to make in the design of the high field (270 MHz) spectrometer using the 56.4 MHz spectrometer described by Vaughan et al.(1) as a model.

The signal to noise ratio is improved in a high field spectrometer for two reasons: the first reason is that the equilibrium magnetization is directly proportional to the size of the Zeeman field, according to Curie's law for magnetization in the high temperature limit, and in pulsed NMR experiments, the size of the NMR signal is proportional to the equilibrium magnetization. The second reason is that we can build a probe which is more sensitive in detecting

the magnetization in our sample by increasing the quality factor (Q) of the probe circut. We can accomplish this without increasing the ringdown time in our probe or decreasing its bandwidth because the ringdown time is related to Q/ω_1 and not Q. Theoretically, the size of the NMR signal is proportional to the Q of the probe circuit so that the total increase in signal to noise is proportional to the square of the Zeeman field. It should be noted, however, that a high Q probe is also more efficient in detecting noise and transmission lines become more lossy with increasing frequency (2) so that we shouldn't expect the complete theoretical enhancement in sensitivity. In addition to improving the sensitivity of the probe, a high Q probe requires less radio-frequency power to produce the same H_1 field strength as a low Q probe.

In some solid state systems, the increased resolving power of a high field spectrometer is more important than the increased sensitivity. The increased resolving power of a high field spectrometer is due to the fact that the value of the chemical shift in absolute frequency units is proportional to H_o while most broadening effects due to pulse imperfections and all nuclear dipole-dipole interactions are independent of H_o. Thus compared to the chemical shift, the heteronuclear and residual homonuclear

dipolar broadening effects are relatively smaller in a high field than in a low field. In the event that residual homonuclear dipolar interactions limit the spectral resolution, we don't have to work as hard in a high field with our multiple pulse cycles to achieve the same resolution as in a low field spectrometer; that is, we can use longer cycle times which are easier to achieve experimentally. In the event heteronuclear dipolar interactions limit the spectral resolution, a high field spectrometer is an alternative to decoupling the heteronuclear dipole by radio-frequency irradiation. A high field spectrometer is especially attractive when a low γ (magneto-gyric ratio) spin with a moderately large quadrupole interaction, like potassium, needs to be decoupled. The improved resolving power of a high field multiple pulse spectrometer is demonstrated at the end of this chapter and in Chapter 7.

The difficulties in building a 270 MHz multiple pulse spectrometer have to do with the high operating frequency, where the dimensions of the radio-frequency circuits are comparable with the quarter wavelength of the radio frequency (22.5 cm for 270 MHz) and where each reactive element (R,L,C) in a circuit cannot be considered as a separate entity; i.e. the self-capacitance of an inductor

cannot be ignored. Also, radio-frequency components like frequency synthesizers, phase shifters, broad banded amplifiers, etc. are less dependable and more expensive with increasing frequency.

THE SPECTROMETER

Figure 1 is a block diagram of the 270 MHz spectrometer which is patterned after the 56.4 MHz spectrometer described by Vaughan et al.(1) in that the 270 MHz spectrometer employs a high Q probe circuit and a high Q transmitter, and that the spectrometer is constructed of commercially available prefabricated units (with the exception of the pulse programmer, the phase locked fast clock, and the intermediate (100W) amplifier). The frequency source for the spectrometer is a 30 MHz frequency synthesizer and the 6.3 tesla magnet, a Bruker super conducting solenoid, operates at a fixed field.

The 270 MHz radio-frequency pulses are obtained by a two step process: first, a 30 MHz signal is divided into four channels for the x, -x, y, and -y pulses and individually gated, phase shifted, and gated again in the same manner as described by Vaughan et al.(1) Secondly, the 30 MHz pulses are heterodyned with 240 MHz in a single side

band mixer to produce 270 MHz pulses. The 240 MHz signal is obtained by octupling the 30 MHZ in a series of double balanced mixers. This two step process allows us to retain the good gating characteristics of the low frequency (30 MHz) electronic switches and take advantage of the longer wavelength of the 30 MHz signal to set the phase of the radio-frequency pulses accurately. However, the heterodyning procedure produces pulses which have turn-on and turn-off transients which are dependent on the relative phases of the input radio-frequencies creating an overall pulse stability problem. This problem is corrected, however, by locking the timing of all pulses to the frequency source at 30 MHz.

The 270 MHz pulses are amplified to 400 watts in three stages: The pre-amplifier consists of a broadband, class B, high gain, 10 watt amplifier that drives the intermediate amplifier which consists of a homebuilt 100 watt class AB, push-pull amplifier (3) with an 8 db gain. The intermediate amplifier is broadbanded from 200 to 400 MHz. The final power amplifier consists of a high power (>400 watts), narrow banded , tunable cavity amplifier (class AB). The quarter wavelength circuit shown in Figure 2 is placed after the power amplifier to insure that the amplifier ringdown time after the pulse is as short as possible and to

prevent oscillations in the amplifier. During the pulse, the peak to peak voltage of the radio-frequency at point A in Figure 2 is typically 400 V, which opens the diodes, thus shorting the quarter wavelength stub. Since a shorted quarter wavelength stub has an infinite impedance, all of the radio-frequency power passes to the probe. When the voltage at point A falls below 1.5 V after the pulse, the crossed diodes close and the 50 Ω terminator dissapates the remainder of the radio-frequency energy in the amplifier. Crossed diodes have been placed after each amplifier from time to time to increase the on-off ratio of the pulses.

The transmitter, probe, and receiver are isolated from each other by the standard quarter wavelength cable arrangement (4,5). Due to the importance of fast receiver recovery times, the receiver is protected further by the circuit shown in Figure 3. This device is a 300Ω quarter wavelength step up-step down transformer. A quarter wavelength cable transforms the voltage according to the equation

$$V_{out} = V_{in}\left(\frac{Z_c}{Z_{in}} \right)$$

where Z_{in} is the impedance of the incoming signal (50Ω) and Z_c is the impedance of the transmission line (300Ω). Thus during the pulse when the voltage at point B is greater than

1/6 x the cut-off voltage of the diodes (1.5 V), the transmission line has infinite impedance. After the pulse, the voltage at point A is less than .25 V and the NMR signal passes through to the receiver.

The receiver itself is essentially the broadband unit described by Vaughan et al. (1). The receiver output at 270 MHz is phase detected with 240 MHz, passed through a 30 MHz phase shifter and finally phase detected with the 30 MHz reference signal. The D.C. signal is sampled by a Biomation waveform recorder capable of sampling rates up to 5 MHz. The Biomation is interfaced to a PDP8-a mini-computer, where the NMR signals are accumulated, signal averaged, and Fourier transformed.

One of the most important components in a high frequency spectrometer is the probe. The probe consists of the circuit shown in Figure 4. We have had the greatest success with high frequency probes when the coil is floating, i.e. when both sides of the coil are not grounded. The coil is a ten turn solenoid made out of flattened, bare copper wire which was wound on a mandrill with an i.d. of about 5 mm and a length of about 15 mm. The coil was annealed while it was in place on the mandrill to insure that the coil did not lose its shape after taking it off the mandrill. The H_1

homogeneity of the coil, which is critical in multiple pulse experiments, is approximately 0.3° . The inductance of the coil is approximately 0.2 μh and the tuning capacitor is approximately 3 pf. The overall dimension of the probe circuit is about 12 cm, which is comparable with the quarter wavelength of 270 MHz, 22.5 cm. The theoretical Q of the isolated probe is approximately 300 based on the bandwidth of the probe as measured by a vector voltmeter.

The tuning of the resonant circuit is very sensitive to the circuit geometry in the probe body due to the low value of the tuning capacitor and the capacitive coupling between the probe circuit and the probe body. The probe is tuned simply by comparing the voltage reflected by the probe and the voltage incident to the probe using a dual directional coupler and a vector voltmeter.

OPERATION OF THE SPECTROMETER

The 270 MHz spectrometer is capable of generating 90° pulses as short as 1μs while the dead time (due to probe ringdown) for an undistorted signal after a 90° pulse is approximately 4μs. The radio-frequency pulses were completely stable when the phase locked fast clock was employed and no power droop problem was encountered. The

radio-frequency phase transients, which are created by the transient response of the high Q probe circut and the high Q transmitter to the rise and fall of the radio-frequency pulse, are controlled by slightly detuning the probe and the transmitter and adjusting the input and output coupling to the transmitter cavity. When the probe and transmitter are detuned, the length of the 90° pulses is increased. H_o homogeneity is approximately 90 Hz, 1/3 ppm.

The linear chemical shift scaling curves for the 8-pulse (6) and 24-pulse (7) cycles are shown in Figure 5 for the well tuned spectrometer; the pulse width is 1.5μ s and the pulse spacing is 4 μ s. The theoretical and experimental chemical shift scaling factors (i.e. the slope of the chemical shift scaling curve) for the 8-pulse cycle are .49 and .48 respectively and for the 24-pulse cycle they are .40 and .38, well within experimental error.

The enhanced resolution of the high field spectrometer (6.3 tesla) is demonstrated in Figure 6, which shows the chemical shift spectrum of the water molecules in a single crystal of gypsum using the 24-pulse cycle. The two peaks are due to two inequivalent water molecules in the unit cell; at room temperature the hydrogen in each water molecule is exchanging rapidly to produce a single line.

The single crystal of gypsum is oriented such that the intra-pair dipolar frequencies for the two water molecules are about 65 kHz and 30 kHz. For this particular experiment, the pulse width was 1.5 μs and the pulse spacing was 4 μs. The full widths at half max. are 1.6 and 2 ppm which can be compared with the linewidths reported by Burum and Rhim (8) at the same orientation, about 3.6 and 4 ppm (shown in Figure 6), in a 1.4 tesla magnetic field. For their experiment, the pulse width was 1.5 μs and the pulse spacing was 2.8 μs. The spectral resolution of the chemical shift spectrum in the high field spectrometer is about twice as good as the low field spectrometer even though the multiple pulse cycle time is 40% slower.

Typical spectra for the case of systems with heteronuclear dipolar broadening (1 kHz) are shown in the next chapter.

Acknowledgements: We wish to acknowledge the many contributions that Professor Cecil Dybowski, Dr. A. Vega, Dr. T.M. Duncan, and Mr. John Yehle have made in the construction of this spectrometer. This work was supported by the National Science Foundation (DMR-7721394).

References

1. R.W. Vaughan, D.D. Elleman, L.M. Stacey, W.K. Rhim, and J.W. Lee, Rev. Sci. Instr. 43, 1356 (1972).
2. R. Myers ed., "The Radio Amateur's Handbook", (Amer. Radio Relay League Inc. Newington Conn. 1976).
3. L.B. Max, Application Note 2.2.8.8E, Communications Transistor Corporation, 1974.
4. U. Haeberlen, Ph.D. thesis (Tech. Hochschule, Stuttgart, 1967).
5. I.J. Lowe and C.E. Tarr, J. Phys. E 1, 604, 320 (1968).
6. W.K. Rhim, D.D. Elleman, L.B. Schreiber, and R.W. Vaughan, J. Chem. Phys. 60, 4595 (1974).
7. R.W. Vaughan, D.D. Elleman, W.K. Rhim, and L.M. Stacey, J. Chem. Phys. 57, 5383 (1972).
8. D.P. Burum and W.K. Rhim, J. Chem. Phys. 70, 3553 (1979).

Figure 1. A block diagram of the spectrometer.

Figure 2. This circuit is placed after the transmitter to dissipate the energy in the transmitter after the radio-frequency pulse has passed. When the voltage at point A is greater than 1.5 V (during the pulse), the horizontal transmission line has infinite impedance. After the pulse, the voltage at point A drops below 1.5 V and the horizontal transmission line has a 50 ohm resistive impedance.

Figure 3. This circuit is a transmission cable step up-step down voltage transformer, which is used to protect the reciever during the intense radio-frequency pulse.

Figure 4. The probe circuit.

Figure 5. The chemical shift scaling curve for the 8- and 24-pulse cycles. The ordinate is the actual offset frequency while the abscissa is the measured offset. The slopes of the two lines are 0.48 and 0.38 for the 8- and 24-pulse cycles respectively.

Figure 6. The chemical shift spectrum of the water molecules in gypsum, observed at 6.3 tesla using the 24-pulse cycle with a pulse width of 1.5 s and a pulse spacing of 4 s. At this orientation, the dipolar interactions for the two water molecules are about 65 KHz and 30 KHz. The linewidth observed at 1.4 tesla with a pulse width of 1.5 s and a pulse spacing of 2.8 s.

Figure 6. The chemical shift spectrum of the water molecules in gypsum, observed at 6.3 tesla using the 24-pulse cycle with a pulse width of 1.5 μs and a pulse spacing of 4 μs. The linewidths are approximately 2 ppm (full width at half max.). At this orientation, the dipolar interactions for the two water molecules are about 65 KHz and 30 KHz. The bars at the top of the spectrum represent the linewidth observed at 1.4 tesla (4 ppm) at the same orientaion with a 1.5 μ s pulse width and a pulse spacing of 2.8 μ s.

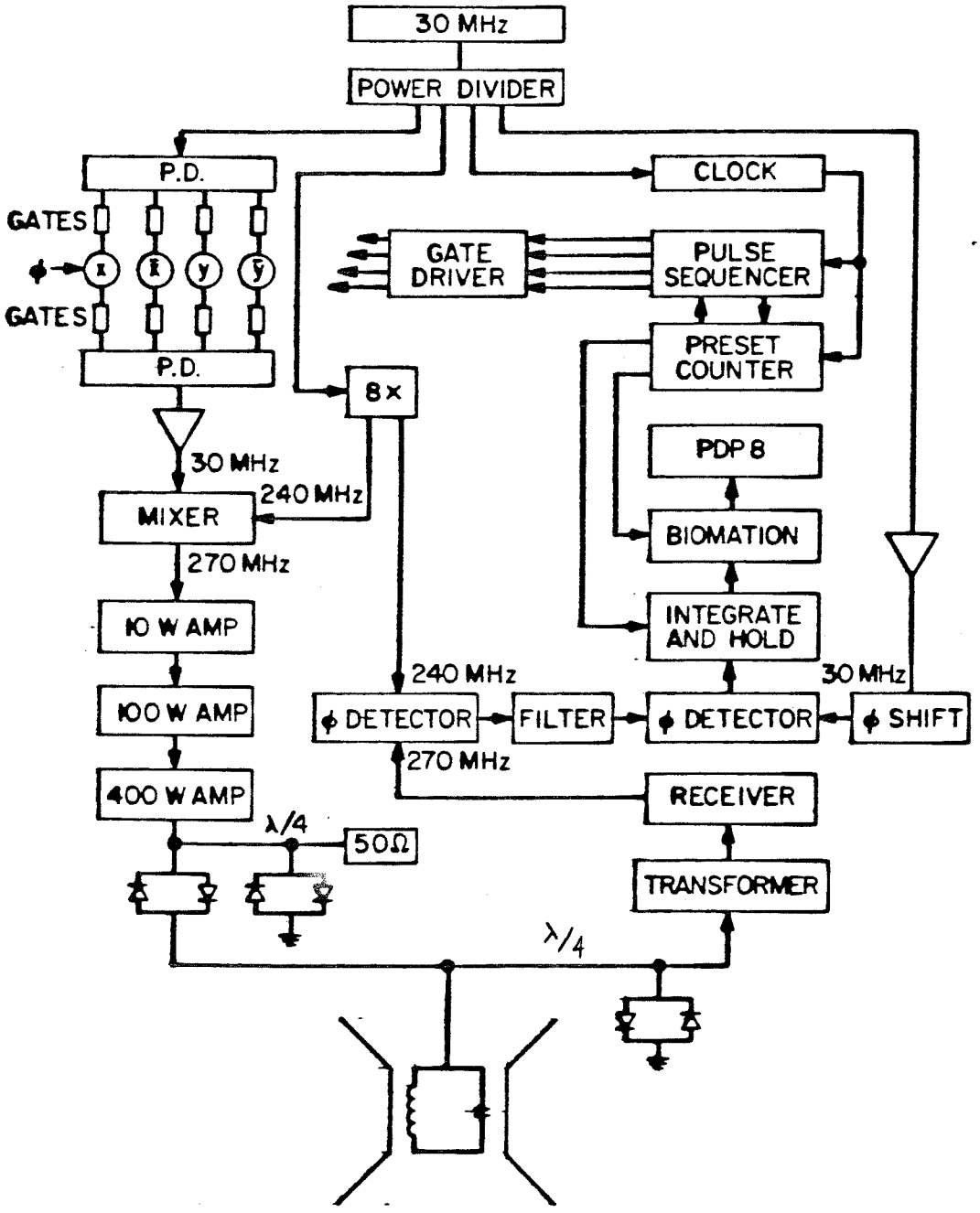
30 MHz
POWER DIVIDER
P.D.
GATES
GATES
P.D.
CLOCK
GATE DRIVER
PULSE SEQUENCER
PRESET COUNTER
8×
PDP 8
BIOMATION
INTEGRATE AND HOLD
30 MHz
240 MHz
MIXER
270 MHz
10 W AMP
100 W AMP
400 W AMP
240 MHz
DETECTOR
FILTER
DETECTOR
SHIFT
30 MHz
270 MHz
RECEIVER
λ/4
50Ω
TRANSFORMER
λ/4

Figure 1.

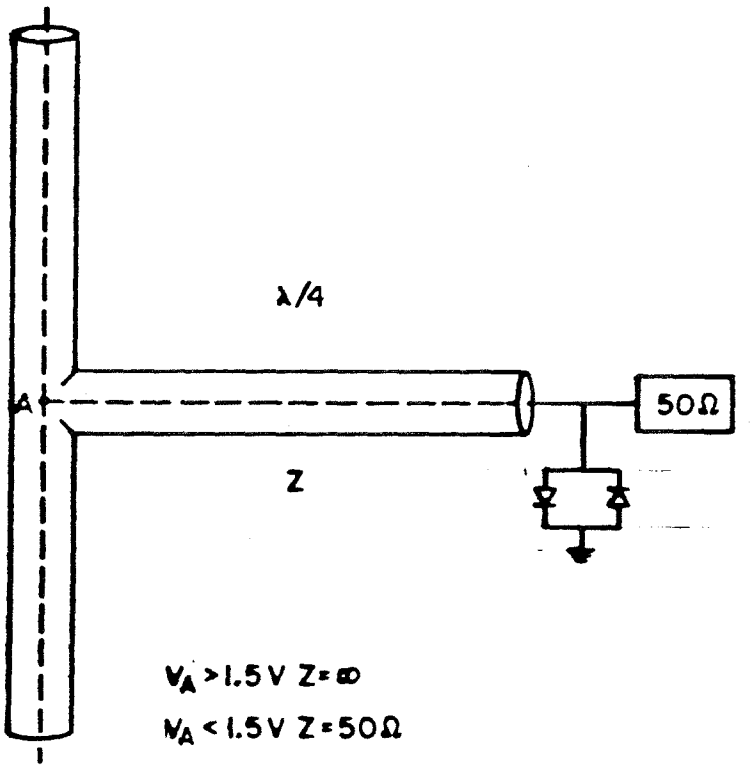

Figure 2.

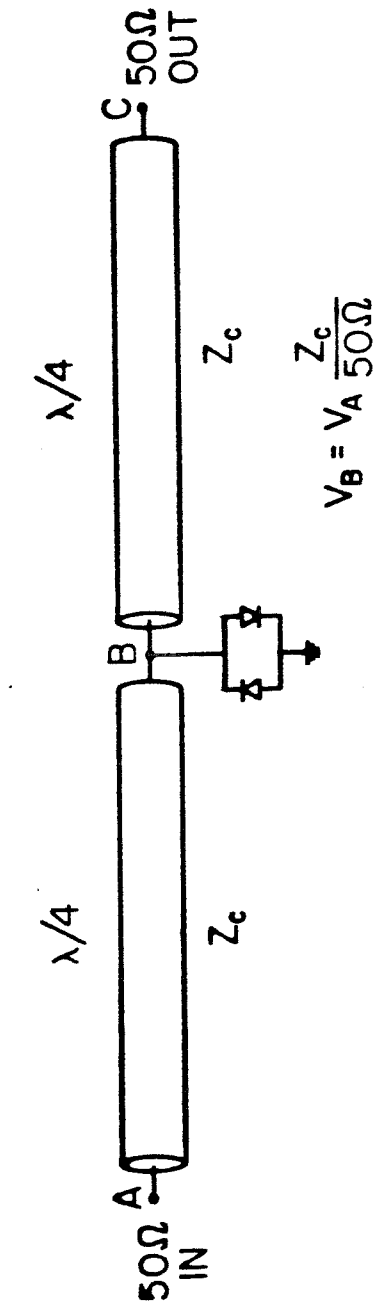

Figure 3.

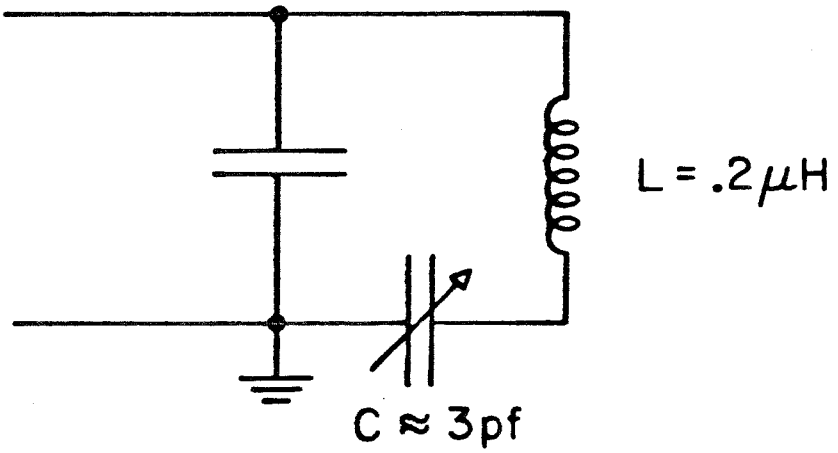

Figure 4.

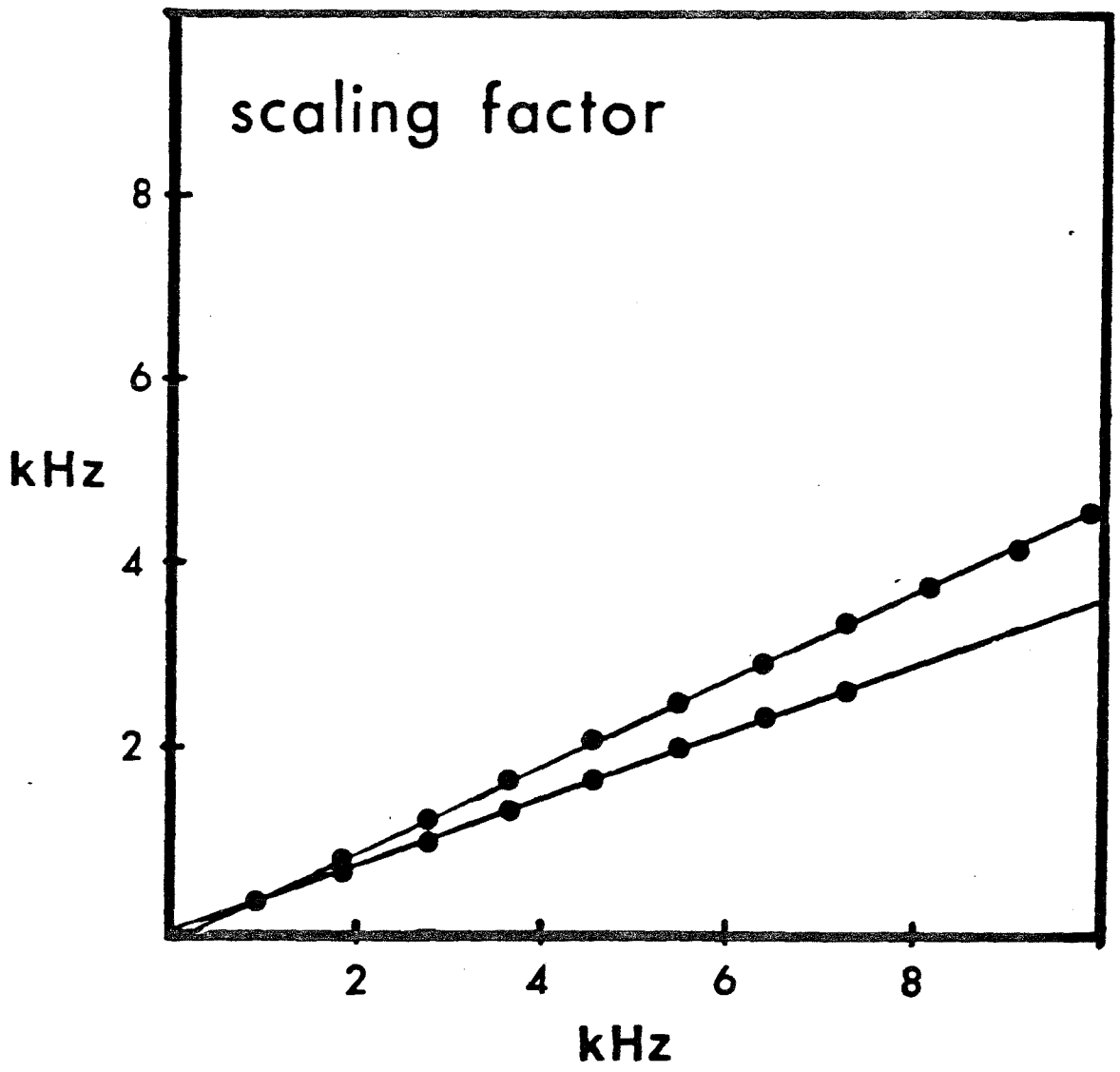

Figure 5.

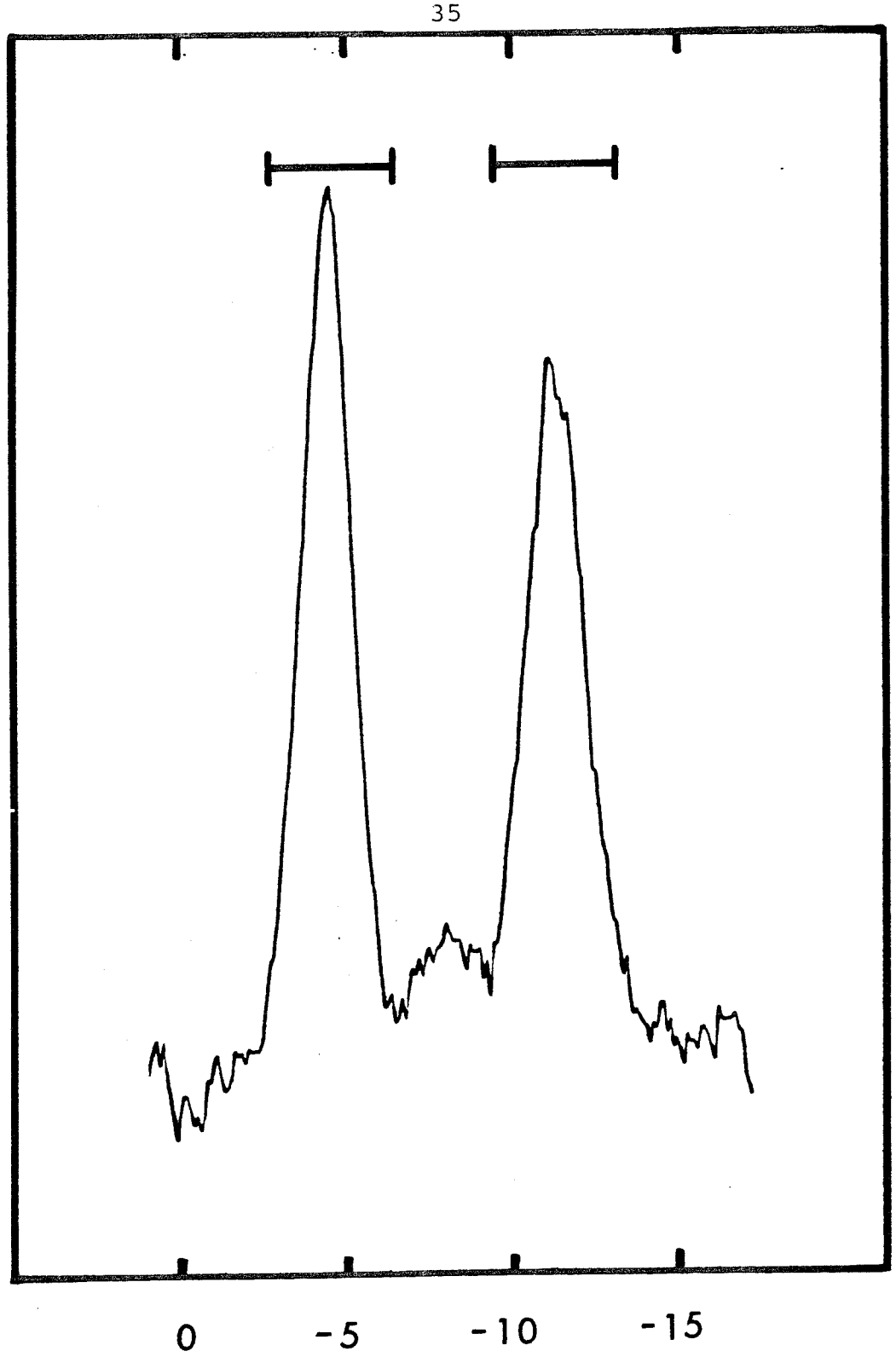

Figure 6.

CHAPTER 4

The Chemical Shift Tensors for Strongly Hydrogen-Bonded Protons: The Carboxylic Protons in $KHCH_2(COO)_2$, $KHO(CH_2COO)_2$, and $KH(C_4H_5O_2)_2$

(Chapter 4 is taken from two articles: The Chemical Shift Tensor for a Strongly Hydrogen-bonded Proton: The Carboxylic Proton in $KHCH_2(COO)_2$, by B. Berglund, D.G. Carson, and R.W. Vaughan which was published in the Journal of Chemical Physics, January 15, 1980, and The Chemical Shift Tensors for Strongly Hydrogen-bonded Protons: The Carboxylic Protons in $KHO(CH_2COO)_2$ and $KH(C_4H_5O_2)_2$, by B. Berglund, J. Allison, D.G. Carson and R.W. Vaughan which has been accepted for publication by the Journal of Magnetic Resonance.)

ABSTRACT

The chemical shift tensors for the carboxylic protons in potassium hydrogen malonate, potassium hydrogen oxydiacetate, and potassium hydrogen dicrotonate have been determined from a proton multiple pulse experiment carried out at 270 MHz. The isotropic part of the chemical shifts relative to a spherical sample of TMS and the anisotropies for the two compounds are -20.5(5), -19.6(7), -18.2(7) ppm and 27.6(6), 28.3(9), 28.9(9) ppm, respectively. The eigenvectors are oriented similarly to those found for other hydrogen bonded systems. The angle between the most shielded direction and the O-H bond vector, for example, is 9(2)° , 4(2)° , and 0(2)° respectively for the three compounds.

INTRODUCTION

The proton chemical shift tensor has now been measured for a number of solid systems since the development of multiple pulse nuclear magnetic resonance in solids (for a review, see Refs. 1-3).

It has been observed that protons involved in hydrogen bonding exhibit chemical shift tensors with a larger anisotropy than found for non-hydrogen- bonded protons and that such hydrogen-bonded proton tensors are nearly axially symmetric in most cases. It has recently been pointed out (3) that both the isotropic value of the chemical shift tensor, $\bar{\sigma}$, and the anisotropy, $\Delta\sigma$, of such hydrogen-bonded protons correlate very well with the hydrogen-bond strength. The anisotropy increases for increasing hydrogen-bond strength, while the isotropic value becomes smaller (more negative relative to tetramethylsilane, TMS). In terms of principal values of the chemical shift tensor (approximated as axially symmetric), the component directed along the O-H direction, $\sigma_{||}$, appears independent of the strength of the hydrogen bond, while components perpendicular to the O-H bond direction, $\sigma_{\perp}$, exhibit a large decrease (become more negative relative to TMS) with the

increasing strength of the hydrogen bond.

Most of the high resolution NMR studies of hydrogen-bonded systems have been performed on materials with weak to moderately strong hydrogen bonds (oxygen-oxygen distances of 2.55-2.65 Å), and the present study was undertaken to provide more information on those systems containing the strongest hydrogen bonds. We have chosen to examine KH malonate, KH oxydiacetate, and KH dicrotonate, since, as appears to be the case for the acid salts of weak carboxylic acids (4,5), they contain particularly strong hydrogen bonds, with an oxygen-oxygen distance of 2.468 (5) Å, 2.476(2) Å, and 2.488(2) Å, and the development of multiple pulse capabilities at 270 MHz allows one to overcome easily the heteronuclear dipolar broadening produced in the spectra by the potassium cation. These bond distances are comparable to the one in KH maleate(2.437 Å), which has been studied previously (6,7) and were the only data on very strong hydrogen bonds used in the correlations (3) discussed above. The study of KH maleate (7) is the only other high-field (270 MHz) study previously reported, and the advantage of using a high- frequency (field) for spreading out the chemical shifts was demonstrated.

The crystal structure of $KHCH_2(COO)_2$ has been studied by

x-ray (8) and neutron diffraction (9). The structure shown in Figure 1 consists of infinite chains of hydrogen malonate residues linked together by a very short O-H-O hydrogen bond across a center of symmetry. The crystal structure of $KHCH_2(COO)_2$ belongs to the monoclinic space group C2/m . (a=9.473 (6), b=11.559 (7), c=4.726(5) Å and β =91.6 (1)°) and consists of one crystallographically independent methylene and one carboxylic proton in the asymmetric unit. The NMR spectra are therefore expected to contain four lines, two from the symmetry-related methylene protons and two from the symmetry-related carboxylic protons.

The crystal structure of KH oxydiacetate has been studied by neutron diffraction (10) and contains hydrogen oxydiacetate chains (Figure 2) with a hydrogen bond length of 2.476 (2) Å between the molecules. The hydrogen bond angle is 174.2(3) ° and the O-H distance 1.152(3) Å showing the significant asymmetry in the bond. The very strong bond is also associated with a small deuterium quadrupole coupling constant, 64 kHz (11).

The structure of KH oxydiacetate belongs to the monoclinic space group $P2_1/c$ (a = 7.102, b = 10.451, c = 8.558 Å and β = 101.44°). The asymmetric unit contains 5 protons and at most 10 lines are expected in the high

resolution spectra of a single crystal. In the presence of the proton-potassium dipolar broadening it is of course extremely difficult to resolve all these lines simultaneously. Since the anisotropy of the shift tensors for carboxylic protons are much larger than for C-H protons (1), it is, however, fairly easy to locate the lines from the carboxylic proton, whereas all the other lines will overlap to one structureless band.

The crystal structure of KH dicrotonate has also been studied by neutron diffraction (12) and it belongs to the triclinic space group $P\bar{1}$ (a = 12.459, b = 6.049, c = 7.452 Å and $\alpha = 65.02^\circ$, $\beta = 104.04^\circ$, $\gamma = 97.44^\circ$). The structure contains dimers of crotonate anions bonded together with a nearly, but not quite, symmetrical hydrogen bond (Figure 3). The O--O distance is slightly longer (2.488(2) Å) than the distance in KH oxydiacetate. The asymmetric unit contains eleven different protons associated with eleven different tensors and at most eleven lines are therefore expected in the high resolution NMR spectrum, one from the carboxylic proton, four from the olefinic protons and six from the CH_3 protons. The lines from all the CH protons will have a small shift relative to TMS for any orientation of the crystal and it is possible to measure the location of the carboxylic line, when it is shifted away from the others.

EXPERIMENTAL DETAILS

Potassium hydrogen malonate was prepared by dissolving equimolar amounts of $KHCO_3$ and malonic acid, and single crystals were grown from a saturated solution by slow evaporation. Two crystals were ground to cylinders (h/l ratio=1.5) with the cylinder axes arbitrarily chosen relative to the unit cell. The crystals were mounted on glass rods so each crystal could be rotated in the magnetic field around an axis parallel to the cylinder axis.

KH dicrotonate was made by dissolving crotonic acid and $KHCO_3$ (2:1) in water and single crystals were grown from a saturated solution by slow exaporation. For KH oxydiacetate, a commercial salt was used and the crystals were grown by the same method. Two different crystals were grown for KH oxydiacetate and four for KH dicrotonate. All crystals were cut to either cylinders or parallel epipeds, with the long axis of the crystal arbitrarily oriented in the unit cell. All crystals were mounted on glass rods, allowing each crystal to be rotated in the magnetic field about an axis parrallel to the axis of the cylinder or parallelepiped.

The rotation axes were determined on a four-circle X-ray diffractometer (syntex $P2_1$) where 10-15 reflections were measured accurately and used in a least-squares refinement of the axis. The rotation axes are given in Table 1. Each crystal was then transferred to a home-built NMR spectrometer operating at 6.3 tesla.

The procedure of rotating the crystals around arbitrary axes has some advantages compared to the more conventional procedure of rotating around three orthogonal axes, usually a, b, c for a monoclinic space group. Most importantly, one does not have to worry about ambiguities which can occur when rotating around axes parallel to symmetry axes, and furthermore, it is usually more convenient experimentally not to have to mount and grind around symmetry axes, especially when the crystals do not have well- developed facets.

The tuning of the spectrometer for the multiple pulse experiments was carried out in a way described elsewhere (13). The epoxy used to mount the crystals to the glass rods was used as a convenient internal reference for the KH malonate and KH dicrotonate samples. In order to determine the chemical shifts relative to a spherical sample of TMS, a spectrum of the crystal plus the epoxy was recorded with a

free induction decay (the epoxy line showed up as a narrow line) and was compared to a spectrum of TMS. The same shift was found for all crystals, and all results are reported relative to the TMS reference. The chemical shifts in the KH oxydiacetate crystals were measured relative to a line from an occluded $KHO(CH_2COO)_2$ solution (-7.2 ppm relative to TMS). The eight-pulse sequence (13) was used with a cycle time of 48 microseconds and the scaling factor was monitored from time to time to confirm proper operation of the sequence. The spin-lattice relaxation time (T_1) in the KH dicrotonate crystal was short due to the CH_3 rotation. For the KH malonate and KH oxydiacetate samples, however, the crystals were doped with Mn^{++}, which reduced T_1 to about one minute.

Figures 4, 5, and 6 give typical spectra for the three samples and demonstrate the resolution obtainable in the presence of the potassium. The relatively large linewidths, due to the proton-potassium coupling, made neither a grinding of the crystals to spheres (14) nor correction for the bulk susceptibility effects (15) warranted. The susceptibility effects are typically of the order of one ppm or less for crystals ground to cylinders, whereas the linewidths are of the order of 3-4 ppm. The reported tensors might, however, be affected by a systematic error of

one ppm or less.

DETERMINATION OF THE CHEMICAL SHIFT TENSORS

The chemical shift for a proton may be written in an arbitrary coordinate system

$$\Delta = \underset{\sim}{u}\ \underset{\sim}{S}\ \underset{\sim}{u} \qquad (1)$$

The vector $\underset{\sim}{u}$ is a unit vector along the magnetic field, and $\underset{\sim}{S}$ is a matrix containing the six elements in the chemical shift tensor. If we write $\underset{\sim}{S}_d$ for the diagonalized form of $\underset{\sim}{S}$ and we choose a coordinate system for Eq. (1) to be an orthogonal crystal fixed system ($\underset{\sim}{i}$, $\underset{\sim}{j}$, $\underset{\sim}{k}$) where $\underset{\sim}{k}$ is along the axis of rotation, the chemical shift may be written

$$\Delta = \underset{\sim}{u}\ \underset{\sim}{P}^{-1}\ \underset{\sim}{R}^{-1}\ \underset{\sim}{L}^{-1}\ \underset{\sim}{S}_d\ \underset{\sim}{L}^{-1}\ \underset{\sim}{R}^{-1}\ \underset{\sim}{P}^{-1}\ \underset{\sim}{u} \qquad (2)$$

$\underset{\sim}{u}$ now has components ($\cos\psi \sin\theta$, $\sin\psi \sin\theta$, $\cos\theta$), where $\psi = \Phi - \phi_0$, ϕ_0 is a reference angle and θ is the angle between the axis of rotation and the magnetic field (usually chosen to be equal to 90^0). The matrix $\underset{\sim}{L}$ transforms a vector from the principal axis system of a particular chemical shift tensor to the crystallographic system. The matrix $\underset{\sim}{R}$ is the translation free part of the transformation of a vector from the asymmetric unit of crystallographic cell to a

symmetry-related unit, i.e., $\underset{\sim}{R}$ is a transformation belonging to the point group isomorphous with a factor group associated with the space group of the crystal. For $KHCH_2(COO)_2$, for example, the space group is C2/m and the two tensors $\underset{\sim}{R}$ are

$$\begin{pmatrix} 1 & 0 & 0 \\ 0 & 1 & 0 \\ 0 & 0 & 1 \end{pmatrix} \quad \text{and} \quad \begin{pmatrix} 1 & 0 & 0 \\ 0 & -1 & 0 \\ 0 & 0 & 1 \end{pmatrix}$$

$\underset{\sim}{P}$, finally, transforms a vector from the crystallographic system to the ($\underset{\sim}{i}$, $\underset{\sim}{j}$, $\underset{\sim}{k}$) system for a particular rotation axis. The chemical shift tensors were refined using the least-squares program QSPL4 (16).

RESULTS AND DISCUSSION

The refined chemical shift tensors for the carboxylic protons in KH malonate, KH oxydiacetate, and KH dicrotonate are given in Table 2 and in Figures 7, 8, and 9, the experimental chemical shifts as a function of the rotation angle are given together with rotation patterns calculated from the tensors given in Table 2.

The three tensors are very similar to each other and also to the tensor reported for KH maleate. In Table 3 the four

tensors are compared, and it can be seen that the isotropic shielding decreases for increasing bond strength (decreasing R_{O--O}). The anisotropies are almost the same and do not correlate with R_{O--O}. Also, the z-principal axes (the most shielded directions) are almost along the O-H vector and the x-principal axes (the least shielded directions) are normal to the plane defined by the carboxylic groups. The errors in the angles are about 2°.

It is interesting to notice that the difference between the components corresponding to the two least shielded directions, $\delta\sigma$, is rather large for all compounds in Table 3 except KH maleate. In KHF (17), which has a very strong F--H--F hydrogen bond, the difference is 7.3 ppm. These values should be compared to differences of 0-4 ppm usually found in weaker hydrogen bonded systems (1). Since the anisotropies, $\Delta\sigma$, are larger for the strongly hydrogen-bonded systems, the asymmetry parameter $\eta = \delta\sigma/(\sigma_{zz} - \bar{\sigma})$, which is a measure of the axial symmetry in the tensor, will not be significantly larger, however. η is usually found to be around 0-0.4 (1) and as can be seen in Table 3, η for KH malonate and KH oxydiacetate is just slightly larger than that. The large values of $\delta\sigma$ are, however, notable. Ditchfield showed (18) that the induced currents on the acceptor oxygen in the O-H--O hydrogen bond

is almost totally responsible for the changes in the anisotropy when the water dimer was formed and this effect is of course increasing as the proton approaches the acceptor oxygen. It would be interesting, however, to follow the variation of the individual eigenvalues of the theoretical shielding tensors with decreasing O--O bond length to see if just the approaching of the acceptor oxygen can be responsible for a larger $\delta\sigma$ value. For an equilibrium value, R_{O--O} = 2.83Å, Ditchfield calculated a $\delta\sigma$ value of 0.4 ppm in the water molecule dimer and 1.4 ppm in the water monomer, so the effect on the two eigenvalues is not the same when the dimer is formed. It is , therefore, reasonable to believe that the two eigenvalues have different variations as a function of R_{O--O} .

Acknowledgements

This work was supported by the National Science Foundation (DMR-7721394) . Thanks are due to Dr. Stan Samson for use of the X-ray diffractometer allowing orientation of the crystals. Dr. Bo Berglund wishes to acknowledge support from the Sweden-America Foundation, the Swedish National Science Research Council and the University of Uppsala, and J. Allison wishes to acknowledge support from the Fannie and John Hertz Foundation.

References

1. U. Haeberlen , "High Resolution NMR in Solids, Selective Averaging," (Academic Press, New York, 1976).

2. M. Mehring, "High Resolution NMR Spectroscopy in Solids," (Springer, New York, 1976).

3. B. Berglund, R.W. Vaughan, J. Chem. Phys. 73,2037(1980)

4. J. C. Speakman, Structure and Bonding 12, 141 (1972).

5. D. Hadzi, Pure Appl. Chem. 11,435 (1965).

6. A. M. Achlama, U. Kohlschutter, and U. Haeberlen, Chem. Phys. 7,287 (1975).

7. A.M. Achlama, H. Post, and U. Haeberlen, Chem. Phys. 31, 203 (1978).

8. J.G. Sime, J. C. Speakman, and R. Parthasarathy, J. Chem. Soc. (A), 1919 (1970).

9. M. Currie and J.C. Speakman, J. Chem. Soc. (A), 1923 (1970).

10. J. Albertsson and J. Grenthe, Acta Cryst. B29, 2751 (1973).

11. L. Mayas, M. Plato, C. J. Winscom and K. Mobius, Mol. Phys. 36, 753 (1978).

12. D. R. McGregor, J. C. Speakman and M. S. Lehmann, J. Chem. Soc. Perkin II, 1740 (1977).

13. W-K.Rhim, D.D. Elleman, and R.W. Vaughan, J. Chem. Phys. 58, 1772 (1973); ibid. 59, 3740 (1973).

14. H.W. Spiess, H. Zimmermann, and U. Haeberlen, Chem. Phys. 12, 123 (1976).

15. L.B. Schreiber, and R.W. Vaughan, Chem. Phys. Lett. 28, 586 (1974).

16. B. Berglund and J. Tegenfeldt, J. Magn. Resonance 30, 451 (1978).

17. P. Van Hecke, H. W. Spiess and U. Haeberlen, J. Magn. Resonance 22, 103 (1976).

18. R. Ditchfield, J. Chem. Phys. 65, 3123 (1976).

Table 1. Rotation axes for the crystals used in the HR-NMR experiment. The axes are given in a coordinate system defined by the unit cell axes.

	Crystal No.	Rotation Axis		
KH malonate	1	-0.0429	-0.0665	0.1020
	2	-0.0106	-0.0022	0.2098
KH oxydiacetate	1	0.0489	0.0726	-0.0574
	2	0.0065	-0.0068	-0.1152
KH diacrotonate	1	-0.0010	0.1639	0.0022
	2	0.0303	0.1506	0.0214
	3	0.0340	-0.0067	-0.1064
	4	-0.0004	-0.0013	0.1345

Table 2. The proton chemical shift tensors determined for the carboxylic protons in the three compounds. The eigenvectors are given in the coordinate system defined by the unit cell axes. The shifts are in ppm relative a spherical sample of TMS.

Eigenvalues	Eigenvectors		
KH malonate:			
-35.1 (3)	-0.0653 (11)	0.0141 (14)	-0.1662 (15)
-24.3 (3)	0.0437 (15)	0.0778 (5)	-0.0276 (29)
- 2.1 (7)	0.0705 (8)	-0.0351 (9)	-0.1281 (19)
	$\bar{\sigma}$ = -20.5 (5)	$\Delta\sigma$ = 27.6 (6)	
KH oxydiacetate:			
-34.7 (6)	0.0806 (40)	0.0081 (21)	0.1100 (15)
-23.4 (3)	0.0869 (40)	-0.0697 (18)	-0.0247 (31)
- 0.7 (10)	0.0823 (18)	0.0656 (19)	-0.0399 (31)
	$\bar{\sigma}$ = -19.6 (7)	$\Delta\sigma$ = 28.3 (9)	
KH dicrotonate:			
-31.7 (4)	0.0001 (33)	-0.1078 (126)	0.1441 (39)
-23.9 (9)	0.0396 (22)	0.1311 (117)	0.0421 (138)
1.1 (8)	0.0727 (12)	-0.0645 (34)	0.0128 (24)
	$\bar{\sigma}$ = -18.2 (7)	$\Delta\sigma$ = 28.9 (9)	

Table 3. Comparison between proton chemical shift tensors for carboxylic protons involved in very strong hydrogen bonds. $\delta\sigma$ is the difference ($\sigma_{yy} - \sigma_{xx}$) and η the asymmetry parameter. α is the angle between the most shielded direction and the O-H direction and β the angle between the least shielded direction and the normal to the plane defined by the carboxylic groups.

	R_{O--O} (Å)	$\bar{\sigma}_{TMS}$ (ppm)	$\Delta\sigma$ ppm	$\delta\sigma$(ppm)	η	α(°)	β(°)
KH maleate	2.437	-21.0	30.3	2.9	0.14	0	2
KH malonate	2.468	-20.5	27.6	10.8	0.59	9	8
KH oxydiacetate	2.476	-19.6	28.3	11.3	0.60	4	4
KH dicrotonate	2.488	-18.2	28.9	7.8	0.40	0	0

FIGURE CAPTIONS

Figure 1. A view of the structure of KH malonate showing the hydrogen bond arrangement.

Figure 2. A view of the structure of KH oxydiacetate showing the hydrogen bond arrangement.

Figure 3. A view of the structure of KH dicrotonate showing the hydrogen bond arrangement.

Figure 4. A multiple pulse NMR spectrum of KH malonate at 270 MHz. The reference is a line from epoxy.

Figure 5. A multiple pulse NMR spectrum of KH oxydiacetate at 270 MHz. The reference is a line from an occluded solution.

Figure 6. A multiple pulse NMR spectrum of KH dicrotonate at 270 MHz. The reference is a line from epoxy.

Figure 7. Angular dependence of the lines associated with the carboxylic proton. The solid curves are calculated from the tensor given in Table 2. Symm 1 and 2 refer to the symmetry operation associated with the symmetry related protons.. The shifts are relative to a spherical sample of TMS.

Figure 8. Angular dependence of the line locations associated with the carboxylic protons in KH oxydiacetate. The solid lines are calculated from the tensor given in Table 2. Symm 1 and 2 refer to the symmetry operation associated with the symmetry related protons.

Figure 9. Angular dependence of the lines associated with the carboxylic protons in KH dicrotonate. The solid lines are calculated from the tensor given in Table 2.

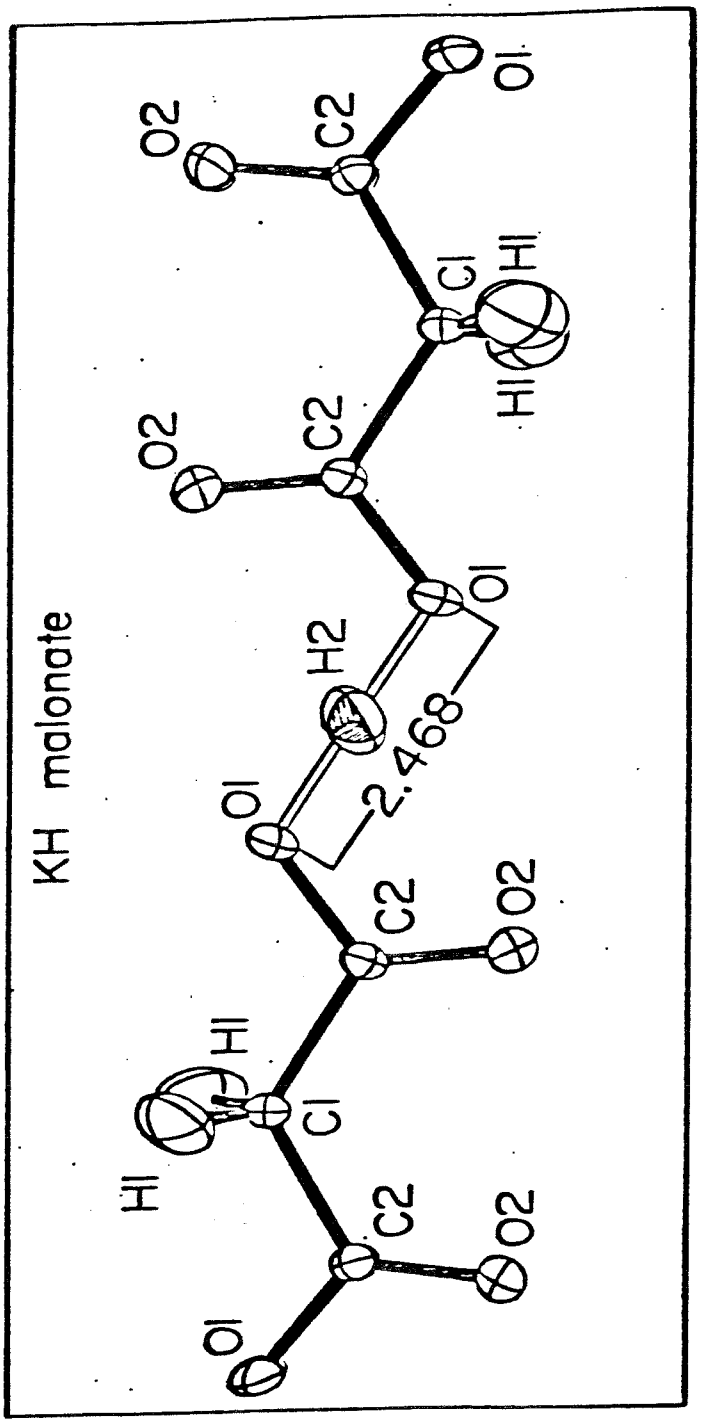
KH malonate
O1
C2
O2
C2
O2
H1
C1
H1
O1
H2
2.468
O1
C2
O2
C2
O2
H1
C1
H1

Figure 1.

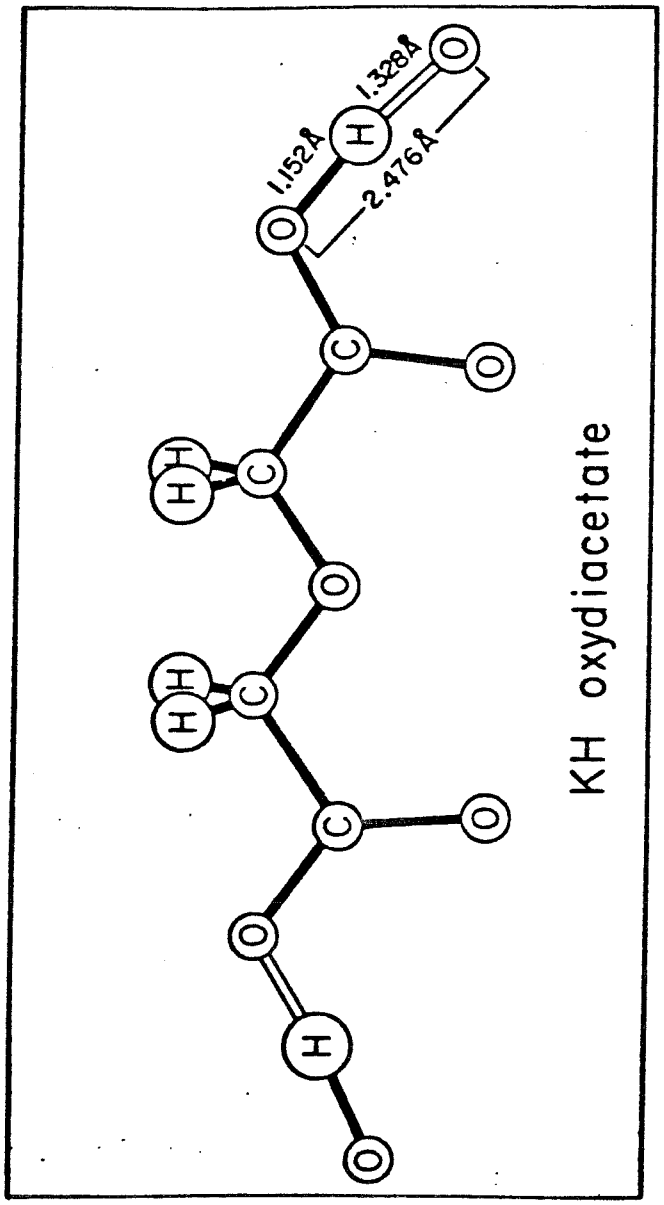

Figure 2.

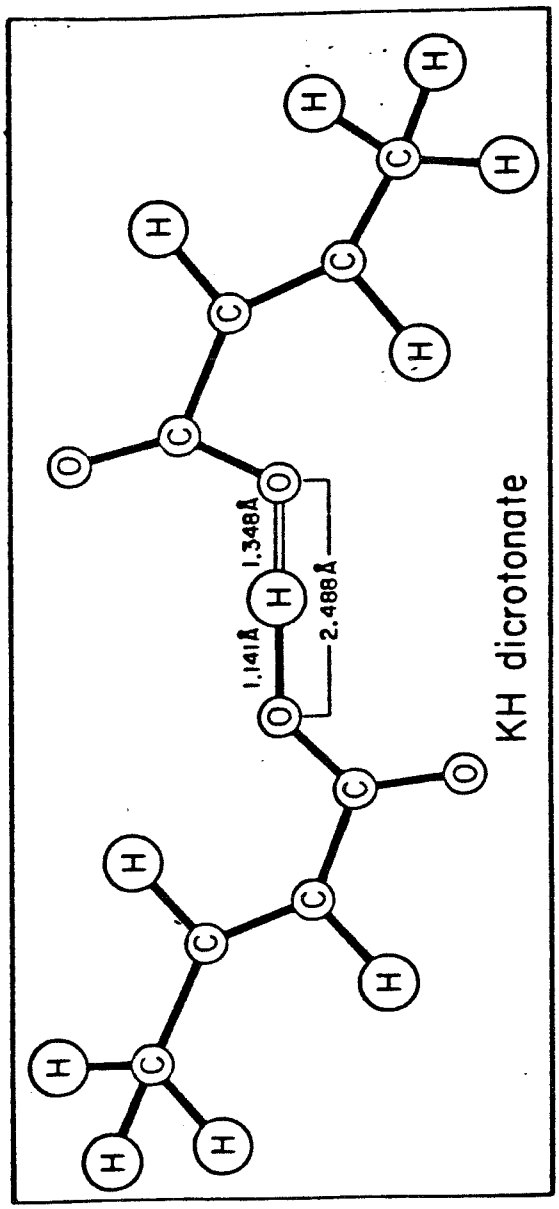

Figure 3.

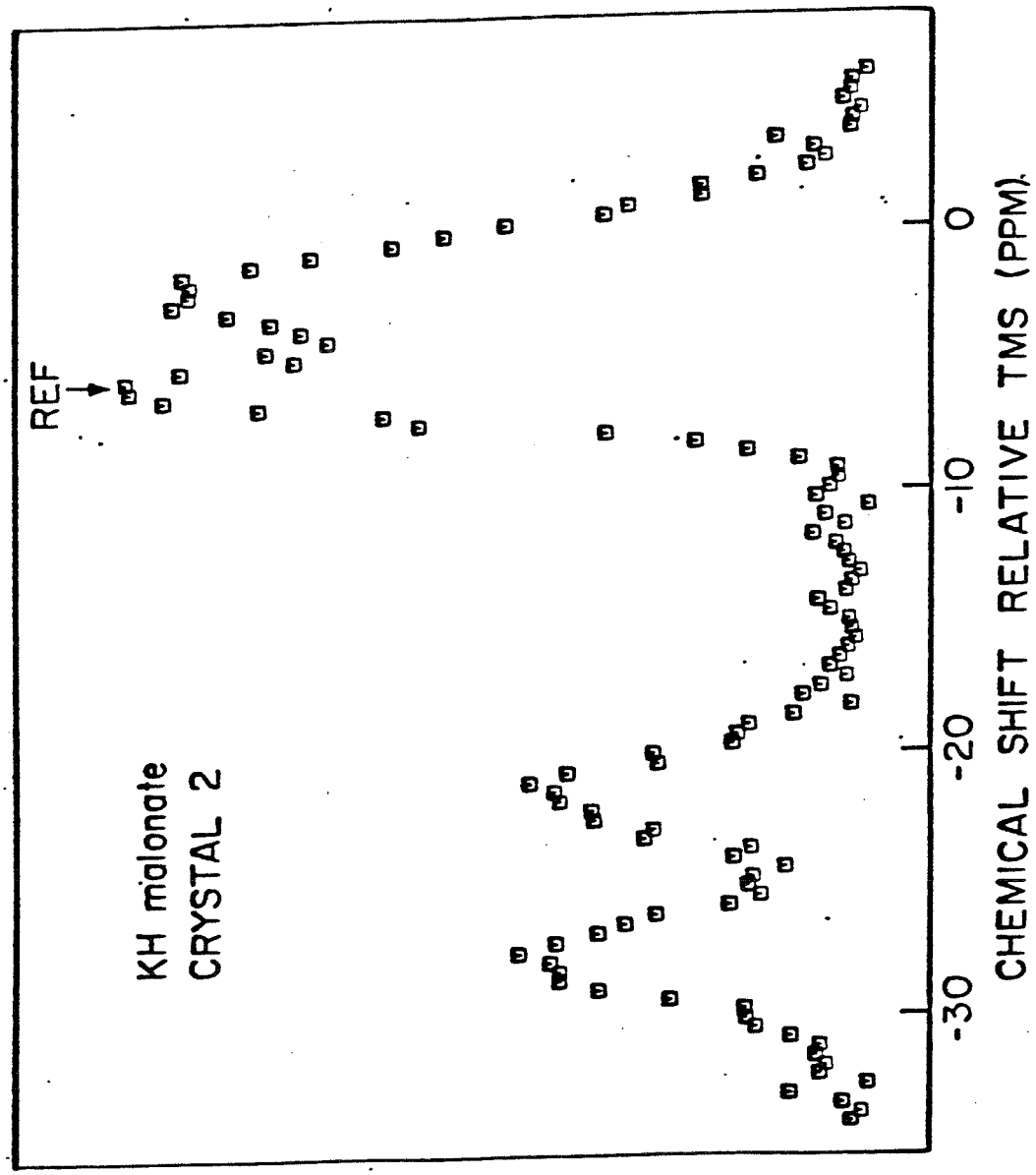
REF
KH malonate
CRYSTAL 2
0
-10
-20
-30
CHEMICAL SHIFT RELATIVE TMS (PPM).

Figure 4.

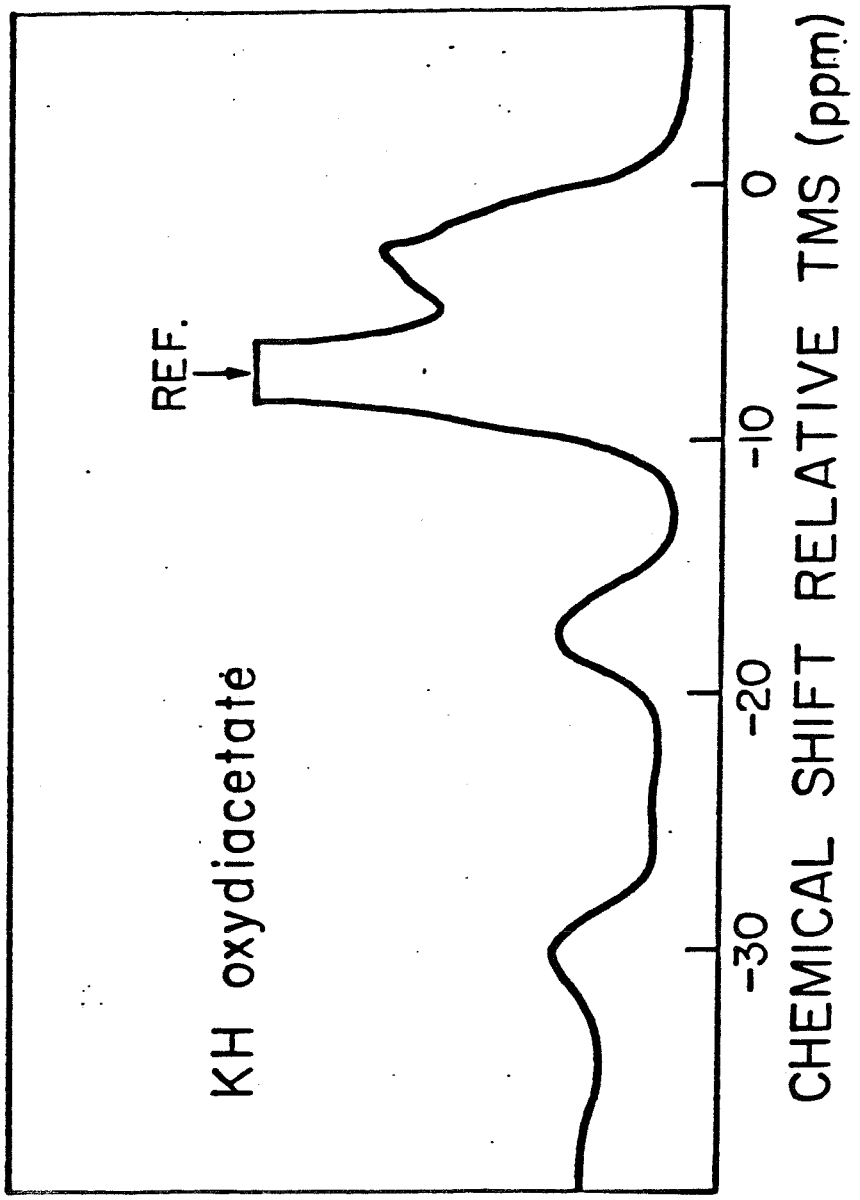
KH oxydiacetate
REF.
0
-10
-20
-30
CHEMICAL SHIFT RELATIVE TMS (ppm)

Figure 5.

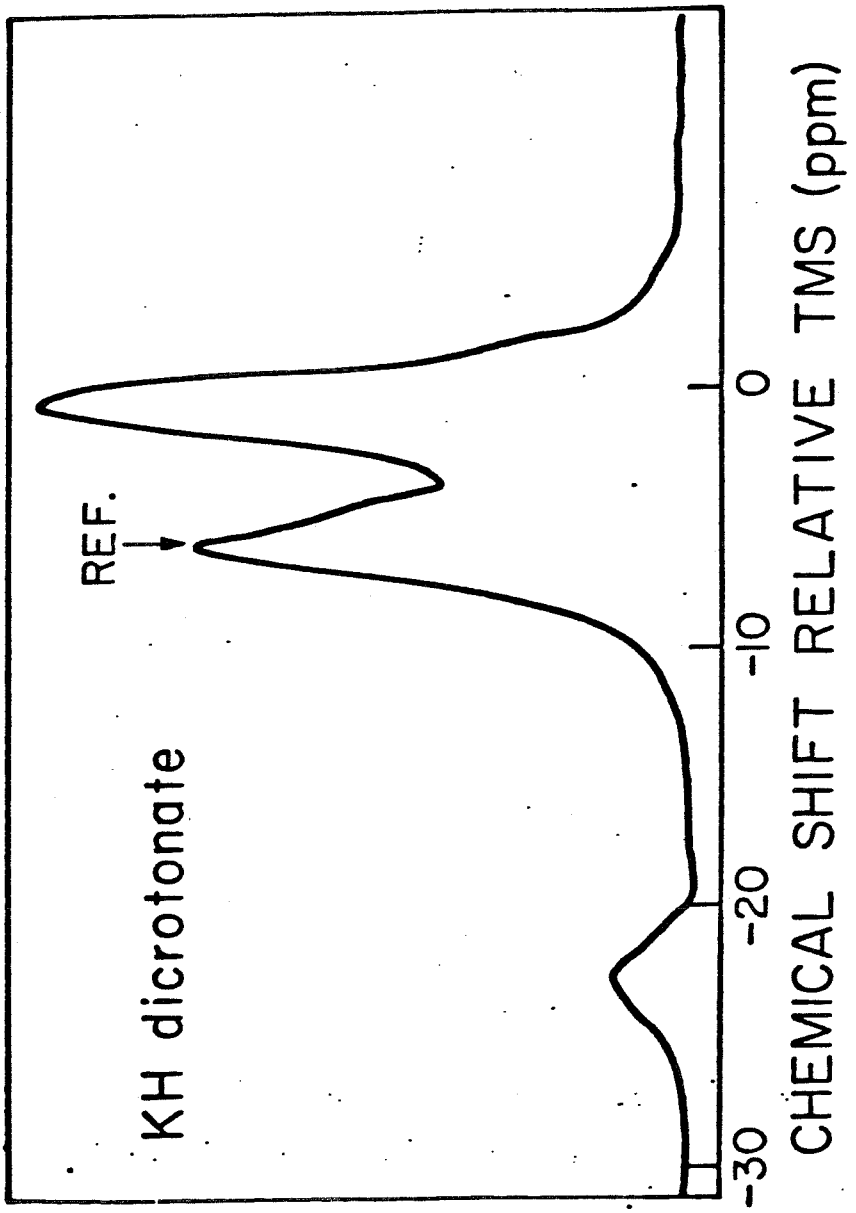
KH dicrotonate
REF.
0
-10
-20
-30
CHEMICAL SHIFT RELATIVE TMS (ppm)

Figure 6.

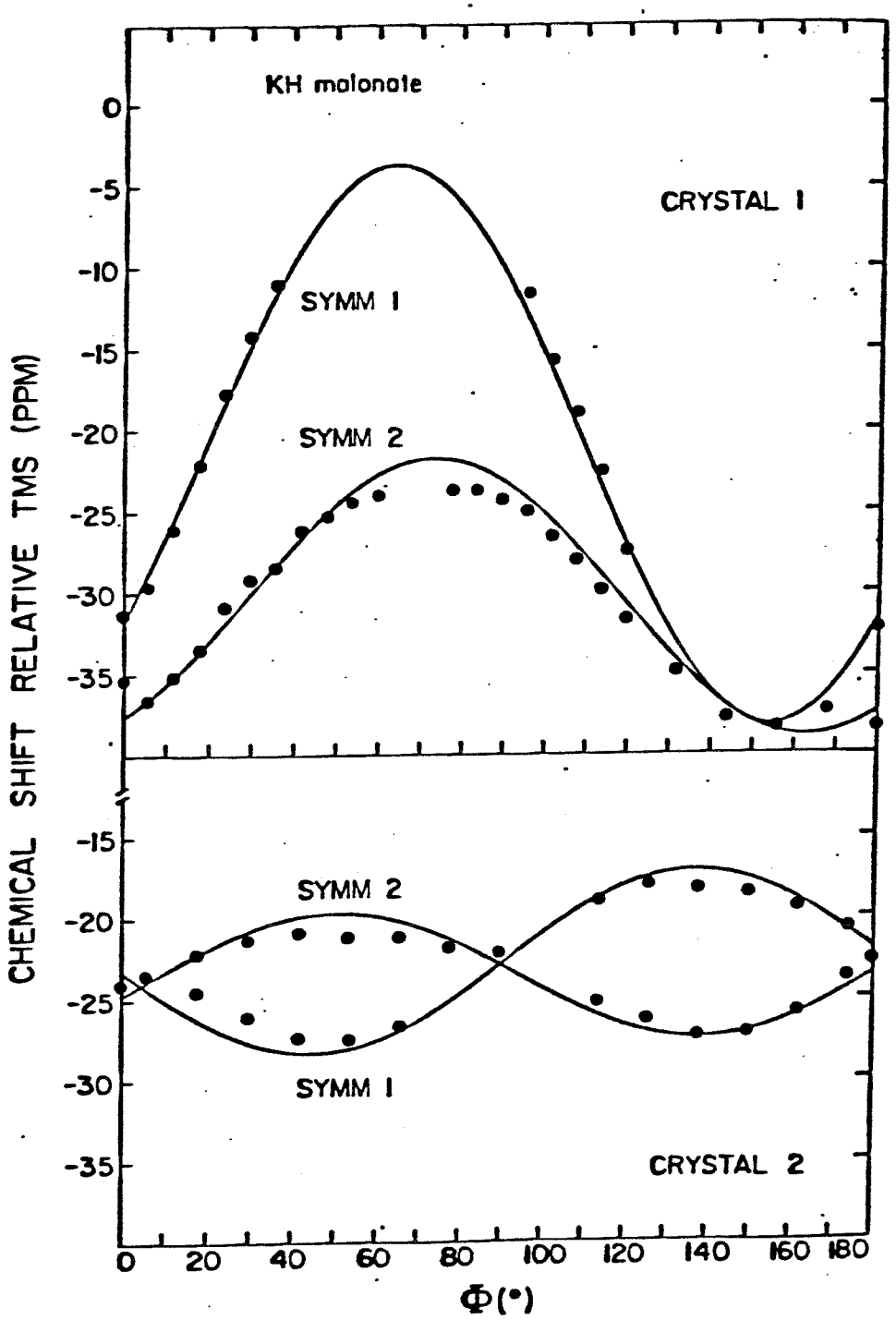
KH malonate
CRYSTAL 1
SYMM 1
SYMM 2
SYMM 2
SYMM 1
CRYSTAL 2
CHEMICAL SHIFT RELATIVE TMS (PPM)
0
-5
-10
-15
-20
-25
-30
-35
0
20
40
60
80
100
120
140
160
180
Φ(°)

Figure 7.

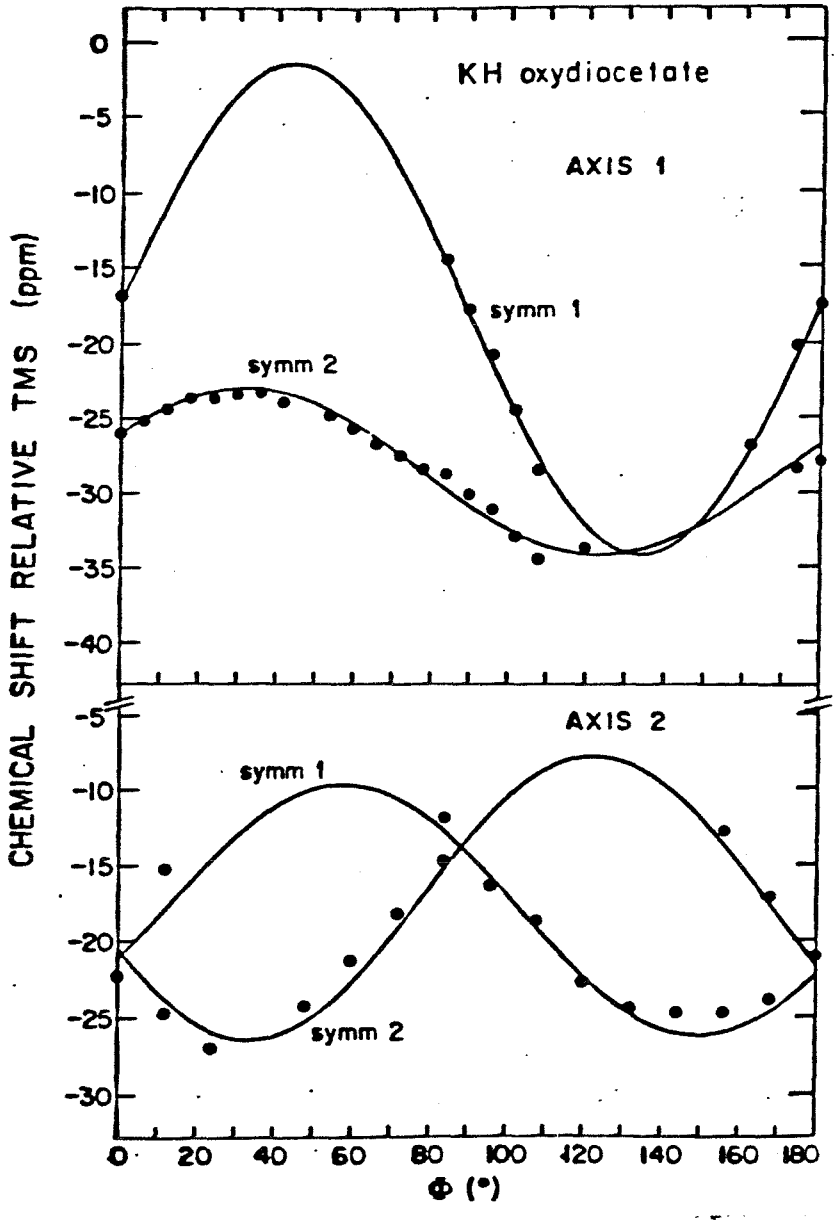
KH oxydiocetate
AXIS 1
symm 1
symm 2
AXIS 2
symm 1
symm 2
CHEMICAL SHIFT RELATIVE TMS (ppm)
Φ (°)
0
-5
-10
-15
-20
-25
-30
-35
-40
0
20
40
60
80
100
120
140
160
180

Figure 8.

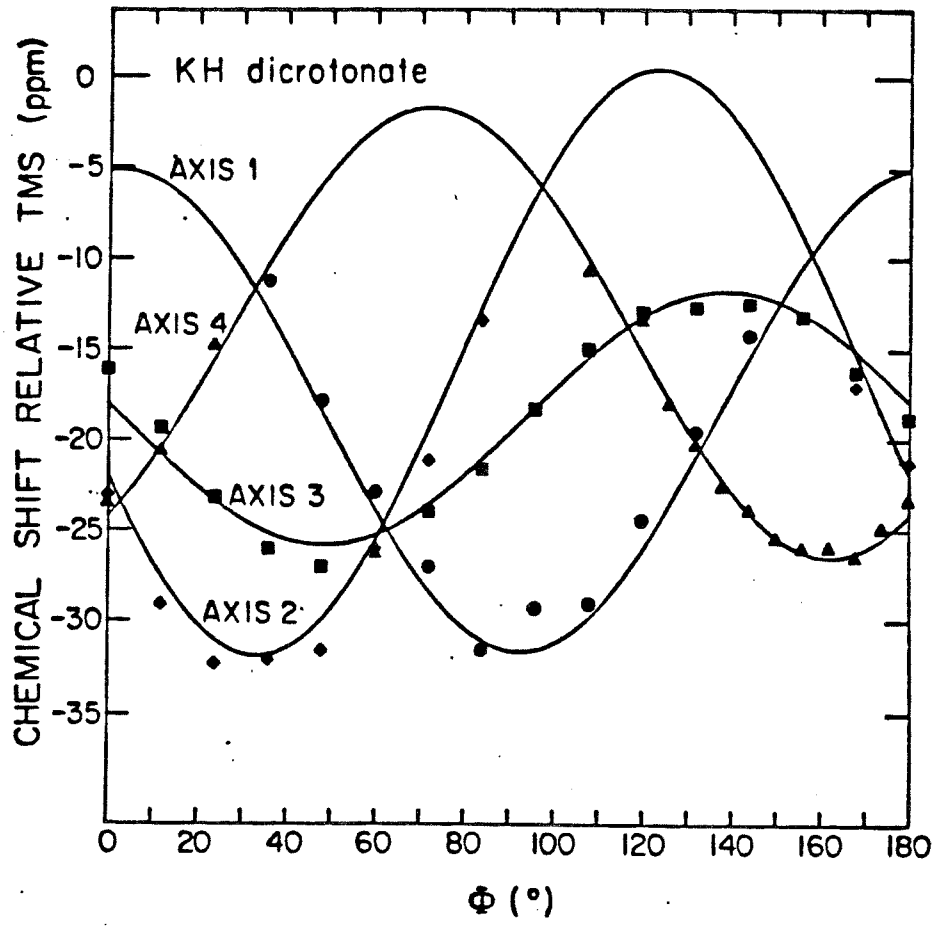
KH dicrotonate
AXIS 1
AXIS 4
AXIS 3
AXIS 2
CHEMICAL SHIFT RELATIVE TMS (ppm)
0
-5
-10
-15
-20
-25
-30
-35
0
20
40
60
80
100
120
140
160
180
Φ (°)

Figure 9.

CHAPTER 5

Analysis of Multiple Pulse NMR in Solids: Spin 1/2 Dipolar Pair Systems

(Chapter 5 is an article by D.G. Carson to be published in the Journal of Chemical Physics)

ABSTRACT

Average hamiltonians are calculated in the dipolar pair-toggling reference frame for the WAHUHA 4-pulse cycle, the MREV 8-pulse cycle, and the Burum-Rhim 24-pulse cycle, thereby extending average hamiltonian theory to cover the case of dipolar pair systems with strong intra-pair dipolar coupling. The residual dipolar interaction for the 24-pulse cycle cannot be reduced further by any multiple pulse cycle based on phase alternated 4-pulse cycles and the residual dipolar interaction for the 4- and 8- pulse cycles is significantly larger than for the 24-pulse cycle.

Finite pulse width effects are calculated exactly for a system of isolated spin 1/2 pairs with an arbitrary intra-pair dipolar coupling. The 24- and 8-pulse cycles perform better than the 4-pulse cycle but the 24-pulse cycle offers no improvement over the 8-pulse cycle in this regard. In this system, for all three multiple pulse cycles, finite pulse width effects can be completely removed to all orders by proper choice of the flip angle, which is a function on the dipolar interaction, pulse width, and pulse spacing.

INTRODUCTION

Recently, new multiple pulse cycles, such as the 24 and 52 pulse cycles (1,2), have been proposed which provide greater line narrowing capability than the "traditional" WAHUHA-4 (3)and MREV-8 (4,5) multiple pulse cycles (henceforth referred to as the 4-pulse and 8-pulse cycles). With the 8 pulse and 24 pulse cycles, proton chemical shifts have been reported for the water molecules in single crystals of gypsum (6) and ice (1,7) at orientations where the proton-proton vector was parallel to the Zeeman field, giving rise to homonuclear interactions greater than 85 KHz. These new multiple pulse cycles have been described by the same average hamiltonian theory (8-12) which was used to describe the 4-pulse and the 8-pulse cycles. However, a critical assumption in the average hamiltonian theory is that the dipolar interaction is very small compared with the time between pulses; that is $H\tau \ll 1$ (13). This assumption does not hold for a dipolar interaction of 85 KHz with a 3μs pulse separation, even though the line is successfully narrowed.

In this paper, I shall extend the average hamiltonian theory to treat multiple pulse cycles in this limit for

certain applications. In particular, I shall extend the theory to handle multiple pulse cycles for the case of strongly interacting spin 1/2 dipolar pairs. Finally, I will discuss the factors which contribute to spectral resolution in a multiple pulse experiment for this case.

REVIEW OF AVERAGE HAMILTONIAN THEORY

Basically, average hamiltonian theory provides the means with which one can calculate in a straightforward manner the time development operator for complicated pulse cycles for extended periods of time (8-12). It is not difficult, in principle, to solve for the complete time development operator at all times for any pulse cycle but its form may not be amenable to interpretation.

The expectation values of the magnetization, $\langle M_x \rangle$, $\langle M_y \rangle$, and $\langle M_z \rangle$ in a nuclear magnetic resonance experiment can be calculated using the equation

$$M_x = tr\{\rho(t) M_x\}$$

where ρ is the density operator. The equation of motion of the density operator is

$$\dot{\rho}(t) = \frac{i}{h} [\rho(t), H(t)]$$

and the formal solution is

$$\rho(t) = U(t)\ \rho(0)\ U^{-1}(t) \qquad \#1$$

U(t) is known as the time development operator. For the case where the hamiltonian is time independent, $U(t) = \exp(-\frac{i}{\hbar} H\, t)$. If $H(t) = H_o + H_1(t)$ and H_o is time independent, equation #1 can be simplified by transforming the density operator to the interaction reference frame dictated by H_o:

$$\rho^*(t) = \exp(\tfrac{i}{\hbar} H_o t)\ \rho(t)\ \exp(-\tfrac{i}{\hbar} H_o t)$$

$$\rho^*(t) = \tfrac{i}{\hbar}[\,\rho^*(t),\ H_1^*(t)\,]$$

$$H_1^*(t) = \exp(\tfrac{i}{\hbar} H_o\, t)\ H_1(t)\ \exp(-\tfrac{i}{\hbar} H_o\, t)$$

For the case where the hamiltonian is time dependent, time dependent pertubation theory must be used, most simply by means of the Magnus expansion (13).

$$U(t) = \exp(-\tfrac{i}{\hbar}\{\,\bar{H}^{(0)} + \bar{H}^{(1)} + \bar{H}^{(2)} + \ldots.\}\ t\ )$$

where

$$\bar{H}^{(0)} = \frac{1}{t}\int_0^t H(t')dt' \quad ; \quad \bar{H}^{(1)} = \frac{-i}{2t}\int_0^t\int_0^{t'} [\,H(t'),H(t")\,]\ dt"dt'$$

Clearly, for the Magnus Expansion to converge we must have $H(t)t \ll 1$.

In general, the time development operator can be

written in terms of the product of time development operators for any set of convenient sub-intervals:

$$U(t_i)=U(t_i,t_{i-1})U(t_{i-1},t_{i-2})U(t_{i-2},t_{i-3}).....U(t_1,0) \qquad \#2$$

$U(t_i,t_{i-1})$ is the time development operator for the time period t_{i-1} to t_i and $U(t_i)=U(t_i,0)$. In particular, equation #2 is useful for evaluating U(t) for a train of radio frequency pulses, where the hamiltonians may be time independent for the time t_{i-1} to t_i but are time dependent overall. But since H_i and H_{i-1} do not neccessarily commute, $U(t_i,t_{i-1})$ and $U(t_{i-1},t_{i-2})$ do not neccessarily commute and thus equation #2 can be a cumbersome expression to evaluate. However, by placing two conditions on the pulse train, termed the periodic condition and cyclic condition, equation #2 can be simplified.

The periodic condition requires that the hamiltonian, including the radio frequency pulses, is periodic in time with periodicity t_c. That is $H(Nt_c+t)= H(t)$, where N is any positive integer. Thus $U(Nt_c)=(U(t_c))^N$, which simplifies the problem of evaluating U(t) to one of evaluating $U(t_c)$.

The cyclic condition requires that the Zeeman reference frame and the interaction reference frame dictated by the radio frequency pulses (termed toggling reference frame) are

coincident at Nt_c.

$$U(Nt_c) = 1$$

This condition allows us to use the Magnus expansion in the toggling reference frame to evaluate $U(t_c)$ provided the dipolar, resonance offset, and pulse error hamiltonians are not too large. Accordingly, the time development operator for a multiple pulse cycle is

$$U(Nt_c) = \exp(-\frac{i}{\hbar}[\,\bar{H}^{(0)*} + \bar{H}^{(1)*} + \ldots]\, Nt_c\,) \qquad \#3$$

$$\bar{H}^{(0)*} = \frac{1}{t_c}\int_0^{t_c} H^*(t)\,dt \quad ; \quad \bar{H}^{(1)*} = \frac{-i}{2t_c}\int_0^{t_c}\int_0^{t'} [\,H^*(t'),H^*(t")\,]\,dt"dt'$$

where $H^*(t)$ is the dipolar and pulse error hamiltonian expressed in the toggling reference frame. Equation #3 is valid only at time Nt_c in the Zeeman reference frame, since in general this is the only time that the Zeeman reference frame and the toggling reference frame are coincident.

If $H^*(t)t_c \ll 1$, it is necessary to calculate only the first couple of terms in the expansion, but if $H^*(t)t_c \not\ll 1$, higher order terms must be kept to insure convergence. Alternatively, the exact form of the time development operator can be obtained by solving an N-body problem where N is the number of coupled spins in the solid, on the order of 10^{20}. Obviously, this is not feasible. On the other hand, the approximate solution for the time development

operator given by average hamiltonian theory (eqn.#3) may not converge when the inequality $\mathcal{H}^{*}(t)t_c \ll 1$ is not satisfied, which is the case for a number solid state systems. However, many of these cases may be treated successfully by solving for the time development operator exactly with respect to a system of dipole pairs of arbitrary strength while using average hamiltonian theory to approximate the net effect of inter-pair interactions. This is accomplished by applying the Magnus expansion in a new interaction reference frame, the dipolar pair-toggling reference frame defined below.

ISOLATED PROTON PAIRS

First, consider the simplest case of a dipolar coupled system, that is, a system of completely isolated, identical dipole pairs such as isolated water molecules. The hamiltonian for free precession in the rotating frame is

$$\mathcal{H} = -\hbar \sum_{i=1,3,5,..} A_i\left(I_{zi}I_{zi+1} - \frac{I_i \cdot I_{i+1}}{3}\right) + \Delta\omega_i(I_{zi} + I_{zi+1}) \qquad \#4$$

For convenience of notation in this section, the hamiltonian can be written

$$\mathcal{H} = -\hbar\left[A\left(I_{z1}I_{z2} - \frac{I_1 \cdot I_2}{3}\right) + \Delta\omega I_z\right]$$

without ambiguity. Accordingly, for free precession,

$$U(t) = \exp\left[iAt\left(I_{z1}I_{z2} - \frac{I_1 \cdot I_2}{3}\right) + i\Delta\omega t I_z \right]$$

From this we obtain the time development operator in the rotating frame at the end of the 4-pulse cycle (Figure 1) applied with delta function pulses:

$$U(6\tau) = \exp(-\tfrac{i}{\hbar} H\tau)\exp(i\tfrac{\pi}{2} I_x)\exp(-\tfrac{i}{\hbar} H\tau)\exp(-i\tfrac{\pi}{2} I_y)$$

$$\exp(-\tfrac{i}{\hbar} 2H\tau)\exp(i\tfrac{\pi}{2} I_y)\exp(-\tfrac{i}{\hbar} H\tau)\exp(-i\tfrac{\pi}{2} I_x)\exp(-\tfrac{i}{\hbar} H\tau)$$

is given by equation #4. Transforming to the interaction reference frame we have

$$U(6\tau) = \exp(i\Delta\omega I_z\tau)\exp(iA(I_{z1}I_{z2} - \tfrac{I_1 \cdot I_2}{3})\tau)\exp(i\Delta\omega I_y\tau)$$

$$\exp(iA(I_{y1}I_{y2} - \tfrac{I_1 \cdot I_2}{3})\tau)\exp(i2\Delta\omega I_x\tau)\exp(i2A(I_{x1}I_{x2} - \tfrac{I_1 \cdot I_2}{3})\tau)$$

$$\exp(i\Delta\omega I_y\tau)\exp(iA(I_{y1}I_{y2} - \tfrac{I_1 \cdot I_2}{3})\tau)\exp(i\Delta\omega I_z\tau)$$

$$\exp(iA(I_{z1}I_{z2} - \tfrac{I_1 \cdot I_2}{3})\tau) \qquad \#5$$

Traditionally, the Magnus expansion is applied at this point to approximate $U(6\tau)$:

$$U(6\tau) = \exp\left(i\frac{\Delta\omega}{3} (I_x + I_z + I_y)6\tau \right) \qquad \#6$$

And we obtain the result originally obtained by Waugh et al. (3). Equation #6 is valid when $A\tau \ll 1$. However, equation #5 can be simplified further before applying the Magnus expansion, by recognizing that $[I_1 \cdot I_2, I_z]=0$, $[I_1 \cdot I_2, I_{z1}I_{z2}]=0$ etc.,

$$\exp(iAI_{z1}I_{z2}\tau) = \cos\left(\frac{A\tau}{4}\right) + i4\, I_{z1}I_{z2} \sin\left(\frac{A\tau}{4}\right)$$

and $$\exp(iA\, I_{z1}I_{z2}\, \tau)\, I_y \exp(-iA\, I_{z1}I_{z2}\, \tau) =$$

$$\left(\cos^2\left(\frac{A\tau}{4}\right) - \sin^2\left(\frac{A\tau}{4}\right) \right) + i8\, I_{z1}I_{z2}\, I_y \left(\cos\left(\frac{A\tau}{4}\right) \sin\left(\frac{A\tau}{4}\right) \right)$$

Thus the exact form of the time development operator is

$$\begin{aligned} U(6\tau) = {} & \exp(i\Delta\omega I_z\tau)\exp\left(i\Delta\omega I_y\left(\cos\left(\frac{A\tau}{2}\right) - i4\, I_{z1}I_{z2}\sin\left(\frac{A\tau}{2}\right)\right)\right) \\ & \exp(i\Delta\omega I_x 2\tau)\exp\left(i\Delta\omega I_y\left(\cos\left(\frac{A\tau}{2}\right) + i4\, I_{z1}I_{z2}\sin\left(\frac{A\tau}{2}\right)\right)\right) \\ & \exp(i\Delta\omega I_z\tau) \end{aligned}$$

This simplification procedure has the same effect as transforming the time development operator to a new interaction reference frame dictated by the dipole pair interaction in each of the inter-pulse intervals. This new reference frame meets the cyclic and periodic conditions previously discussed. Now, applying the Magnus expansion:

$$U(N6\tau) = \exp\left(i\, \frac{\Delta\omega}{3}\, \left(I_x + I_z + I_y\cos\left(\frac{A\tau}{2}\right)\right) N6\tau\right) \qquad \#7$$

Equation #7 is valid provided $\Delta\omega\tau << 1$. The difference between equation #6 and equation #7 is that the average hamiltonian in equation #6 was calculated in the interaction reference frame dictated by the radio frequency pulses while the average hamiltonian in equation #7 was calculated in the interaction reference frame dictated by both the radio

frequency pulses and the dipolar-pair interaction. Because the dipolar hamiltonian is generally larger than the resonance offset hamiltonian, equation #7 is more accurate than equation #6. At $t = N6\tau$, all reference frames are coincident.

The exponent in equation #6 is the chemical shift scaling factor currently used for the 4-pulse cycle and is independent of the dipolar interaction. However, the more accurate chemical shift scaling factor given by equation #7 is dipolar interaction dependent. For the 4-pulse cycle, a liquid sample has a different chemical shift scaling factor than a system of rigid dipole pairs, even though the dipolar broadening is successfully removed.

The 8-pulse cycle (Figure 1) is obtained by putting two 4-pulse cycles together and replacing the x pulse with a -x pulse, and vice-versa, in the second 4-pulse cycle. Thus, the traditionally calculated time development operator is

$$U(12N\tau) = \exp\left(i \frac{\Delta\omega}{3} (I_x + I_z) 12N\tau \right)$$

Equation #8 is valid when $A\tau \ll 1$. The exact time development operator in the dipolar pair-toggling interaction frame is

$$U(12\tau) = \exp(i\Delta\omega I_z \tau)\exp\left(-i\Delta\omega I_y \tau\left(\cos\left(\frac{A\tau}{2}\right) - i4I_{z1}I_{z2}\sin\left(\frac{A\tau}{2}\right)\right)\right)$$

$$\exp(i\Delta\omega I_x 2\tau)\exp(-i\Delta\omega I_y \tau(\cos\left(\frac{A\tau}{2}\right) + i4I_{z1}I_{z2}\sin\left(\frac{A\tau}{2}\right))$$

$$\exp(i\Delta\omega I_z 2\tau)\exp(\ i\Delta\omega I_y \tau(\cos\left(\frac{A\tau}{2}\right) - i4I_{z1}I_{z2}\sin\left(\frac{A\tau}{2}\right))$$

$$\exp(i\Delta\omega I_x 2\tau)\exp(\ i\Delta\omega I_y \tau(\cos\left(\frac{A\tau}{2}\right) + i4I_{z1}I_{z2}\sin\left(\frac{A\tau}{2}\right))$$

$$\exp(i\Delta\omega I_z \tau)$$

Applying the Magnus expansion at this point yields

$$U(12N\tau) = \exp(\ i\ \frac{\Delta\omega}{3}\ (I_x + I_z)12N\tau) \qquad \#9$$

Equation #9 is valid when $\Delta\omega\tau << 1$. There is no difference between equations #8 and #9. The chemical shift scaling factor is invariant with respect to the dipolar hamiltonian.

I have thus shown that by dealing with the intra-pair interaction explicitly by going to the dipolar pair-radio-frequency pulse (toggling) interaction reference frame, it is possible to calculate the time development operator to 0th order more accurately than using the traditional method to 2nd order. I shall now apply the dipolar pair-toggling reference frame concept to non-isolated proton pairs.

NON-ISOLATED PROTON PAIRS

Proton-proton pairs may be considered isolated as in

the previous section if the inter-pair dipolar interaction is small compared with the desired resolution of the chemical shift spectrum, which is typically on the order of 50 Hz, depending on the size of H_o. In general, the inter-pair dipolar interaction is large compared with the chemical shift and must be included in the hamiltonian.

$$H = -\hbar \sum_i \Delta\omega_i I_{zi} - \hbar \sum_{i=1,3,5} \left(A_i (I_{zi} I_{zi+1} - \frac{I_i \cdot I_{i+1}}{3}) \right. \qquad \#10$$

$$\left. + \sum_{j\ i+1} [B_{ij} (I_{zi} I_{zj} - \frac{I_i \cdot I_j}{3}) + B_{i+1j} (I_{zi+1} I_{zj} - \frac{I_{i+1} \cdot I_j}{3})] \right)$$

The dipolar hamiltonian in equation #10 is a pairwise sum of all of the dipole-dipole interactions in the solid but is written in terms of the intra-pair dipolar interactions (of strength A_i) and the inter-pair dipolar interactions (of strength B_i). For a system of isolated dipolar pairs, B =0 and equation #10 is equivalent to equation #4. Equation #10 is also valid for a general system of coupled dipoles not paired. In this case, there is no distinction between the magnitudes of A and B .

For this more complex hamiltonian, the time development operator at (6τ) for the 4-pulse cycle with delta function pulses in the interaction reference frame of the pulses is

$$U(6\tau) = \exp(\frac{-i}{\hbar} H_z \tau) \exp(\frac{-i}{\hbar} H_y \tau) \exp(\frac{-i}{\hbar} H_x 2\tau) \exp(\frac{-i}{\hbar} H_y \tau)$$

$$\exp(\frac{-i}{\hbar} H_z \tau)$$

$$H_k = -\hbar\sum_i \Delta\omega_i I_{ki} - \hbar \sum_{i=1,3,..} \Big(A_i (I_{ki}I_{ki+1} - \frac{I_i \cdot I_{i+1}}{3}) + \sum_{j>i+1} [B_{ij}(I_{ki}I_{kj} - \frac{I_i \cdot I_j}{3}) + B_{i+1j}(I_{ki+1}I_{kj} - \frac{I_{i+1} \cdot I_j}{3})] \Big) \qquad \#11$$

where k is either x, y, or z. If the Magnus expansion is used at this stage, then we have

$$U(6N\tau) = \exp(i \sum_i \frac{\Delta\omega_i}{3} (I_{xi} + I_{zi} + I_{yi}) 6N\tau)$$

However, equation #11 can be simplified further by transforming to the interaction reference frame dictated by the intra-pair dipolar interaction as discussed in the previous section. In this reference frame, the hamiltonian is given by

time	hamiltonian
$0 - \tau$	H_z
$\tau - 2\tau$	$U_z^{-1} H_y U_z$
$2\tau - 3\tau$	$U_x H_x U_x^{-1}$
$3\tau - 4\tau$	H_x
$4\tau - 5\tau$	$- U_x^{-1} H_y U_x$
$5\tau - 6\tau$	$U_z H_z U_z^{-1}$

$$H_k = \sum_{i+1,3,..}\left(\frac{(\Delta\omega_i+\Delta\omega_{i+1})}{2}(I_{ki}I_{ki+1}) + \right.$$

$$\left. \frac{(\Delta\omega_i-\Delta\omega_{i+1})}{2}(I_{ki}-I_{ki+1})\exp(-i\frac{A_i}{3}(I_{ki}I_{ki+1} - \frac{I_i \cdot I_{i+1}}{3})2t)\right)$$

$$+ \sum_{\substack{i=1,3... \\ j>i+1}} \exp(iA_i(I_{ki}I_{ki+1}-\frac{I_i \cdot I_{i+1}}{3})t)\exp(iA_j(I_{kj}I_{kj+1}-\frac{I_j \cdot I_{j+1}}{3})t)$$

$$\left\{B_{ij}(I_{ki}I_{kj}-\frac{I_i \cdot I_j}{3})+B_{i,j+1}(I_{ki}I_{kj+1}-\frac{I_i \cdot I_{j+1}}{3})\right.$$

$$\left. B_{i+1,j}(I_{ki+1}I_{kj}-\frac{I_{i+1} \cdot I_j}{3}) + B_{i+1,j+1}(I_{ki+1}I_{kj+1}-\frac{I_{i+1} \cdot I_{j+1}}{3})\right\}$$

$$\exp(-iA_i(I_{ki}I_{ki+i}-\frac{I_i \cdot I_{i+1}}{3})t)\exp(-iA_j(I_{kj}I_{kj+1}-\frac{I_j \cdot I_{j+1}}{3})t)$$

$$U_k \equiv \exp\left[\sum_i iA_i(I_{ki}I_{ki+1}-\frac{I_i \cdot I_{i+1}}{3})\tau\right]$$

t is measured from the beginning of each time interval. H can be seen to be time dependent at all times. Provided $B_{ij}\tau << 1$, the Magnus expansion can be used to calculate the time independent average hamiltonian. The general expression for the 0th order term in B_{ij} and $\Delta\omega$ for the 4-pulse cycle is given in Table 1. The first term in Table 1 is due to the resonance offset hamiltonian. The analogous term for the 8-pulse cycle is given in Table 1 also. Note that even for the 8-pulse cycle, the resonance offset hamiltonian is a function of the intra-pair dipolar interaction.

The second term in Table 1 is the residual dipolar hamiltonian, which is the same for both the 4-pulse and 8-pulse cycles. The intra-pair dipolar interaction (A_i) is zero to all orders but the 0th order inter-pair dipolar interaction is a function of A (a_{ij},b_{ij}, etc.=$f(A_i,A_j)$). This residual dipolar hamiltonian is anisotropic in spin space; that is, it commutes with I_y but not I_x or I_z. Of course, alternative 8-pulse cycles can be constructed to commute with I_x or I_z by properly choosing the phases of the radio-frequency pulses. The Burum-Rhim 24 pulse cycle (2) (Figure 1) is composed of three 8-pulse cycles, one which commutes with I_x, another with I_y, and the third with I_z. The factor by which the inter-dipolar hamiltonian for the 24-pulse cycle is scaled is the average of the factors for the 3 different 8-pulse cycles. Thus, the 24-pulse cycle has an average hamiltonian which is isotropic in spin space, to 0th order in B (see Table 1).

FINITE WIDTH PULSES

An important aspect of multiple-pulse NMR which heretofore has been neglected in this treatise is the effect of finite width pulses. I will now show that the effect of finite width pulses can be treated exactly for the case of isolated pairs of identical spin 1/2 nuclei, no matter how

large the dipolar interaction is and including non-negligble double quantum effects.

In general, the time development operator for a multiple pulse cycle can be written in the form of equation #2, where the sub-intervals are defined as the time intervals between pulses and the time intervals during the pulses. In the rotating frame, the respective hamiltonians are

$$\frac{-H_f}{h} = \Delta\omega I_z + A(I_{z1}I_{z2} - \frac{I_1 \cdot I_2}{3})$$

$$\frac{-H_{pk}}{h} = \Delta\omega I_z + A(I_{z1}I_{z2} - \frac{I_1 \cdot I_2}{3}) + \omega_1 I_k \qquad (k=x,-x,y,-y)$$

and the respective time development operators for the sub-intervals are

$$U_F(t_i,t_{i-1}) = \exp(-\frac{i}{h} H_F(t_i - t_{i-1}))$$

$$U_{pk}(t_i,t_{i-1}) = \exp(-\frac{i}{h} H_{pk}(t_i - t_{i-1}))$$

For the 4-pulse cycle

$$U(6) = U_F(6\tau,5\tau+t_w/2)U_{px}(5\tau+t_w/2,5\tau-t_w/2)U_F(5\tau-t_w/2,4\tau+t_w/2)$$

$$U_{py}(4\tau+t_w/2,4\tau-t_w/2)U_F(4\tau-t_w/2,2\tau+t_w/2)U_{py}(2\tau+t_w/2,2\tau-t_w/2)$$

$$U_F(2\tau-t_w/2,\ \tau+t_w/2)U_{px}(\tau+t_w/2,\tau-t_w/2)U_F(\tau-t_w/2,0) \qquad \#12$$

where t_w is the pulse width and τ is the pulse spacing. It is well known that a system of isolated pairs of identical spin 1/2 nuclei which forms a three level system so that H_F,

H_{pk}, U_F, and U_{pk} can be expressed as 3 X 3 matrices. With the basis set $|\alpha\alpha\rangle$, $\sqrt{2}(|\alpha\beta\rangle + |\beta\alpha\rangle)$, and $|\beta\beta\rangle$,

$$\frac{H_F}{h} = \begin{pmatrix} A/6+\Delta\omega & 0 & 0 \\ 0 & -A/3 & 0 \\ 0 & 0 & A/6-\Delta\omega \end{pmatrix} \qquad \frac{H_{px}}{h} = \begin{pmatrix} A/6+\Delta\omega & \omega_1/\sqrt{2} & 0 \\ \omega_1/\sqrt{2} & -A/3 & \omega_1/\sqrt{2} \\ 0 & \omega_1/\sqrt{2} & A/6-\Delta\omega \end{pmatrix}$$

$$U_F(t',t") = \begin{pmatrix} \exp(-i(\frac{A}{6}+\Delta\omega)(t'-t")) & 0 & 0 \\ 0 & \exp(-i(\frac{A}{3})(t'-t")) & 0 \\ 0 & 0 & \exp(-i(\frac{A}{6}-\Delta\omega)(t'-t")) \end{pmatrix}$$

$$U_{px}(t',t") = T^{-1}\begin{pmatrix} \exp(\frac{-i}{h}\lambda_1(t'-t")) & 0 & 0 \\ 0 & \exp(\frac{-i}{h}\lambda_2(t'-t")) & 0 \\ 0 & 0 & \exp(\frac{-i}{h}\lambda_3(t'-t")) \end{pmatrix} T$$

$$T\,H_{px}T^{-1} = \begin{pmatrix} \lambda_1 & 0 & 0 \\ 0 & \lambda_2 & 0 \\ 0 & 0 & \lambda_3 \end{pmatrix}$$

where T is the unitary transformation that diagonalizes H_{pk} and λ_1, λ_2, and λ_3 are the eigenvalues of H_{pk}. In the event $\Delta\omega = 0$,

$$U_{px}(t',t") = \exp(\frac{-iA}{12}(t'-t"))\begin{pmatrix} \alpha & \beta & \gamma \\ \beta & \delta & \beta \\ \gamma & \beta & \alpha \end{pmatrix} \qquad X = \sqrt{\omega_1^2 + (\frac{A}{4})^2}\,(t'-t")$$

$$\alpha = \tfrac{1}{2}[\cos(X) + \frac{iA(t'-t")}{X}\sin(X) + \exp(\frac{iA}{4}(t'-t"))]$$

$$\gamma = \alpha - \exp(\frac{iA}{4}(t'-t")) \qquad \beta = \frac{i\omega_1(t'-t")}{\sqrt{2}\ X} \sin(X)$$

$$\delta = \cos(X) - \frac{A}{4X} \sin(X)$$

Note that U_{px} is an exact expression for the time development operator of a radio-frequency pulse and includes all double quantum effects. Thus calculating $U(6\tau)$ exactly for the 4-pulse cycle from equation #12 is a matter of matrix multiplication. Multiple pulse cycles which have more pulses are handled in the same manner but there are more matrices to be multiplied.

The on-resonance time development operators for an isolated spin 1/2 system using the 4-pulse and 8-pulse cycles with finite width pulses are given in Table 2. Ideally, the time development operator should be the unity operator at the end of the pulse cycle. The resolution of the pulse cycles is limited by the broadening expressed in the time development operators given in Table 2.

In general, $A < \omega_1$ and the magnitude of the broadening is governed by the spin function which has the lowest order term in A/ω_1. For the 4-pulse cycle, there are two terms which are 1st order in A/ω_1, and to 2nd order, the time development operator is

$$U(6N\tau) = \exp(4i[\frac{A}{4}_1 \cos(\frac{A\tau}{2}) + \left(\frac{A}{4\omega_1}\right)^2 \frac{\pi}{4} \sin(\frac{A\tau}{2})]$$
$$[\, I_{y1}(I_{x2} + I_{z2}) + I_{y2}(I_{x1} + I_{z1})\,]\, N)$$

A is the dipolar interaction, τ is the pulse spacing, ω_1 is the pulse strength t_w is the pulse width, and $t_w\ \omega_1 = \pi/2$.

Note that as τ increases, the broadening due to finite width pulses decreases until

$$\cos(\frac{A\tau}{2}) = -\frac{A\ \pi}{16\omega_1} \sin(\frac{A\tau}{2})$$

at which point the time development operator is the unity operator to second order in A/ω_1.

The exact time development operator for the 4-pulse cycle given in Table 2 can be compared with the results of an average hamiltonian treatment of the finite width pulse problem. The 0th order dipolar term in the average hamiltonian is (12)

$$\bar{H}^{(0)}_D = -\frac{2A}{6\pi\tau} t_w\ (I_{y1}(I_{x2} + I_{z2}) + I_{y2}(I_{x1} + I_{z1}))$$

The 1st order term is 0. Accordingly $U(6\tau) = \exp[-\frac{i}{h} H_D 6\tau]$ which is precisely the expression #13 when $\tau = 0$.

For the 8-pulse cycle, there are three terms from Table 2 which are 2nd order in A/ω_1 in the time development operator,

$$U(12N\tau) = \exp(-4i\left(\frac{A}{4\omega_1}\right)^2 \sin(A\tau)\{ I_{x1}I_{z2}+I_{z1}I_{x2}+I_{z1}I_{z2}-I_{x1}I_{x2}\}N)$$

and for the 24-pulse cycle, there three terms from Table 2 which are 2nd order in A/ω_1 in the time development operator

$$U(36N\tau) = \exp(-4i\left(\frac{A}{4\omega_1}\right)^2 \sin(A\tau)\{ I_{x1}I_{z2} + I_{z1}I_{x2} + I_{x1}I_{y2} + I_{y1}I_{x2} + I_{y1}I_{z2} + I_{z1}I_{y2}\}N)$$

Note that in both cases, the 2nd order term is ~0 when $A\tau << 1$ and increases when $A\tau$ increases. The 0th and 1st order dipolar terms in the average hamiltonian (11) are both 0 for finite width pulses which is consistent with the exact time development operator when $A\tau << 1$. Also, when $\sin(A\tau)=0$, the time development operator is the unity operator.

DISCUSSION

The utility of the time development operators derived in the previous section is in characterizing multiple pulse cycles for systems of strongly coupled spin 1/2 dipolar-pairs, such as rigid H_2O and CH_2 groups. This treatment is equally valid for weakly coupled spin 1/2 dipolar-pairs, thus all spin 1/2 systems, but has no real advantage over the time development operators calculated in the toggling reference frame discussed elsewhere (8-12). Thus this discussion will be limited to the case of strongly

coupled dipolar pairs. For such cases, the time development operators calculated in the dipolar pair-toggling reference frame point out some limits in resolution for multiple pulse schemes due to the strongly coupled dipolar-pairs. These limits fall into four categories; residual dipolar broadening for ideal pulse cycles, changes in the intercept and slope of the chemical shift scaling factor curve as a function of the dipolar coupling, finite pulse-width effects, and pulse errors. I will consider the 4 pulse cycle, 8-pulse cycle, and the BR-24 pulse cycle, since they are representative of three generations of homonuclear decoupling multiple pulse cycles.

First of all, to get a feeling for the magnitude of the residual dipolar broadening, consider the following average hamiltonian for the simplified case of $B_{ij}=B_{ij+1}=B_{i+1j}=B_{i+1j+1}$ when the pulses are perfect delta-functions:

$$= \frac{1}{6}\sum_{\substack{i=1,3,5\ldots \\ j \text{ odd} > i}} (4B_{ij}) \left[a_{ij}(I_{yi}+I_{yi+1})(I_{yj}+I_{yj+1}) - \frac{a'_{ij}}{3}(I_i+I_{i+1})\cdot(I_j+I_{j+1}) \right] \qquad \#14$$

$$- \frac{16}{3} B_{ij}d_{ij}\left((I_i\cdot I_j)(I_{i+1}\cdot I_{j+1}) + (I_i\cdot I_{j+1})(I_{i+1}\cdot I_j) \right)$$

$$+ \frac{32}{3} B_{ij}d_{ij} \quad (F_x + F_y + F_z)$$

$$- \frac{32}{3} B_{ij}d'_{ij} \quad (F_x + F_z)(I_{yi} + I_{yi+1})(I_{yj} + I_{yj+1})$$

where $F_x = I_{xi}I_{xi+1}I_{xj}I_{xj+1}$

8-pulse: $$a_{ij} = \frac{1}{3}\cos\left(\frac{A_i}{2}\right)\cos\left(\frac{A_j}{2}\right) - 1$$

$$a'_{ij} = \frac{\sin\left[(A_i+A_j)\tau/2\right]}{(A_i + A_j)\tau} + \frac{\sin\left[(A_i-A_j)\tau/2\right]}{(A_i - A_j)\tau} - 1$$

For the 4-pulse and 8-pulse cycles, the first two terms in equation 14 with coefficients a_{ij} and a'_{ij} resemble closely the dipolar hamiltonian for a spin 1 nucleus except that the residual dipolar hamiltonian commutes with I_y instead of I_z and the ratio $a_{ij}:a'_{ij}$ is not quite unity. Thus, if $\Delta\omega_i = \Delta\omega_{i+1} = \Delta\omega_j = \Delta\omega_{j+1}$ and the magnetization is along y, these terms do not contribute to the linewidth but if the magnetization is along x or z, the a_{ij} term does contribute to the linewidth which is consistent with the fact that the experimental linewidths are broader for y pre-pulses than for x pre-pulses. Also, the d_{ij} and d'_{ij} terms in equation #14 do not commute with either I_x, I_y, or I_z and thus contribute to the linewidth. On the other hand, for the 24-pulse cycle, the average hamiltonian has fewer terms and is completely isotropic in spin space. The only term which does not commute with either I_x, I_y, or I_z is the d_{ij} term in equation #14.

The 2nd and 4th terms in equation #14 are dot product terms which are like some kind of residual scalar coupling. These terms, which are common to all three pulse cycles,

commute with I_x, I_y, and I_z and thus contribute to the linewidth only in the event that the chemical shifts for the i, i+1, j, and j+1 nuclei are not the same.

Thus in general, the coefficients a_{ij}, a'_{ij}, and d_{ij} in equation #14 determine the magnitude of the residual dipolar interaction provided $B_{ij} = B_{ij+1} = B_{i+1j} = B_{i+1j+1}$. Figure 2 shows a_{ij}, a'_{ij}, and d_{ij} as a function of $A_i/(A_i+A_j)$ assuming that $(A_i+A_j)\tau=0.64$ for both the 8-pulse and 24-pulse cycles (the 4-pulse cycle is the same as the 8-pulse cycle). Figure 3 shows a_{ij}, a'_{ij}, and d_{ij} as a function of A_i assuming $A_i=A_j$. The a_{ij}'s and d_{ij}'s for the 24-pulse cycle are an order of magnitude smaller than a_{ij}'s and d_{ij}'s for the 8-pulse cycle in all cases. Note that $d_{ij}=0$ when $A_i = 0$ irrespective of the size of A_j and if $A_i+A_j=$ a constant, d_{ij} is a maximum when $A_i=A_j$ (see Figure 2). Thus the largest residual dipolar broadening for the i,i+1 spin 1/2 pair does not necessarily occur when A_i is a maximum. This is due to the fact that the residual dipolar interactions given in equation #14 are due to a 4-body interaction and are subsequently a function of the environment of all four spins. The dipolar broadening experienced by one spin in a quartet of spins is the same for all four spins.

Note that one of the consequences of the fact that the

residual dipolar interaction for the 24-pulse cycle is isotropic in spin space and is invariant under a 90° rotation about x, y, or z, is that any "super cycle" based on any combination of phase alternated 4-pulse cycles will do no better at removing dipolar interactions than the 24-pulse cycle.The d_{ij} term in equation #14 can be reduced by second averaging (10,12) or sample spinning (14,15), but it will not be completely eliminated. Also, the a_{ij} term is a dot product and is invariant under any rotation so it will always be present.

Another factor which may limit the resolution is a multiple pulse experiment is the functional dependence of the chemical shift scaling factor on the strength of the intra-pair dipolar interaction (A). This factor is potentially serious since the chemical shift scaling factor in a multiple pulse experiment usually is determined experimentally with a convenient liquid sample (A=0) with a known chemical shift and then the chemical shift in the solid sample is measured relative to this chemical shift scaling factor.

The hamiltonian in question for perfect delta function pulses is the term in Table 1. All three multiple pulse cycles have error terms of the form

$$\frac{(\Delta\omega_i - \Delta\omega_{i+1})}{2} (I_{zi} - I_{zi+1}) \left(\frac{\sin\left(\frac{A_i\tau}{3}\right)}{\left(\frac{A_i\tau}{3}\right)} - 1 \right)$$

Essentially, this term changes the intercept of the chemical shift scaling factor curve (υ_{real} vs $\upsilon_{obs.}$) only in the event that the chemical shifts of the i and i+1 nuclei are different from each other, and is significant if A is large. For example, if A=80 kHz, τ =4.0 , then this term is $0.073\ (\frac{\Delta\omega_i - \Delta\omega_{i+1}}{2})\ (I_{zi} - I_{zi+1})$.

Additionally, the 4-pulse cycle has an error term of the form

$$\left(\frac{\Delta\omega_i + \Delta\omega_{i+1}}{2}\right) (I_{yi} + I_{yi+1})\left(1 - \cos\left(\frac{A_i\tau}{2}\right)\right)$$

which changes the slope of the chemical shift scaling factor curve. (i.e. the error is offset frequency dependent). For example , if A=57 kHz, τ = 4.0 , the error is

$$0.25(\Delta\omega_i + \Delta\omega_{i+1})/2 \quad I_y$$

Due to second averaging, the actual change in the slope of the chemical shift scaling factor is 8%. For large values of $\Delta\omega$ this error is quite significant. It should be noted that neither of these error terms is responsible for line broadening but actually shift the resonant frequencies as a function of A.

The third factor that can limit the resolution in a multiple pulse experiment is the residual intra-pair dipolar broadening due to finite pulse widths. The expressions which describe this broadening for the 4-pulse and the 8-pulse cycles are complex functions of A, τ, ω_1 and t_w (see Table 2). But, there is one factor, F, that is common to all spin operator terms in the time development operators for both the 4-pulse and 8-pulse cycles.

$$F = 2i\left[\cos(\chi t_w)\sin\left(\frac{A(\tau - t_w/2)}{2}\right) + \frac{A}{4\chi}\sin(\chi t_w)\cos\left(\frac{A(\tau - t_w/2)}{2}\right)\right]$$

$$\chi = \sqrt{\omega_1^2 + \left(\frac{A}{4}\right)^2}$$

Additionally, there is another factor, G, common to all spin operator terms for the 8-pulse cycle.

$$G = 2\left[\cos(\chi t_w)\cos\left(\frac{A(\tau - t_w/2)}{2}\right) - \frac{A}{4\chi}\sin(\chi t_w)\sin\left(\frac{A(\tau - t_w/2)}{2}\right)\right]$$

In the limiting case of $A\tau \ll 1$, F and G are the same common factors calculated to 1st order in A using standard average hamiltonian theory (10,12).

$$G^{(1)} = 2\cos(\omega_1 t_w) \; ; \; F^{(1)} = iA(\tau - t_w/2)\cos(\omega_1 t_w) + \frac{\sin(\omega_1 t_w)}{(\omega_1(2\tau - t_w))}$$

Note that for given values of and ω_1 and τ, and an arbitrarily large value of A, there is a unique value of t_w for which F=0 and an unique value of t_w for which G=0. This means that we can set the pulse width at a certain value, t_o,

which has the effect of completely and exactly eliminating the intra-pair dipolar interactions. However, t_o is a function of both A and ω_1, so that in general there is no unique value of t for the entire sample due to different values of A in powders and different values of throughout the sample due to radio-frequency inhomogeneity. Thus, it is important to know the residual dipolar broadening as a function of radio-frequency field strength, ω_1 .

The best way to see what the residual intra-pair dipolar broadening is as a function of ω_1 near the point $t_w \omega_1 = \pi/2$ is to calculate the coefficients of the spin operator terms from Table 2 for specific values of A, t_w , and τ. For example, consider a proton resonance experiment with A=40 kHz, t_w =1.5μs, and τ =4.0 μ s. For this case, the $I_x I_y + I_y I_x$ and $I_x I_z + I_z I_x$ terms dominate the residual dipolar broadening for the 4-pulse cycle and the $I_{z1} I_{z2} - I_{x1} I_{x2}$ and $I_x I_z + I_z I_x$ terms dominate the residual dipolar broadening for the 8 pulse cycle so we need to consider only these terms. Accordingly,

4-pulse:

$$U(6N\tau) = \exp(F\{(I_xI_y + I_yI_x) + (I_zI_y + I_yI_z)\}N) \qquad \#15$$

8-pulse:

$$U(12N\tau) = \exp(FG\{2I_{z1}I_{z2} - 2I_{x1}I_{x2} + (I_xI_z + I_zI_x)\}N)$$

Figures 4a and 4b show the coefficients of the spin

operator terms (F and FG) as a function of flip angle, $\beta = \omega_1 t_w$ with $\tau = 4.0\mu s$, $\omega_1 = 166$ kHz, and with A=40 kHz and A=80 kHz respectively. The qualitative behavior of the coefficients as a function of t_w is the same as the coefficients calculated using standard average hamiltonian theory but the zero crossings occur at different flip angles. The "standard" zero crossings, which are independent of A, are marked with an X in Figure 4.

Finite pulse width effects can be estimated for other multiple pulse cycles which are based on the 8-pulse cycle for the experimental conditions given above by using equation #15. Thus we can approximate the time development operator for the 24-pulse cycle as

$$U(36N\tau) = \exp[FG\{(I_xI_z+I_zI_x)+(I_xI_y+I_yI_x)+(I_yI_z+I_zI_y)\}N]$$

Comparing equations #15 and #16, it is evident that the 24-pulse cycle is no better at reducing the residual dipolar broadening due to finite width pulses than the 8-pulse cycle. However, it is possible to construct a multiple pulse cycle which is better at reducing the residual dipolar broadening due to finite pulse widths without losing the benefits of the 24-pulse cycle. We can accomplish this by replacing the 8-pulse cycle as the building block for the 24-pulse cycle with a 16-pulse cycle consisting of two phase

altered 8-pulse cycles (i.e. interchange y and -y pulses in the second 8-pulse cycle). For the 16 pulse cycle we have

$$U(24N\tau) = \exp(2\ FG\ (I_{z1}I_{z2} - I_{x1}I_{x2})\ N\ )$$

The resulting 48 pulse cycle (x,y,-y,-x,-x,y,-y,x,x,-y,y,-x, -x,-y,y,x,y,x,-x,-y,-y,x,-x,y,y,-x,x,-y,-y,-x, y,x,-x,-y,-y, x,-x,y,y,-x,x,-y,-y,-x,x,y,x,y) will have a time development operator which contains terms of the order $F\ G\ \frac{A}{4\omega_1}$ and $F\ G\ \cos(\omega_1 t_w)$ which is an order of magnitude better than the 24-pulse cycle for the conditions A=40 kHz, τ =4.0 μs, ω_1=166.7 kHz, t_w=1.5 μs. The averaged resonance offset hamiltonian is along the (1,1,1) direction but is severely scaled, by approximately $\sqrt{3}/9$; thus other broadening mechanisms become relatively larger for the 48-pulse cycle than the 24-pulse cycle.

The final factor that can limit the resolution in a multiple pulse experiment is pulse imperfections. Table 3 summerizes the 0th order pulse error hamiltonians and the 1st order coupling between resonance offset and the pulse imperfections calculated in the dipolar-pair-toggling reference frame for the 4-pulse and 8-pulse cycles. The main difference between the terms in Table 3 and previous pulse error calculations (11) is that the terms in Table 3 include the complete intra-pair dipolar coupling with the

pulse imperfections. Note that for the 8-pulse cycle, there is no 0th order radio-frequency inhomogeneity term and that both the 0th order pulse length and phase error terms become smaller as A becomes larger. The 0th order phase transient term is independent of A .

The remainder of Table 3 shows the dependence of the 1st order resonance offset-pulse imperfection couplings on A. For $A\tau \not\ll 1$, this dependence has the effect of adding new constraints to a well tuned spectrometer, such as $\delta_y + \delta_{\bar{y}} - 2\delta_x = 0$ for the 8-pulse cycle. However, due to second averaging, many of the added terms have no adverse effect on the multiple pulse cycle. For example, the resonance offset-phase errors for the 8-pulse cycle are a function of A but are completely second averaged provided $\phi\tau \ll 1$, and, the resonance offset-phase transient errors actually are attenuated with increasing A . Also, the most serious pulse imperfection problem, that of resonance offset-radio-frequency homogeneity coupling, remains unaffected by the size of A .

CONCLUSIONS

Average hamiltonian theory can be extended to describe multiple pulse cycles in coupled dipole pair systems where

the intra-pair dipolar interaction is arbitrarily large by applying the Magnus expansion in the dipolar pair-toggling reference frame. The 0th order average dipolar hamiltonian calculated in this reference frame for the 4-, 8-, and 24-pulse cycles is a function of the inter-pair dipolar interactions and in general is non zero, unlike the average hamiltonian calculated in the toggling reference frame which is zero to second order.

The resultant 0th order term for the residual dipolar interaction in the 24-pulse cycle is isotropic in spin space and invariant under 90° rotations about the x, y, or z axis, indicating that the residual dipolar interaction cannot be reduced further by any multiple pulse cycle based on the 4-pulse cycle. Also, the residual dipolar interaction is a sum of 4 body interaction and thus the dipolar broadening is governed by the environment (i.e. geometry) of all 4 interacting spins.

Finite pulse width calculations for the 4- and 8-pulse cycles in a system of isolated pairs of identical spin 1/2 nuclei show that the intra-pair dipolar interaction is not completely eliminated for $\pi/2$ pulses as in the delta function case. However, an arbitrarily large intra-pair dipolar interaction can be completely and exactly eliminated

by choosing the proper flip angle, which is a function of the dipolar interaction, pulse width, and pulse spacing.

Acknowledgements: I wish to thank Professor S.I. Chan and J.R. Reimer for helpful discussions and I acknowledge the support of the National Science Foundation (NSF DMR-7721394).

References

1. D.P. Burum and W.K. Rhim, J. Chem. Phys. 70, 3553 (1979); W.K. Rhim, D.P. Burum, and D.D. Elleman, J. Chem. Phys. 71, 3239 (1979).
2. D.P. Burum and W.K. Rhim, J. Chem. Phys. 71, 944 (1979).
3. J.S. Waugh, L.M. Huber, and U. Haeberlen, Phys. Rev. Lett. 20, 180 (1968).
4. W.K. Rhim, D.D. Elleman, and R.W. Vaughan, J. Chem. Phys. 58, 1772 (1973).
5. P. Mansfield, J. Phys. C 4, 1444 (1971).
6. D.P. Burum and W.K. Rhim, J. Mag. Resonance 34, 24 (1979).
7. L.M. Ryan, R.C. Wilson, and B.C. Gerstein, Chem. Phys. Lett. 52, 341 (1977).
8. W.A.B. Evens, Ann. Phys. 48, 72 (1968).
9. U. Haeberlen and J.S. Waugh, Phys. Rev. 175, 453 (1968).
10. M. Mehring, High Resolution NMR Spectroscopy in Solids: Basic Principles and Progress (Springer, Berlin, 1976).
11. W.K. Rhim, D.D. Elleman, L.B. Schreiber, and R.W. Vaughan, J. Chem. Phys. 59, 3740 (1973).
12. U. Haeberlen, High Resolution NMR in Solids, Selective Averaging (Academic Press, New York 1976).
13. W. Magnus, Comm. Pure Appl. Math., 7, 649 (1954).

14. B.C. Gerstein, R.G. Pembleton, R.C. Wilson, and L.M. Ryan, J. Chem. Phys. 66, 361 (1977).

15. R.E. Taylor, R.G. Pembleton, L.M. Ryan, and B.C. Gerstein, J. Chem. Phys. 71, 4541 (1979).

16. M. Mehring, Z. Naturforsch A 27, 1634 (1972).

Table 1.

The 0th order average dipolar and resonance offset hamiltonians calculated in the dipolar pair-toggling reference frame for the 4- 8- and 24- pulse cycles. Perfect delta function pulses were assumed. The intra-pair and inter-pair dipolar interactions are symbolized by A and B respectively.

TABLE 1

$$\bar{H}^{(0)} = \bar{H}^{(0)}_{\Delta\omega} + \bar{H}^{(0)}_{\text{dipolar}}$$

$$\bar{H}^{(0)}_{\Delta\omega} = \frac{\beta_1}{3} \sum_{i=1,3,5..} \frac{(\Delta\omega_i + \Delta\omega_{i+1})}{2} (I_{zi}+I_{zi+1}+I_{xi}+I_{xi+1}+\alpha_1(I_{yi}+I_{yi+1}))$$

$$+ \frac{(\Delta\omega_i - \Delta\omega_{i+1})}{2} \left((I_{zi}-I_{zi+1}+I_{xi}-I_{xi+1}+\beta_2(I_{yi}-I_{yi+1})) \sin(\frac{A_i\tau}{3})/(\frac{A_i\tau}{3}) \right.$$

$$\left. + \beta_2(I_{yi}-I_{yi+1})(\cos(\frac{A_i\tau}{3}) - 2i\sin(\frac{A_i\tau}{3})(I_{xi}I_{xi+1} + I_{zi}I_{zi+1}) \right)$$

$$\bar{H}^{(0)}_{\text{dip}} = \frac{1}{6} \sum_{\substack{i=1,3,5... \\ j=3,5,7... \; j>i}} B_{1ij} \left(a_{ij}(I_{yi}+I_{yi+1})(I_{yj}+I_{yj+1}) - \frac{a'_{ij}}{3}(I_i+I_{i+1})\cdot(I_j+I_{j+1}) \right)$$

$$B_{2ij} \left(b_{ij}(I_{yi}+I_{yi+1})(I_{yj}-I_{yj+1}) - \frac{b'_{ij}}{3}(I_i+I_{i+1})\cdot(I_j-I_{j+1}) \right)$$

$$B_{3ij} \left(c_{ij}(I_{yi}-I_{yi+1})(I_{yj}+I_{yj+1}) - \frac{c'_{ij}}{3}(I_i-I_{i+1})\cdot(I_j+I_{j+1}) \right)$$

$$-\frac{4}{3}B_{1ij}\, d_{ij} \left((I_i\cdot I_j)(I_{i+1}\cdot I_{j+1}) + (I_i\cdot I_{j+1})(I_{i+1}\cdot I_j) - 2(F_x+F_y+F_z) \right)$$

$$-\frac{4}{3}B_{2ij}\, e_{ij} \left((I_i\cdot I_j)(I_{i+1}\cdot I_{j+1}-2I_{yi+1}I_{yj+1}) + (I_{i+1}I_j)(I_i\cdot I_{j+1}-2I_{yi}I_{yj+1}) \right.$$

$$\left. -2(F_x-F_y+F_z) \right)$$

$$-\frac{4}{3}B_{3ij}\, f_{ij} \left((I_i\cdot I_j-2I_{yi}I_{yj})(I_{i+1}\cdot I_{j+1}) + (I_{i+1}\cdot I_j-2I_{yi+1}I_{yj})(I_i\cdot I_{j+1}) \right.$$

$$\left. - 2(F_x-F_y+F_z) \right)$$

$$+8B_{4ij} \left((F_x+F_z)(I_{yi}+I_{yi+1})(I_{yj}+I_{yj+1}) \right)$$

$$F_x \equiv I_{xi}I_{xi+1}I_{xj}I_{xj+1}$$

$$B_{1ij} = B_{ij} + B_{i+1j} + B_{ij+1} + B_{i+1j+1}$$

$$B_{2ij} = B_{ij} + B_{i+1j} - B_{ij+1} - B_{i+1j+1}$$

$$B_{3ij} = B_{ij} - B_{i+1j} + B_{ij+1} - B_{i+1j+1}$$

4-pulse: $\beta_1 = 1 \quad \alpha_1 = \cos(\frac{A_i\tau}{2}) \quad \beta_2 = 0 \quad \alpha_2 = \frac{\sin(\frac{A_i\tau}{6})}{\frac{A_i}{6}}$

8-pulse: $\beta_1 = 1 \quad \alpha_1 = 0 \quad \beta_2 = 0 \quad \alpha_2 = 0$

24-pulse: $\beta_1 = 2/3 \quad \alpha_1 = 1 \quad \beta_2 = 1 \quad \alpha_2 = 0$

4- and 8-pulse:

$$a_{ij} = \frac{1}{3}\left(\cos(\frac{A_i\tau}{2})\cos(\frac{A_j\tau}{2}) - 1\right)$$

$$a'_{ij} = \frac{\sin(\frac{A_i\tau+A_j\tau}{2})}{(A_i + A_j)\tau} + \frac{\sin(\frac{A_i\tau-A_j\tau}{2})}{(A_i - A_j)\tau} - 1$$

$$b_{ij} = \frac{9A_i^2}{A_j(9A_i^2 - A_j^2)\tau}\, 2\sin(\frac{A_j\tau}{6})\cos(\frac{A_i\tau}{2}) - \sin(\frac{A_j\tau}{3})$$

$$b'_{ij} = \frac{18A_i\sin(\frac{A_i\tau}{2})\cos(\frac{A_j\tau}{6})}{(9A_i^2 - A_j^2)\tau} - \frac{27A_i^2\sin(\frac{A_j\tau}{3})}{A_j(9A_i^2-A_j^2)\tau}$$

$$c_{ij} = \frac{9A_j^2}{A_i(9A_j^2 - A_i^2)\tau} \quad 2\sin(\frac{A_i\tau}{6})\cos(\frac{A_j\tau}{2}) - \sin(\frac{A_i\tau}{3})$$

$$c'_{ij} = \frac{18A_j\sin(\frac{A_j\tau}{2})\cos(\frac{A_i\tau}{6})}{(9A_j^2 - A_i^2)\tau} - \frac{27A_j^2\sin(\frac{A_i\tau}{3})}{A_i(9A_j^2 - A_i^2)\tau}$$

$$d_{ij} = \frac{\sin(\frac{A_i\tau - A_j\tau}{2})}{3(A_i - A_j)\tau} - \frac{\sin(\frac{A_i\tau + A_j\tau}{2})}{3(A_i + A_j)\tau}$$

$$e_{ij} = \frac{6A_i}{(9A_i^2 - A_j^2)\tau}\left(\frac{\sin(\frac{A_j\tau}{3})}{2} - \sin(\frac{A_j\tau}{6})\cos(\frac{A_i\tau}{2})\right)$$

$$f_{ij} = \frac{6A_j}{(9A_j^2 - A_i^2)\tau}\left(\frac{\sin(\frac{A_i\tau}{3})}{2} - \sin(\frac{A_i\tau}{6})\cos(\frac{A_j\tau}{2})\right)$$

$$B_{4ij} = -B_{2ij}\,e_{ij} - B_{3ij}\,f_{ij} - \frac{1}{3}\sin(\frac{A_i\tau}{2})\sin(\frac{A_j\tau}{2})\,B_{1ij}$$

24-pulse:

$$a_{ij} = 0$$

$$a'_{ij} = -\frac{2}{3} + \frac{\sin(\frac{A_i\tau + A_j\tau}{2})}{(A_i + A_j)\tau} + \frac{\sin(\frac{A_i\tau - A_j\tau}{2})}{(A_i - A_j)\tau} - \frac{\cos(\frac{A_i\tau}{2})\cos(\frac{A_j\tau}{2})}{3}$$

$$b_{ij} = 0$$

$$b'_{ij} = \frac{18A_i^2}{A_j(9A_i^2 - A_j^2)\tau} \quad \frac{A_j}{A_i}\sin(\frac{A_i\tau}{2})\cos(\frac{A_j\tau}{6}) - \sin(\frac{A_j\tau}{3}) - \sin(\frac{A_j\tau}{6})\cos(\frac{A_i\tau}{2})$$

$$c_{ij} = 0$$

$$c'_{ij} = \frac{18A_j^2}{A_i(9A_j^2 - A_i^2)\tau} \quad \frac{A_i}{A_j}\sin(\frac{A_j\tau}{2})\cos(\frac{A_i\tau}{6}) - \sin(\frac{A_i\tau}{3}) - \sin(\frac{A_i\tau}{6})\cos(\frac{A_j\tau}{2})$$

$$d_{ij} = -\frac{1}{9}\sin(\frac{A_i\tau}{2})\sin(\frac{A_j\tau}{2}) + \frac{1}{3}\frac{\sin(\frac{A_i\tau - A_j\tau}{2})}{(A_i - A_j)\tau} - \frac{1}{3}\frac{\sin(\frac{A_i\tau + A_j\tau}{2})}{(A_i + A_j)\tau}$$

$$e_{ij} = 0 \qquad f_{ij} = 0 \qquad B_{4ij} = 0$$

Table 2.

The exact time development operator for the 4- and 8- pulse cycles evaluated at the end of the cycle for the case of finite width pulses. Isolated proton pairs of arbitrary coupling were assumed. Any deviation from the unity operator represents residual dipolar broadening.

TABLE 2

$$U(t_c) = a\mathbf{1} + b(4I_{z1}I_{z2}) + c(4I_{x1}I_{x2}) + d(I_x) + e(I_z) + f(I_xI_z + I_zI_x) + g(I_xI_y + I_yI_x) + h(I_yI_z + I_zI_y)$$

4-pulse:

$a = 1 + F(F - \delta^3)/2$

$b = F(\delta^* + \delta\gamma + \delta^3)/2$

$c = F(\gamma - 1)\delta/2$

$d = 0$

$e = 0$

$f = F(\beta\delta)$

$g = F(1 - \gamma)$

$h = F\beta(1 - \delta^2)$

8-pulse:

$a = 1 + FG(F\delta^5 + F^2\delta^2 + F\delta^* + 2F\delta - \delta^2)/2$

$b = F\,G(1 + F^2(1 + \delta^2 + \delta^4) - F\delta^3 + 2\delta^2)/2$

$c = F\,G((\gamma - 1)(1 + F(2\delta + \delta^3))/2$

$d = F^2G\,\beta(1 + \delta^2 + \delta^4)$

$e = F\,G(\gamma - 1)\delta^2$

$f = -F\,G\,\beta(F\delta^3 - 1)$

$g = 0$

$h = 0$

$$F = 2i \cos\left(\sqrt{\omega_1^2 + \left(\frac{A}{4}\right)^2}\, t_w\right)\sin\left(\frac{A}{2}\left(\tau - \frac{t_w}{2}\right)\right) + \frac{A}{4\sqrt{\omega_1^2 + \left(\frac{A}{4}\right)^2}} \sin\left(\sqrt{\omega_1^2 + \left(\frac{A}{4}\right)^2}\, t_w\right)\cos\left(\frac{A}{2}\left(\tau - \frac{t_w}{2}\right)\right)$$

$$G = 2 \cos\left(\sqrt{\omega_1^2 + \left(\frac{A}{4}\right)^2}\, t_w\right)\cos\left(\frac{A}{2}\left(\tau - \frac{t_w}{2}\right)\right) - \frac{A}{4\sqrt{\omega_1^2 + \left(\frac{A}{4}\right)^2}} \sin\left(\sqrt{\omega_1^2 + \left(\frac{A}{4}\right)^2}\, t_w\right)\sin\left(\frac{A}{2}\left(\tau - \frac{t_w}{2}\right)\right)$$

$$\delta = \exp\left(-i\,\frac{A}{2}\left(\tau - \frac{t_w}{2}\right)\right) \cos\left(\sqrt{\omega_1^2 + \left(\frac{A}{4}\right)^2}\, t_w\right) - \frac{i\,A}{4\sqrt{\omega_1^2 + \left(\frac{A}{4}\right)^2}} \sin\left(\sqrt{\omega_1^2 + \left(\frac{A}{4}\right)^2}\, t_w\right)$$

$$\gamma = \cos\left(\sqrt{\omega_1^2 + \left(\frac{A}{4}\right)^2}\, t_w\right) - \frac{i\,A}{16\omega_1^2 + A^2} \sin\left(\sqrt{\omega_1^2 + \left(\frac{A}{4}\right)^2}\, t_w\right)$$

$$\beta = \frac{\omega_1}{\sqrt{\omega_1^2 + \left(\frac{A}{4}\right)^2}} \sin\left(\sqrt{\omega_1^2 + \left(\frac{A}{4}\right)^2}\, t_w\right)$$

t_w = pulse length

τ = pulse spacing

ω_1 = pulse strength

A = dipole-dipole interaction

Table 3.

0th order pulse error hamiltonians calculated in the dipolar pair-toggling reference frame.

δ ; pulse length error

ϕ ; pulse phase error

ε ; radio-frequency inhomogeneity

T ; phase transient error:

$$J_1 = \int_0^{t_w} \omega_T(t)(\sin\omega_1 t - \cos\omega_1 t)dt$$

$$J_2 = \int_0^{t_w} \omega_T(t)(\sin\omega_1 t + \cos\omega_1 t)dt$$

4-pulse:

$$\bar{H}^{(0)}_{\delta} = \frac{1}{t_c} \sum_{i=1,3,5..} \cos(\frac{A_i\tau}{2}) \quad (I_{xi} + I_{xi+1})(\delta_{-x} - \delta_x) + (I_{zi} + I_{zi+1})(\delta_y - \delta_{-y})$$
$$+ 2\sin(\frac{A_i\tau}{2}) \quad (I_{yi}I_{zi+1} + I_{zi}I_{yi+1})(\delta_{-x} + \delta_x) + (I_{yi}I_{xi+1} + I_{xi}I_{yi+1})(\delta_y + \delta_{-y})$$

$$\bar{H}^{(0)}_{\phi} = \frac{1}{t_c} \sum_{i=1,3..} (I_{zi} + I_{zi+1})(\phi_x - \phi_{-x}) + (I_{xi} + I_{xi+1})(\phi_y - \phi_{-y})$$
$$+ \cos(\frac{A_i\tau}{2})(I_{yi} + I_{yi+1})(\phi_{-x} - \phi_x + \phi_{-y} - \phi_y)$$
$$- 2\sin(\frac{A_i\tau}{2})(I_{xi}I_{zi+1} + I_{zi}I_{xi+1})(\phi_{-x} - \phi_y - \phi_{-y} + \phi_x)$$

$$\bar{H}^{(T)} = \frac{1}{t_c} \sum_{i=1,3...} (I_{zi} + I_{zi+1} + I_{xi} + I_{xi+1})\, J_1 + 2\cos(\frac{A_i}{2})(I_{yi} + I_{yi+1})\, J_1$$

8-pulse:

$$\bar{H}^{(0)}_{\delta} = \frac{2}{t_c} \sum_{i=1,3,..} \cos(\frac{A_i\tau}{2})(I_{xi} + I_{xi+1})(\delta_{-x} - \delta_x)$$

$$\bar{H}^{(0)}_{\phi} = \frac{2}{t_c} \sum_{i=1,3..} (I_{xi} + I_{xi+1})(\phi_y - \phi_{-y}) + \cos(\frac{A_i\tau}{2})(I_{yi} + I_{yi+1})(\phi_{-x} - \phi_x)$$

$$\bar{H}^{(0)}_{T} = \frac{2}{t_c} \sum_{i=1,3...} (I_{zi} + I_{zi+1} + I_{xi} + I_{xi+1})\, J_1$$

$$\bar{H}^{(0)}_{\varepsilon} = 0$$

$$\bar{H}^{(0)}_{\varepsilon} = \frac{1}{t_c} \sum \left(2\sin(\frac{A_i\tau}{2}) \quad I_{yi}(I_{zi+1} + I_{xi+1}) + I_{yi+1}(I_{zi} + I_{xi})\right)\varepsilon$$

1st order resonance offset-pulse imperfection hamiltonians.

4-pulse cycle:

$$\bar{H}^{(1)}_{\Delta\omega-\delta} = \sum_{i=1,3..} \frac{\Delta\omega_i}{6} \Big[-(I_{zi} + I_{zi+1})(\delta_{-x} + \delta_x)\cos^2(\tfrac{A_i\tau}{2}) - (I_{xi} + I_{xi+1})(\delta_{-y} + \delta_y)\sin^2(\tfrac{A_i\tau}{2})$$
$$-(I_{yi}I_{zi+1} + I_{zi}I_{yi+1})(\delta_y - \delta_{-y})\sin(A_i\tau) - (I_{xi}I_{yi+1} + I_{yi}I_{xi+1})(\delta_{-x} - \delta_x)\sin(A_i\tau)$$
$$-(I_{yi} + I_{yi+1})(\delta_y + \delta_{-y})\cos(\tfrac{A_i\tau}{2}) - 2(I_{xi}I_{zi+1} + I_{zi}I_{xi+1})(\delta_{-y} - \delta_y)\sin(\tfrac{A_i\tau}{2})$$
$$-4(I_{zi}I_{zi+1} - I_{yi}I_{yi+1})(\delta_x - \delta_{-x})\sin(\tfrac{A_i\tau}{2}) \Big]$$

$$\bar{H}^{(1)}_{\Delta\omega-\phi} = \sum_{i=1,3..} \frac{\Delta\omega_i}{6} \Big[-(I_{xi} + I_{xi+1})(\phi_x + \phi_{-x})\cos(\tfrac{A_i\tau}{2}) + (I_{zi} + I_{zi+1})(\phi_x + \phi_{-x} - \phi_y - \phi_{-y})\cos(\tfrac{A_i\tau}{2})$$
$$+ (I_{yi} + I_{yi+1})(\phi_x + \phi_{-x}) + 2(I_{xi}I_{yi+1} + I_{yi}I_{xi+1})(-2\phi_y + \phi_x + \phi_{-x})\sin(\tfrac{A_i\tau}{2})$$
$$+ 2(I_{xi}I_{xi+1} - I_{zi}I_{zi+1})(\phi_x - \phi_{-x} - \phi_{-y} + \phi_y)\sin(\tfrac{A_i\tau}{2}) \Big]$$

$$\bar{H}^{(1)}_{\Delta\omega-T} = \sum_{i=1,3..} \frac{\Delta\omega_i}{6} \Big[(I_{xi} + I_{xi+1})J_2\cos(\tfrac{A_i\tau}{2}) - (I_{yi} + I_{yi+1})J_2 - 2(I_{yi}I_{xi+1} + I_{xi}I_{yi+1})J_1\sin(\tfrac{A_i\tau}{2})$$
$$+ 4(I_{zi}I_{zi+1} - I_{xi}I_{xi+1})\sin(A_i\tau) \Big]$$

$$\bar{H}^{(1)}_{\Delta\omega-\varepsilon} = \sum_{i=1,3..} \frac{\Delta\omega_i}{6} \Big[-2(I_{zi} + I_{zi+1})\cos^2(\tfrac{A_i\tau}{2}) - 2(I_{yi} + I_{yi+1})\cos(\tfrac{A_i\tau}{2}) - 2(I_{xi} + I_{xi+1})\sin^2(\tfrac{A_i\tau}{2}) \Big]\varepsilon$$

8-pulse cycle:

$$\bar{H}^{(1)}_{\Delta\omega-\delta} = \sum_{i=1,3..} \frac{\Delta\omega_i}{6} \Big[(I_{zi} + I_{zi+1})(-2\delta_{-x})\cos^2(\tfrac{A_i\tau}{2}) - (I_{xi} + I_{xi+1})(\delta_y + \delta_{-y})\sin^2(\tfrac{A_i\tau}{2}) + (I_{zi}I_{yi+1} + I_{yi}I_{zi+1})(\delta_{-y} - \delta_y)\sin(A_i\tau) - (I_{zi}I_{zi+1} - I_{yi}I_{yi+1})(4\delta_x)\sin(\tfrac{A_i\tau}{2}) + (I_{xi}I_{xi+1} - I_{yi}I_{yi+1})(2\delta_y + 2\delta_{-y})\sin(\tfrac{A_i\tau}{2}) + (I_{yi} + I_{yi+1})(\delta_y - \delta_{-y})\cos(\tfrac{A_i\tau}{2}) + 2(I_{xi}I_{zi+1} + I_{zi}I_{xi+1})(\delta_x + \delta_{-x} - \delta_y - \delta_{-y})\sin(\tfrac{A_i\tau}{2}) \Big]$$

$$\bar{H}^{(1)}_{\Delta\omega-\phi} = \sum_{i=1,3..} \frac{\Delta\omega_i}{6} \Big[(I_{yi} + I_{yi+1})(2\phi_x) + (I_{xi} + I_{xi+1})(\phi_{-y} - \phi_y)\cos(\tfrac{A_i\tau}{2}) + 2(I_{zi}I_{yi+1} + I_{yi}I_{zi+1})(\phi_x + \phi_{-x} - \phi_y - \phi_{-y})\sin(\tfrac{A_i\tau}{2}) - 2(I_{zi}I_{zi+1} - I_{xi}I_{xi+1})(\phi_y - \phi_{-y})\sin(A_i\tau) - 2(I_{xi}I_{yi+1} + I_{yi}I_{xi+1})(2\phi_x - \phi_y - \phi_{-y})\sin(\tfrac{A_i\tau}{2}) \Big]$$

$$\bar{H}^{(1)}_{\Delta\omega-T} = \sum_{i=1,3..} \frac{\Delta\omega_i}{6} \Big[-(I_{yi} + I_{yi+1})J_2 + (I_{xi} + I_{xi+1} - I_{zi} - I_{zi+1})J_1\, 3\cos(\tfrac{A_i\tau}{2}) \Big]$$

$$\bar{H}^{(1)}_{\Delta\omega-\varepsilon} = \sum_{i=1,3...} \frac{\Delta\omega_i}{6} \Big[-(I_{zi} + I_{zi+1})2\cos^2(\tfrac{A_i\tau}{2}) - (I_{xi} + I_{xi+1})2\sin^2(\tfrac{A_i\tau}{2}) + (I_{xi}I_{xi+1} - I_{zi}I_{zi+1})4\sin(\tfrac{A_i\tau}{2}) \Big]\, \varepsilon$$

Figure 1. A schematic diagram for the 4-pulse, 8-pulse and 24-pulse cycles.

Figure 2. The coefficients for the reduction in the inter-pair dipolar interaction as a function of $A_i/(A_i + A_j)$ assuming $(A_i + A_j)\tau = 0.64$. This corresponds to $(A_i + A_j) = 80$ KHz with $\tau = 4$ μ s. When $a_{ij} = 1$, there is no reduction in the inter-pair interaction for that particular term.

Figure 3. The coefficients for the reduction in the inter-pair dipolar interaction as a function of A assuming $A_i = A_j$. For the condition $\tau = 4$ μ s and A = 80 KHz, $A\tau = \pi/2$.

Figure 4. The broadening due to finite width pulses for the 4-pulse (F) , 8-pulse (FG) , and 24-pulse (FG) cycles is plotted as a function of flip angle for the conditions $\omega_1 = 2\pi$ 166 KHz , $\tau = 4$ μ s , and a) A = 40 KHz and b) A = 80 KHz.

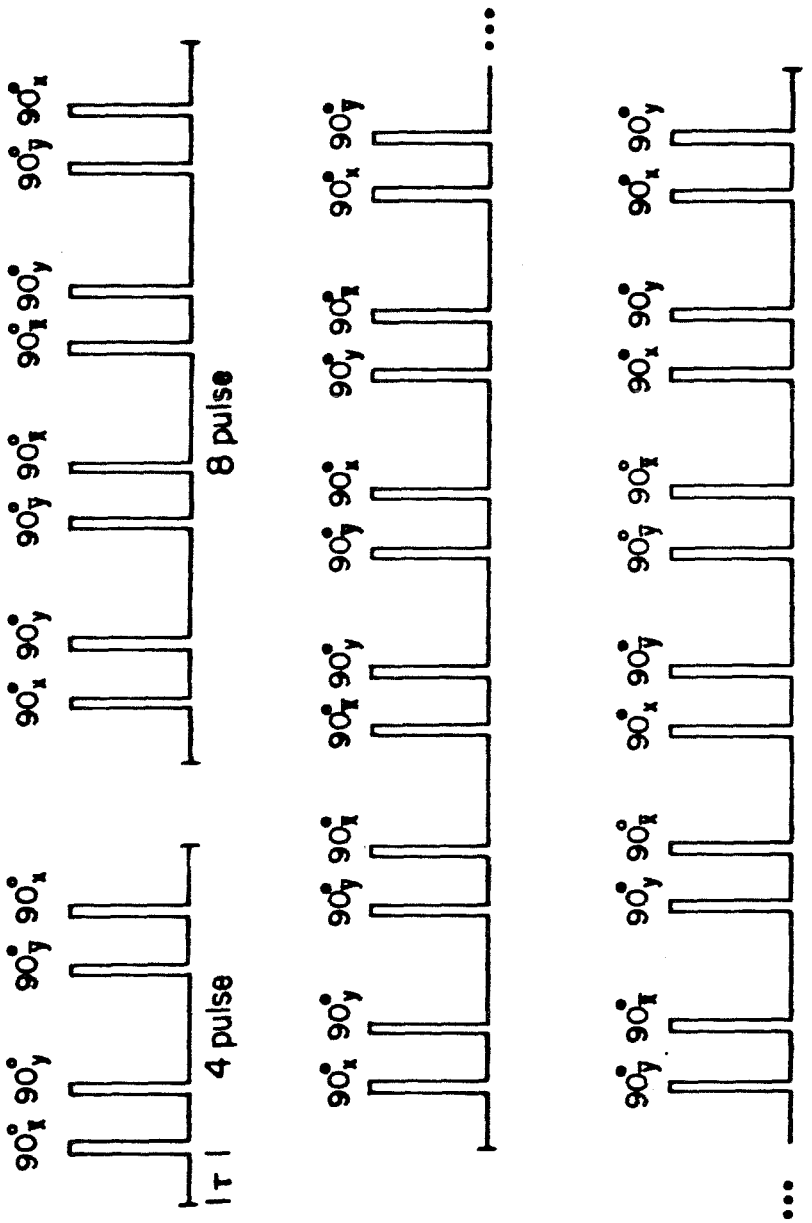

Figure 1.

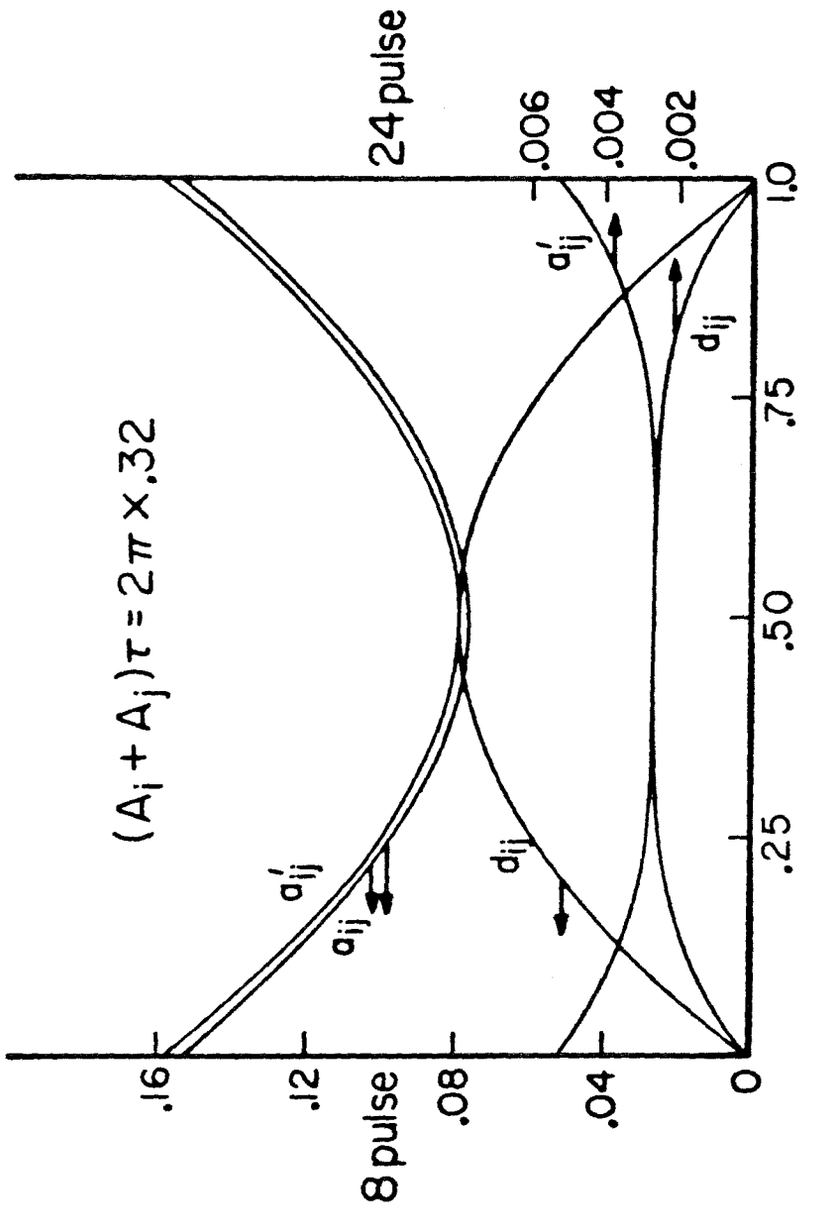
24 pulse
8 pulse
$(A_i + A_j)\tau = 2\pi \times .32$
a'_{ij}
a_{ij}
d_{ij}
.16
.12
.08
.04
0
.006
.004
.002
.25
.50
.75
1.0
$\frac{A_i}{(A_i + A_j)}$

Figure 2.

Figure 3.

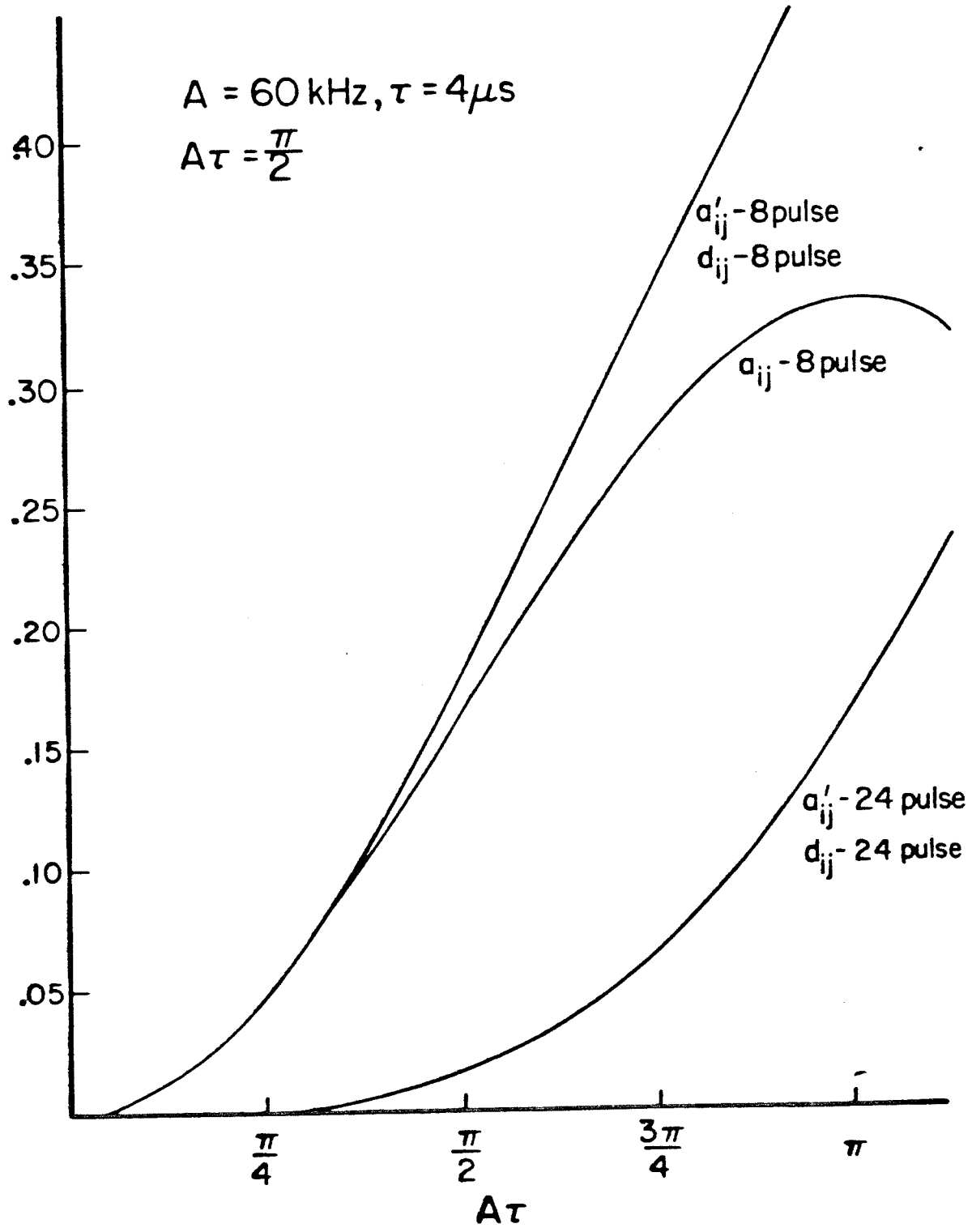
A = 60 kHz, τ = 4μs
Aτ = π/2
.40
.35
.30
.25
.20
.15
.10
.05
a'_{ij} - 8 pulse
d_{ij} - 8 pulse
a_{ij} - 8 pulse
a'_{ij} - 24 pulse
d_{ij} - 24 pulse
π/4
π/2
3π/4
π
Aτ

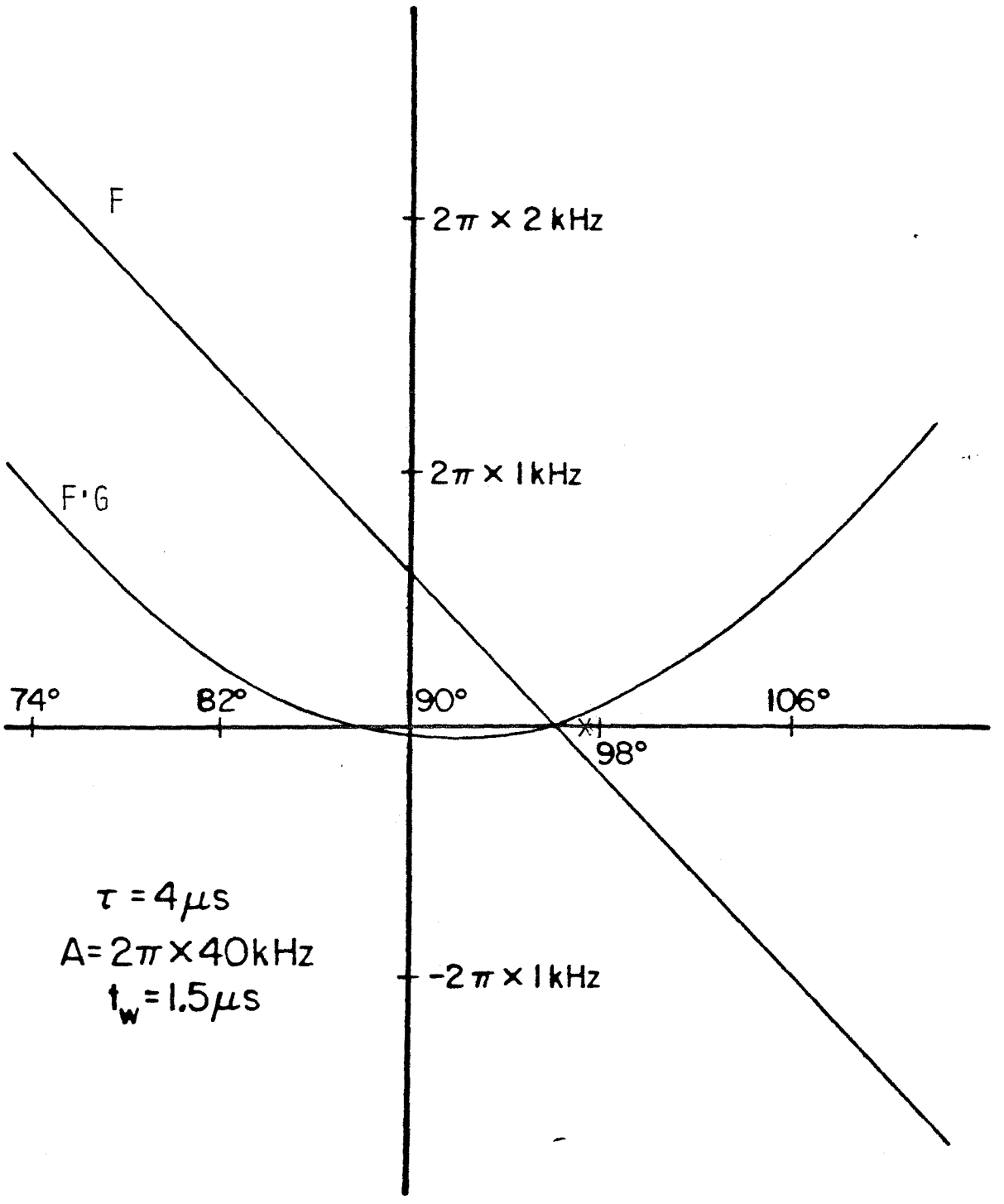
F
F·G
2π × 2 kHz
2π × 1 kHz
-2π × 1 kHz
74°
82°
90°
98°
106°
τ = 4μs
A = 2π × 40 kHz
t_w = 1.5μs

Figure 4a.

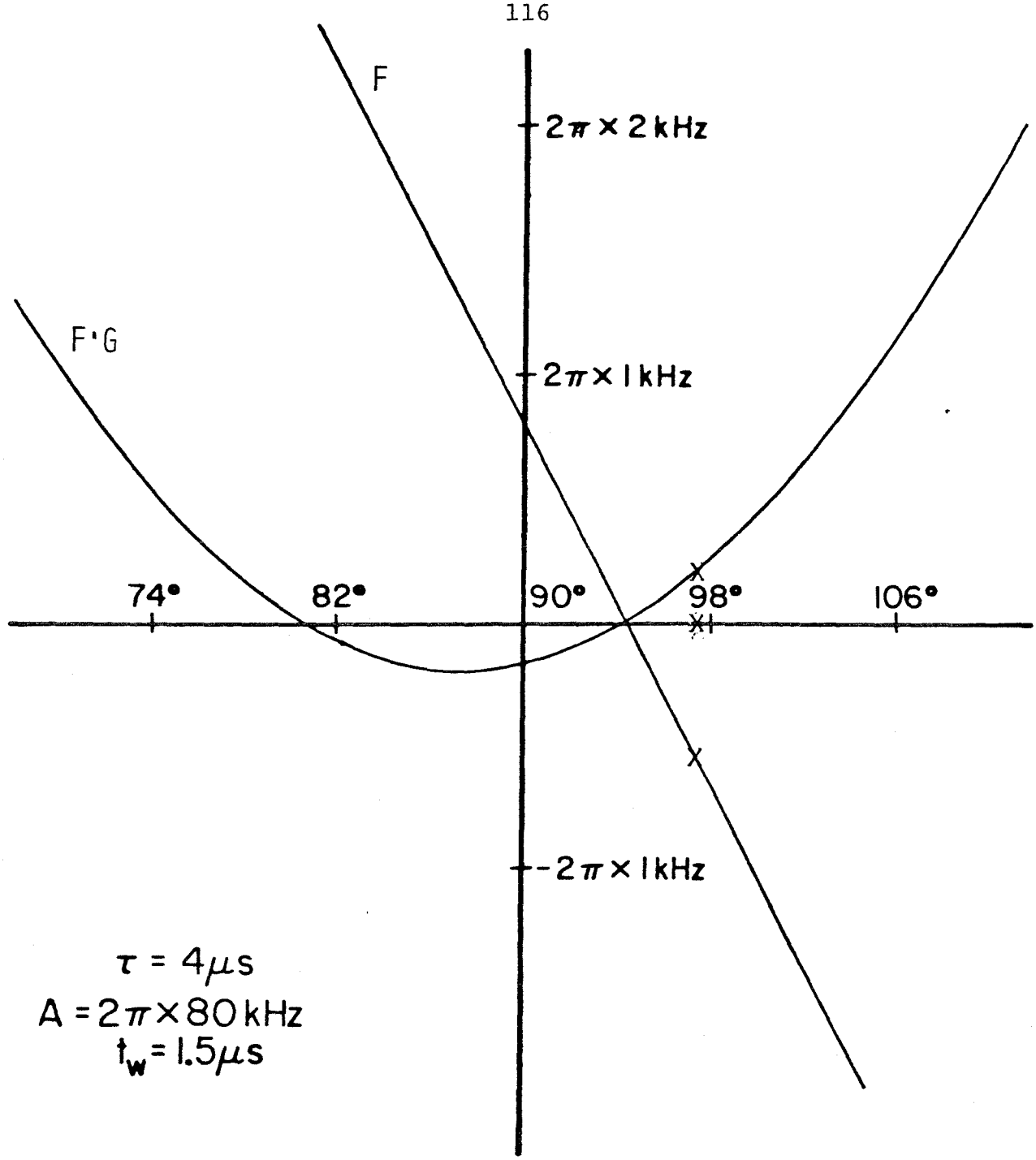
F
2π × 2 kHz
F·G
2π × 1 kHz
74°
82°
90°
98°
106°
-2π × 1 kHz
τ = 4μs
A = 2π × 80 kHz
t_w = 1.5μs

PART II

The Determination of Pake Doublet Splittings in Inhomogeneously Broadened Systems

CHAPTER 6

Introduction to Part II

It is well known that the NMR spectrum of a pair of isolated, identical spin 1/2 nuclei consists of a doublet whose splitting (A) is a function the inter-nuclear distance (r), the angle (θ) between the external magnetic field and the inter-proton vector, and the gyromagnetic ratio of the nucleus (γ) (1):

$$A = \frac{3}{2}\gamma^2 h \left\langle \frac{1 - 3\cos^2\theta}{r^3} \right\rangle \qquad \#1$$

Ever since 1948 when Pake first observed dipolar pair doublets in a proton magnetic resonance spectrum of the water molecules in gypsum and presented equation #1, many researchers have used NMR spectra to deduce structural information about rigid water molecules in crystalline hydrates (see references 2 and 3 for a review). NMR data are in close agreement with the neutron diffraction data (2) for cases where neutron diffraction data are available. However, in general, the proton-proton distances determined by NMR are longer than the distances determined by neutron diffraction: mean values of 1.60 Å and 1.563 Å respectively are given in the review by El Saffar. The median difference in θ is 1.6° . The discrepancy in r between NMR results and neutron diffraction results is due to the thermal vibrations and librations of the water molecule (4) and due to the fact that the averaging processes are different. Neutron

diffraction gives the position of each individual proton based on the maximum of a distribution of scattering density while in a NMR experiment the NMR average of the proton-proton distance is given according to equation #1.

Besides thermal vibration effects, the accuracy of the NMR results is determined by the spectral resolution, which in turn, is limited by either homogeneous broadening (such as homonuclear dipolar interactions) or inhomogeneous broadening (such as heteronuclear dipolar interactions or paramagnetic interactions). In the event the spectral resolution is limited by homogenous broadening, the spectral resolution cannot be improved by spin manipulation. However, in the event the spectral resolution is limited by heterogeneous broadening , there are techniques, in principle, that will improve the resolution in terms of measuring A.

For instance, consider a 90° τ 180° pulse echo experiment (5). At time 2τ after the 90° pulse, the inhomogeneous interactions will be refocused by the 180° pulse. Thus by varying τ and recording the echo amplitude at 2τ, we can observe the frequency A. However, this technique requires many experiments (>200) varying τ to produce 1 spectrum and thus is quite time consuming. A

Carr-Purcell sequence (6), which consists of a train of refocussing 180° pulses, can be used to provide the complete spectrum with 1 experiment, but in general, the intra-pair dipolar interaction for a water molecule is rather large, on the order of 50 kHz depending on the orientation of the proton-proton vector in the external magnetic field, so that finite pulse width effects are very large and the pulse sequence actually alters the measured dipolar frequency. Clearly this is unacceptable.

Alternatively, we can use double quantum NMR techniques to measure the intra-pair dipolar coupling in inhomogeneously broadened systems of spin 1/2 pairs. Double quantum techniques are well suited for this kind of experiment because the double quantum transition probability is a strong function of the dipolar coupling, the resonance offset (i.e. inhomogeneous interactions), and the intensity of the perturbing radio-frequency field (7-9). On the basis of this functional dependence, an easy-to-use , two pulse double quantum experiment is presented in Chapter 7 which provides the intra-pair dipolar interaction directly and unambiguously in one experiment. The resolution, as in the $90^\circ\tau\ 180^\circ$ experiment, is limited by the homogeneous broadening.

The utility of the two pulse double quantum experiment is demonstrated in Chapter 8, where the orientation and motional properties of the water molecule in cordierite are elucidated by measuring the Pake doublet splittings as a function of orientation and temperature. The orientation of the water molecule has been the subject of a recent controversy (see Chapter 8) and the NMR data provide an important piece to the puzzle.

References

1. G.E. Pake, J. Chem. Phys. 16, 327 (1948).

2. Z.M. El Saffar, J. Chem. Phys. 45, 4643 (1966).

3. R. Chidambarum, J. Chem. Phys. 36, 2361 (1962).

4. B. Pedersen, J. Chem. Phys. 41, 122 (1964).

5. E.L. Hahn, Phys. Rev. 80, 580 (1950).

6. H.Y. Carr and E.M. Purcell, Phys. Rev. 94, 630 (1954).

7. R. G. Brewer and E.L. Hahn, Phys. Rev. A 11, 1641 (1975).

8. S. Vega and A. Pines, J. Chem. Phys. 66, 5624 (1977).

9. A. Wokaun and R.R. Ernst, J. Chem. Phys. 67, 1752 (1977).

CHAPTER 7

The Determination of Pake Doublet Splittings in Inhomogeneously Broadened Systems Using Double Quantum NMR

(Chapter 7 is an article by D.G. Carson and R.W. Vaughan to be published in the Journal of Magnetic Resonance.)

Multiple quantum transient nutations in NMR were first observed in 1975 by Hanakata et al.(1) and in 1976 by Pines et al. (2). Since that time, several pulse techniques have been developed to create and detect multiple quantum coherence (3-10). These techniques are useful in the measurement of the deuterium chemical shift in solids (3), in the measurement of multiple quantum relaxation times (4), in the measurement of intra-molecular interactions (5,6), in proton-deuteron cross polarization (9,10), and the list keeps growing.

Basically, multiple quantum coherence is a superposition state involving non-adjacent levels in a multi-level spin system (Figure 1). There are a number of ways to create multiple quantum coherence; such as with low intensity, selective radio-frequency pulses, where the multiple quantum transition probability is a function of $\delta\omega$, the resonance offset, and the strength of the pulse (11,12), or we can create multiple quantum coherence non-selectively with intense radio-frequency pulse schemes (13). In all cases, the time scale for inducing multiple quantum transitions is governed by $\delta\omega$. Most experiments performed to date have been concerned with inducing and monitoring multiple quantum coherences.

Double quantum NMR techniques are well suited to measure the intra-pair dipolar coupling in systems of isolated pairs of identical spin 1/2 nuclei which are inhomogeneously broadened. This is because the double quantum transition probability is a function of the dipolar coupling, the resonance offset, and the intensity of the perturbing radio-frequency field (10-13). However, this system poses a problem. In real systems, the dipolar pairs are never completely isolated and there is some spin communication between the dipolar pairs, thus limiting the time scale of any spin manipulation experiment. On the other hand, we want to be as selective as possible in inducing only double quantum transitions so that the results of our experiment will provide the Pake doublet splitting unambiguously, which is done on a long time scale.

The following two pulse experiment solves this problem by using a radio-frequency pulse which is approximately the same intensity as the intra-pair couping. However, for this case, both single and double quantum transitions are induced and the approximative method for calculating the transition probability will not work (11-13).

Consider the two pulse experiment depicted in Figure 1,

which is designed to measure the inter-pair dipolar interaction (A) in a system of isolated proton pairs which is inhomogeneously broadened. The purpose of the double quantum pulse (the first pulse in Figure 2) is to selectively invert the magnetization of only those spins for which $\Delta\omega = 0$. At the conclusion of the double quantum pulse, there is intensity in all elements of the density matrix, to some extent. The off diagonal elements will relax and decay to 0 according to T_2 processes while the diagonal elements $\langle I_z \rangle$ will remain unchanged provided $\tau_2 << T_1$. At a time after the double quantum pulse, an intense 90° pulse is applied, rotating the z magnetization into the xy plane where it can be observed. Then during the subsequent free induction decay, these spins will evolve according to the free precession hamiltonian but they will be 180° out of phase with the rest of the spins, thus providing a direct measurement of A upon Fourier transformation.

What we need to know for this two pulse double quantum experiment is the density matrix at time τ_1 as a function of A and $\Delta\omega$. We can start by calculating the time development operator , U(t), during radio-frequency irradiation of a system of isolated pairs of identical protons in a large external magnetic field. U(t) is defined by the equation

$$\rho(t) = U(t)\ \rho(t)\ U^{-1}(t) \qquad \#1$$

and the equation of motion for the density operator, $\rho(t)$, is

$$\frac{d\rho(t)}{dt} = \frac{i}{\hbar}[\rho(t), H(t)] \qquad \#2$$

The hamiltonian for this system can be written in the rotating frame as

$$-H_p(t) = \hbar\Delta\omega\,(I_{z1} + I_{z2}) + \hbar A\,(I_{z1}I_{z2} - \frac{I_1 \cdot I_2}{3}) + \hbar\omega_1\,(I_{x1} + I_{x2})$$

$2\omega_1$ is the strength of the radio-frequency irradiation, $\Delta\omega = \omega - \omega_o$ (ω_o is the Larmor frequency) and $A = \frac{3\gamma^2\hbar}{2r^3}(1-3\cos^2\theta)$. Since H_p is time independent, we obtain the formal solution

$$U(t) = \exp(i\Delta\omega(I_{z1} + I_{z2}) + iA(I_{z1}I_{z2} - I_1 \cdot I_2/3) + i\omega_1(I_{x1} + I_{x2})t)$$

However, in its present form, U(t) is useful only if A is effectively 0. This is because only single quantum transitions are induced during the pulse and we can use a vector representation for the phase coherence of the spins (i.e. the magnetization) and the exponential operators are simple vector rotation operators. But if $A \neq 0$, both single and double quantum transitions may be induced simultaneously. For this reason, a vector representation of the phase coherence and exponential operators are no longer possible.

Accordingly, U(t) is more conveniently written in matrix notation.

$$U_{ij}(t) = \exp(-\frac{i}{h} H_p t)$$

$$= T \begin{pmatrix} \exp(-\frac{i}{h}\lambda_1 t) & 0 & 0 \\ 0 & \exp(-\frac{i}{h}\lambda_2 t) & 0 \\ 0 & 0 & \exp(-\frac{i}{h}\lambda_3 t) \end{pmatrix} T^{-1}$$

where T is the transformation that diagonalizes H_p and λ_1, λ_2, and λ_3 are the eigenvalues of H_p. In general, we have to solve a cubic equation to obtain the eigenvalues of H_p for this particular system. Thus

$$\exp(-\frac{i}{h} {}_p t) = \begin{pmatrix} r_{11} & r_{12} & r_{13} \\ r_{12} & r_{22} & r_{32} \\ r_{13} & r_{32} & r_{33} \end{pmatrix}$$

r_{12}, r_{13}, r_{22}. are given in Table 1 in terms of λ_1, λ_2, and λ_3 in the eigenbase of the equilibrium hamiltonian ($|1\rangle = |\alpha\alpha\rangle$, $|0\rangle = (|\alpha\beta\rangle + |\beta\alpha\rangle)/\sqrt{2}$, $|-1\rangle = |\beta\beta\rangle$). In the event $\Delta\omega =$ 0 we have

$$r_{11} = r_{33} = \frac{1}{2}(\cos\chi t + \frac{iA}{4\chi}\sin\chi t + \exp(iAt/4)) \qquad \chi = \sqrt{\omega_1^2 + A^2/16}$$

$$r_{12} = r_{32} = \frac{i\omega_1}{\sqrt{2}\chi}\sin\chi t \quad ; \quad r_{13} = r_{11} - \exp(iAt/4)$$

$$r_{22} = \cos\chi t - (iA/4\chi)\sin\chi t$$

which essentially is the solution obtained by Brewer and Hahn (13). Other closed form solutions exist whenever $\Delta\omega$ satisfies the equation

$$\Delta\omega^2 = A^2S^2/16 - \left(A^2/16 + \omega_1^2 \right) \frac{S + 1}{S - 1} \qquad \text{for any } S$$

then $\lambda_1 = AS/4 - A/12$

$$\lambda_2 = \frac{A}{8}\left(\frac{1}{3} - S \right) + \sqrt{\left(\frac{A}{4}\right)^2 (5 + 2S - 3S^3) + 4\omega_1 + 4\Delta\omega^2}$$

$$\lambda_3 = \frac{A}{8}\left(\frac{1}{3} - S \right) - \sqrt{\left(\frac{A}{4}\right)^2 (5 + 2S - 3S^2) + 4\omega_1 + 4\Delta\omega^2}$$

The matrix $U_{ij}(t)$ also may be expressed in terms of the fictitious spin 1/2 operators proposed by Vega and Pines (11) or Wokaun and Ersnt (12). These operators are useful when there are transitions induced between only two of the three levels in the three level system while the third level remains unchanged (i.e. $\Delta\omega = 0$ or $\Delta\omega = \pm A/2$) In this case, we can retain a vector representation for the phase coherence and think of spin transitions simply as vector rotations.

One of the most important experimental parameters is the strength of ω_1 because it controls both the selectivity (in $\Delta\omega$) and the efficiency of both single and double quantum transitions. By efficiency we mean the time required to completely invert the magnetization. This is an important factor due to the fact that in most samples, proton pairs are not completely isolated and we want the length of the double quantum pulse to be shorter than the time for inter-pair spin diffusion. We can examine the efficiency of the double quantum pulse by following $\langle I_z \rangle$ during the pulse. Assuming $\rho(0) = c\, I_z$ and $\Delta\omega = 0$,

($\Delta\omega = 0$ is the most efficient condition for inducing double quantum transitions) and using equations 2 and 3;

$$\langle I_z(t)\rangle = \frac{c}{2}\left(1 - \frac{A}{4\chi}\right)\cos[(\chi + A/4)\,t\,] + \frac{c}{2}\left(1 + \frac{A}{4\chi}\right)\cos[(\chi - A/4)\,t\,]$$

If we apply a very selective pulse, $\omega_1 << A$, then equation 4 reduces to

$$\langle I_z(t)\rangle = \cos(2\omega_1^2\, t/A)$$

and $\langle I_z(t_I)\rangle = -\langle I_z(0)\rangle$ when $t_I = (4\pi/A)(A^2/8\omega_1^2)$. On the other hand, if we apply a nonselective, intense pulse, $\omega_1 >> A$

$$\langle I_z(t')\rangle = \cos(\omega_1 t')\cos(At'/4)$$

(Note that if we only allow $\omega_1 t' = n2\pi$ where n = any positive integer, then the strong pulse case is the same as a 90°_x t' 90°_x pulse sequence (5)) $t_I' = 4\pi/A$ for inversion through the double quantum transition. $t_I = 2(A/4\omega_1)^2 t_I'$; the nonselective intense pulse is more efficient than the weak selective pulse. Thus we have a trade-off between efficency and selectivity; the size of ω_1 must be chosen for each case.

The selectivity of a double quantum pulse can be seen graphically in Figure 2 which shows $\langle I_z(t)\rangle$ vs $\Delta\omega/A$ for

specific values of ω_1/A and τ_1 A (the Figure is presented with dimensionless parameters for generality). Here, we have neglected relaxation effects. When $\omega_1 \ll A$, single quantum transitions are induced at $\Delta\omega = \pm A/2$ and double quantum transitions are induced at $\Delta\omega = 0$. Note that even when $\omega_1 = A/4$, we maintain a reasonable amount of selectivity. For proton pair systems, the fine structure and oscillations shown in Figure 2b are smoothed out somewhat due to inter-pair dipolar interactions, which generally limits the resolution to about 1 KHz or greater. This is actually benificial for the experiment at hand since we are not interested in the complicated oscillations but only the intra-pair dipolar interaction.

EXPERIMENTAL RESULTS

The two pulse double quantum experiment was performed on the pulsed NMR spectrometer operating at 270 MHz described in Chapter 3. The intensity of the double quantum radio-frequency pulse was chosen to be a little less than the magnitude as the dipolar coupling (1 to 5 gauss) and the intense 90° pulse was about 50 gauss. In general, some *a priori* knowledge of the dipolar coupling is necessary to set the intensity and duration of the double quantum pulse. A can be estimated by the free induction decay linewidth or

established by trial and error. For water molecules, we know that $0 < A < 90$ KHz. Finite pulse width effects for the intense pulse were neglected. All experiments were performed on resonance; that is, close to the center of gravity of the broad line.

The sample was a single crystal of cordierite in the form of a 4 mm cube. The structure of cordierite is a network of stacked rings of alumino-silicates forming continuous channels where water molecules reside about 6 Å apart. All of the water molecules have the same inter-proton dipolar interaction. 6 Å away from the water molecules are Fe ions in octohedral symmetry. These paramagnetic ions are a source of inhomogeneous broadening for the protons (see Chapter 8 for more details).

The spin 1 nature of the proton pairs in the water molecules in cordierite can be seen directly from a double quantum echo experiment; the double quantum pulse in Figure 1 is an intense pulse, which is highly non-selective creating double quantum coherence for all of the spins , provided $A = 0$, irrespective of $\Delta\omega$. During the time after the double quantum pulse, the double quantum coherence evolves with the frequency $2\Delta\omega$. The intense pulse transfers the double quantum coherence into an observable coherence

(I_x or I_y), and evolves with $-\Delta\omega$. Therefore at time = $2\tau_2$ after the 90° pulse, the coherence is refocussed and we have an echo. Note that this echo is not a quadrupolar echo; quadrupolar echos at $2\tau_2$ for a spin 1 particle are strictly forbidden. The dipolar hamiltonian is not refocussed, but since we have a single crystal, all spins are evolving with the same dipolar frequency. The double quantum echos are shown in Figure 3. The double quantum pulse was 10 μs long with an intensity of 15 gauss; τ_2 was 80 μs. By changing the phase of the double quantum pulse by ϕ , the phase of the double quantum echo is changed by 2ϕ . This effect can also be seen in Figure 3.

The result of the two pulse double quantum experiment to measure A is shown in Figure 4. The intensity of the double quantum pulse is 2 gauss and τ_1 = 800 μs, τ_2 = 1ms. Figure 4a shows the Fourier transform of a simple free induction decay of the cordierite at an arbitrary orientation. The free induction decay was recorded on resonance at two orthogonal phases and then a complex Fourier transformation was performed. Due to receiver dead time, the lineshape may be distorted slightly. Figure 4b shows the Fourier transform of a free induction decay at the same orientation with the double quantum pre-pulse and Figure 4c shows the difference between 4a and 4b. The

doublet splitting is 20 KHz (5 gauss). Since the double quantum absorption peaks are narrow compared with the dead time, a linear phase correction of the spectrum will leave the doublet splitting undistorted.

Figure 5 shows the theoretical results under the same experimental conditions using a 20 KHz Lorentzian function to model the inhomogeneous broadening and a 1 KHz broadening function to model the homogeneous broadening. The intra-pair dipolar frequency was assumed to be 20 KHz. The peaks in the theoretical spectrum are narrower than the experimental spectrum due to the fact that we have ignored inter-pair spin communication during the pulse. Nonetheless, the resolution in Figure 4 is more than sufficient to assign a Pake doublet splitting.

References

1. H. Hatanaka, T. Terao, and T. Hashi, J. Phys. Soc. Jpn. 39, 835 (1975); H. Hatanaka and T. Hashi, *ibid*. 39, 1139 (1975).

2. S. Vega, T.W. Shattuck, and A. Pines, Phys. Rev. Lett. 37, 43 (1976).

3. G. Drobny, A. Pines,S. Sinton, D Weidekamp, and D. Wemmer, Trans. Faraday Soc. (in press).

4. G. Bodenhausen, R. L. Vold, and R. R. Vold, J. Mag. Reson. 37, 93 (1980).

5. W.S. Warren, D.P. Weitekamp, and A. Pines, J. Chem Phys. 73, 2084 (1980).

6. A. Bax, R. Freeman,and S.P. Kempsell, J. Am. Chem. Soc. 102, 4849 (1980).

7. M.E. Stoll, A.J. Vega, and R.W. Vaughan, J. Chem. Phys. 67, 2029 (1977).

8. W.P. Aue, E. Bartholdi, and R.R. Ernst, J. Chem. Phys. 64, 2229 (1976).

9. S. Vega, T.W. Shattuck, and A. Pines, Phys. Rev. A 22, 638 (1980).

10. P. Brunner, M. Reinhold, and R.R. Ernst., J. Chem. Phys. 73, 1086 (1980).

11. S. Vega and Pines, J. Chem. Phys. 66, 5624 (1977).

12. A. Wokaun and R.R. Ernst, J. Chem. Phys. 67, 1752 (1977).

13. R.G. Brewer and E.L Hahn, Phys. Rev. A 11, 1641 (1975).

Table 1. The matrix elements for the time development matrix of a radio-frequency pulse applied to a system of isolated proton pairs (a three level system). The matrix elements are a function of the intra-pair coupling, the strength of the pulse, the duration of the pulse, and the resonance offset.

$$r_{ij} = \sum_k a_{ijk} \exp(-i\lambda_k t)$$

$$a_{11k} = \frac{(\omega_1)^4}{D_k} \qquad a_{22k} = \frac{2(\omega_1)^2(\lambda_k - A/4 - \Delta\omega)^2}{D_k}$$

$$a_{33k} = \frac{(\omega_1)^4 - 4(\omega_1)^2(\lambda_k - A/4 - \Delta\omega)(\lambda_k + A/4)}{D_k} + \frac{4(\lambda_k - A/4 - \Delta\omega)^2(\lambda_k + A/4)^2}{D_k}$$

$$a_{12k} = \frac{\sqrt{2}(\omega_1)^3(\lambda_k - A/4 - \Delta\omega)}{D_k}$$

$$a_{13k} = \frac{2(\omega_1)^2(\lambda_k - A/4 - \Delta\omega)(\lambda_k + A/4)}{D_k}$$

$$a_{32k} = \frac{2\sqrt{2}\,\omega_1(\lambda_k - A/4 - \Delta\omega)^2(\lambda_k + A/4) - \sqrt{2}\,(\omega_1)^3(\lambda_k - A/4 - \Delta\omega)}{D_k}$$

$$D_k = 2(\omega_1)^4 + 2(\omega_1)^2(\lambda_k - A/4 - \Delta\omega)(-\lambda_k - 3A/4 - \Delta\omega)$$

Figure 1. Above, an energy level diagram for a multi-level spin system. Provided $\delta\omega \neq 0$, double quantum transitions can be induced from between levels 1 and 3 without perturbing level 2. Below, a schematic diagram of a two pulse experiment to measure the Pake doublet splitting in an inhomogeneously broadened system of spin 1/2 pairs.

Figure 2. $\langle I_z(t) \rangle$ during the double quantum pulse is plotted as a function of $\Delta\omega/A$ for various values of ω_1/A and $A\tau_1$. a) $\omega_1 = A/40$ and $T = 2\pi 8.0/A$. Single quantum transitions are induced only at $\Delta\omega = \pm A/2$ and double quantum transitions are induced only at $\Delta\omega = 0$. b) $\omega_1 = A/4$ and $T = 2\pi 0.2/A$. The single quantum transition probability at $\Delta\omega = 0$ is small but non-zero. c) $\omega_1 = 2.5A$ and $T = 2\pi .08/A$. The single quantum transition probability is large everywhere.

Figure 3. Double quantum echos observed using a non-selective, intense double quantum pulse. When the relative phase between the double quantum pulse and the intense $\pi/2$ pulse is changed by ϕ the phase of the double quantum echo changes by 2ϕ.

Figure 4. a) The Fourier transform of a simple free induction of rigid water molecules in cordierite. The Pake doublets are completely obscured by the inhomogeneous broadening. b) The Fourier transform of a free induction decay preceded by a double quantum pulse. The strength of the pulse was approximately A/4. c) A difference spectrum, a) - b).

Figure 5. A theoretical spectrum corresponding to the double quantum experiment in Figure 4b. A 20 KHz broadening function was used to model the inhomogeneous broadening and a 2 KHz broadening function was used to model the homogeneous broadening after the intense 90° pulse.

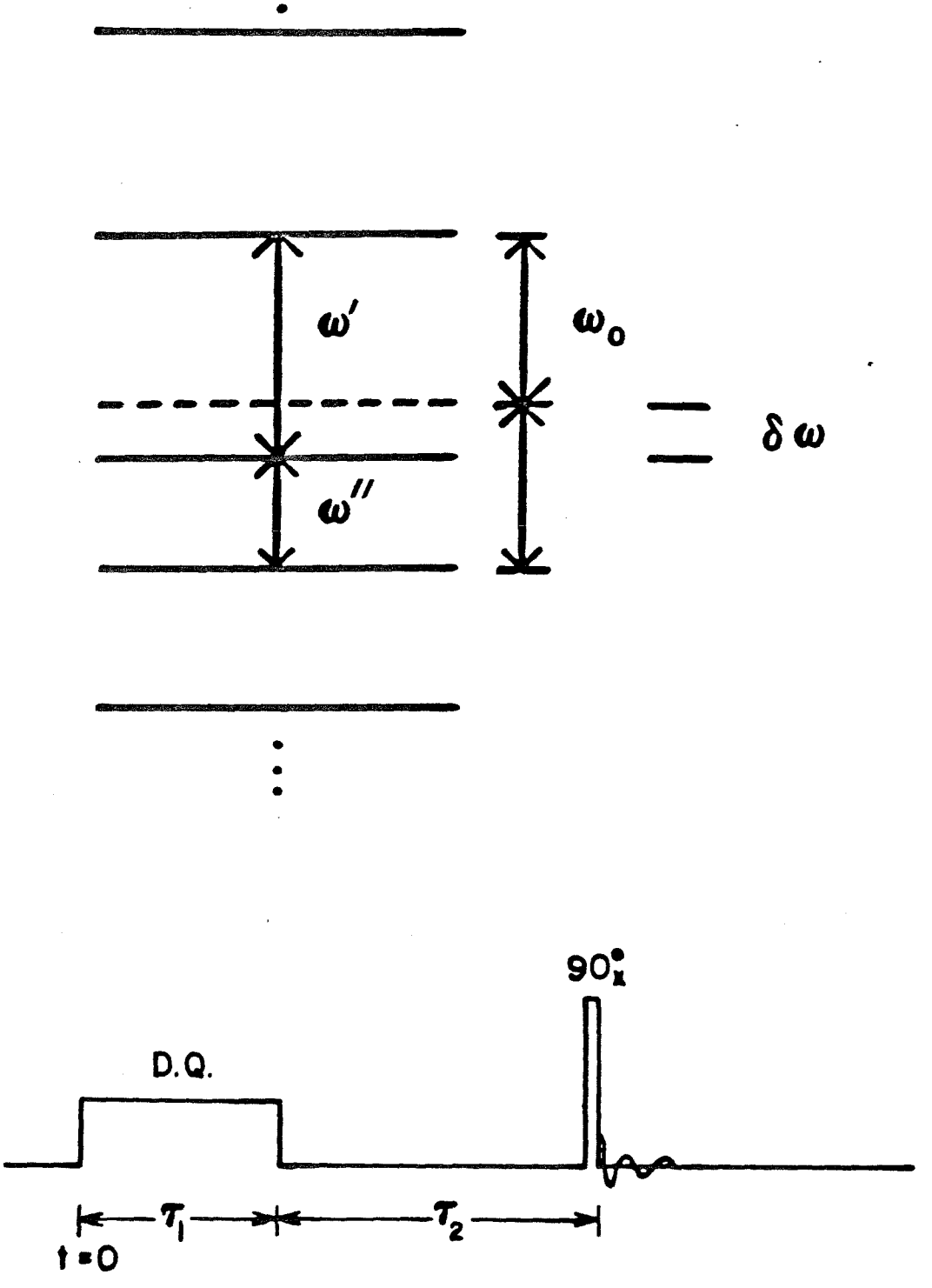

Figure 1.

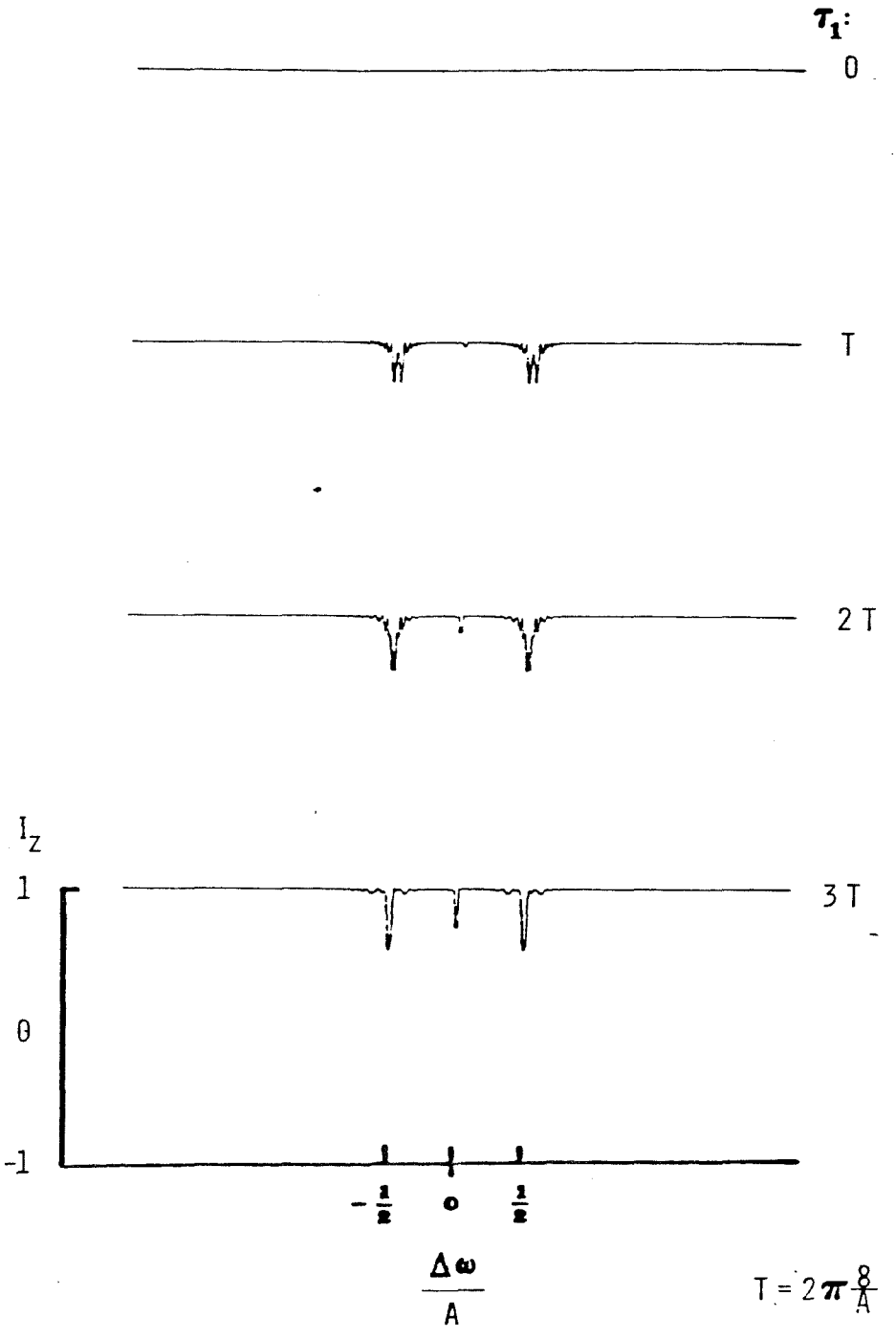
τ_1:
0
T
2 T
3 T
I_z
1
0
-1
$-\frac{1}{2}$
0
$\frac{1}{2}$
$\frac{\Delta\omega}{A}$
$T = 2\pi\frac{8}{A}$

Figure 2a.

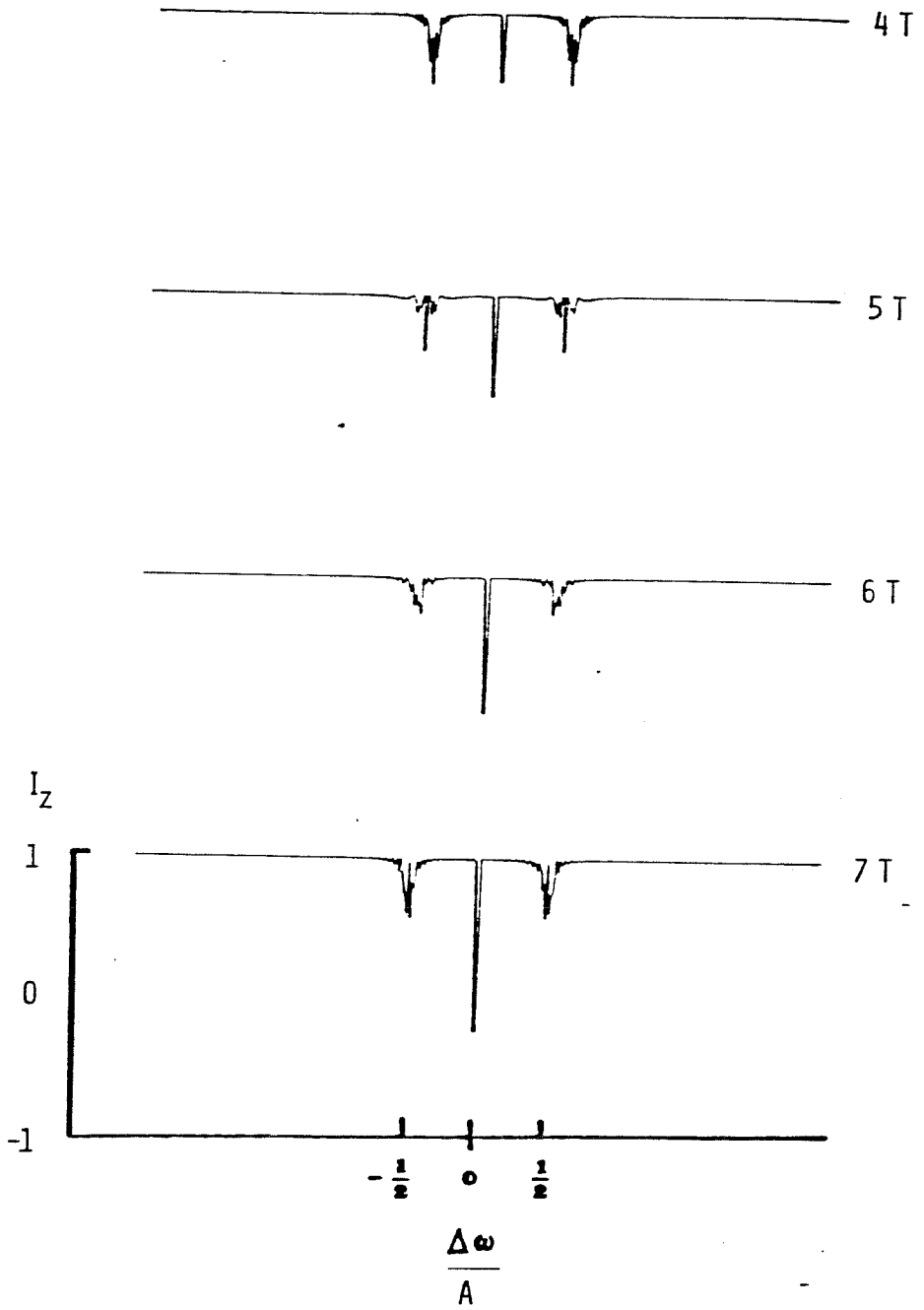
4 T
5 T
6 T
7 T
I_z
1
0
-1
$-\frac{1}{2}$
0
$\frac{1}{2}$
$\frac{\Delta\omega}{A}$

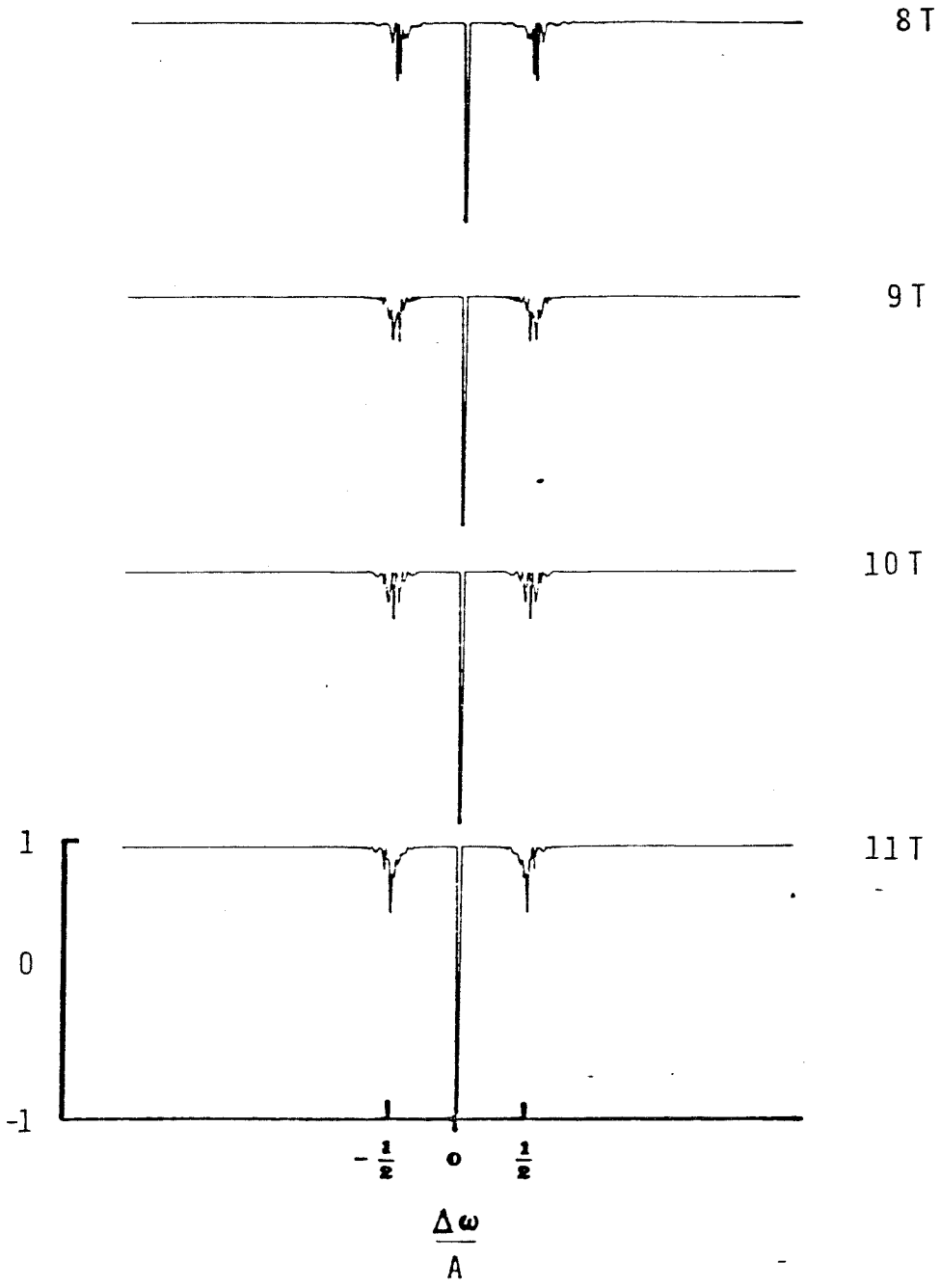
8 T
9 T
10 T
11 T
1
0
-1
$-\frac{1}{2}$
0
$\frac{1}{2}$
$\frac{\Delta\omega}{A}$

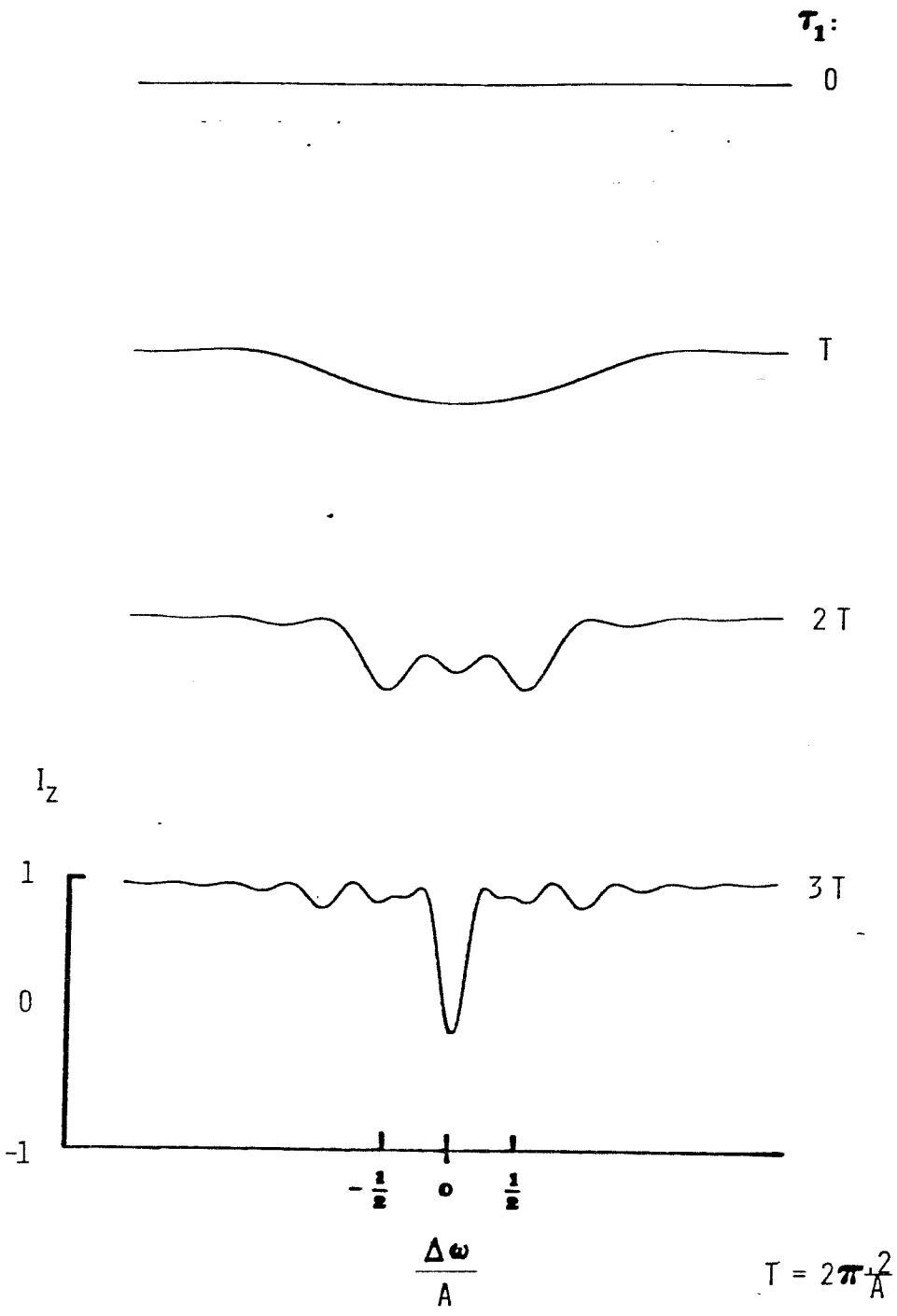
τ_1:
0
T
2 T
3 T
I_z
1
0
-1
$-\frac{1}{2}$
0
$\frac{1}{2}$
$\frac{\Delta\omega}{A}$
$T = 2\pi \frac{2}{A}$

Figure 2b.

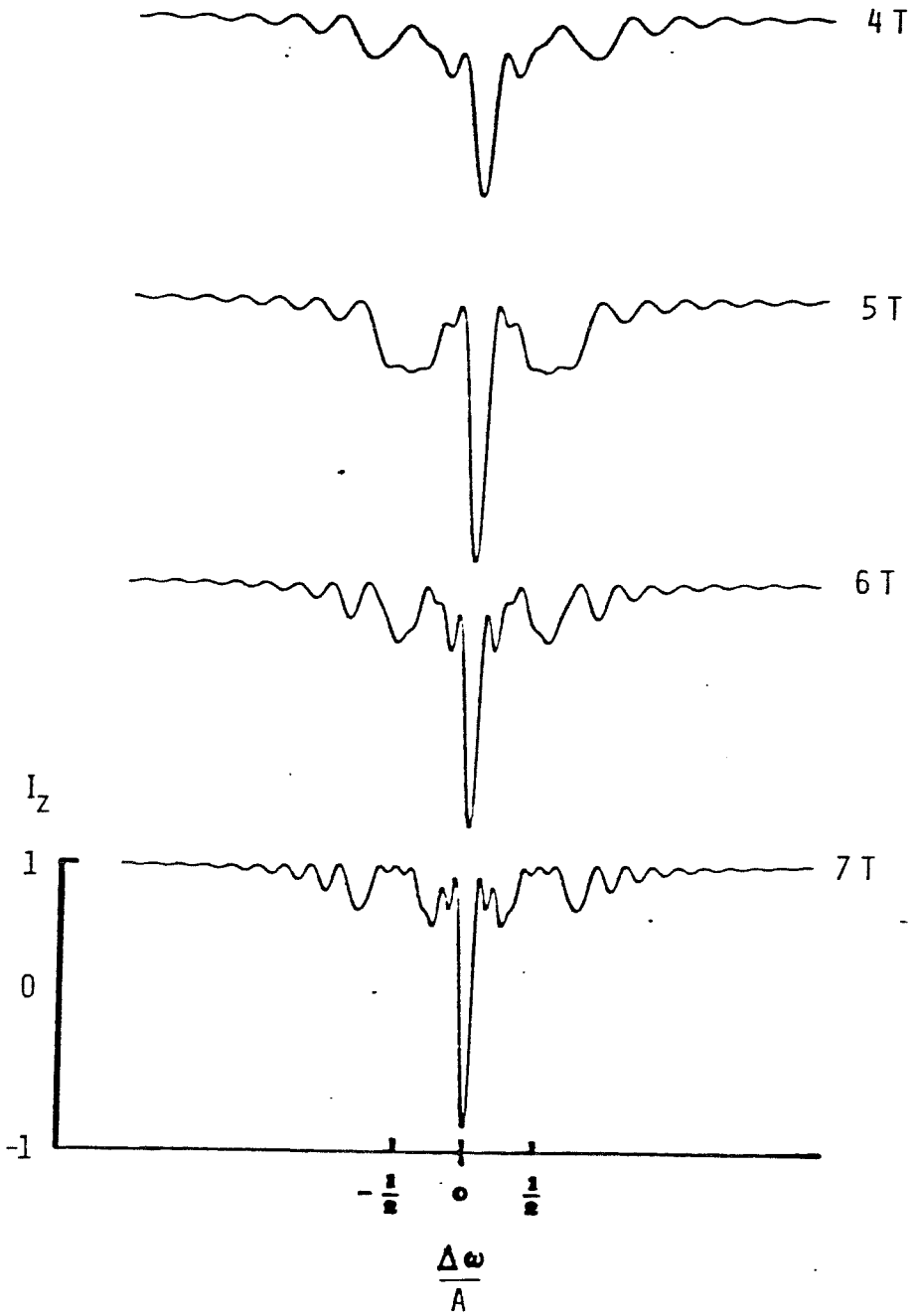
4 T
5 T
6 T
7 T
I_z
1
0
-1
$-\frac{1}{2}$
0
$\frac{1}{2}$
$\frac{\Delta\omega}{A}$

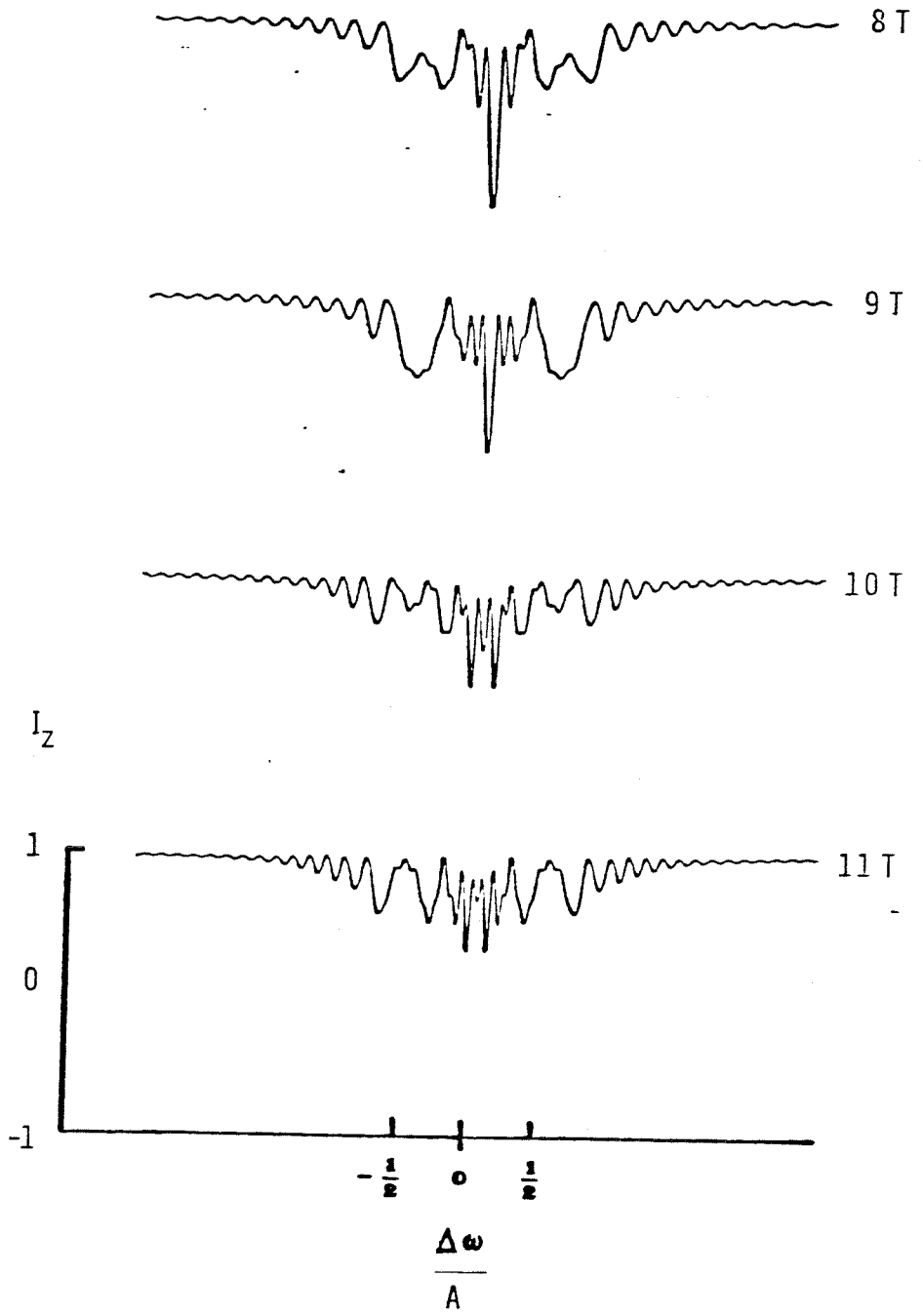
8 T
9 T
10 T
I_z
1
0
-1
11 T
$-\frac{1}{2}$
0
$\frac{1}{2}$
$\frac{\Delta\omega}{A}$

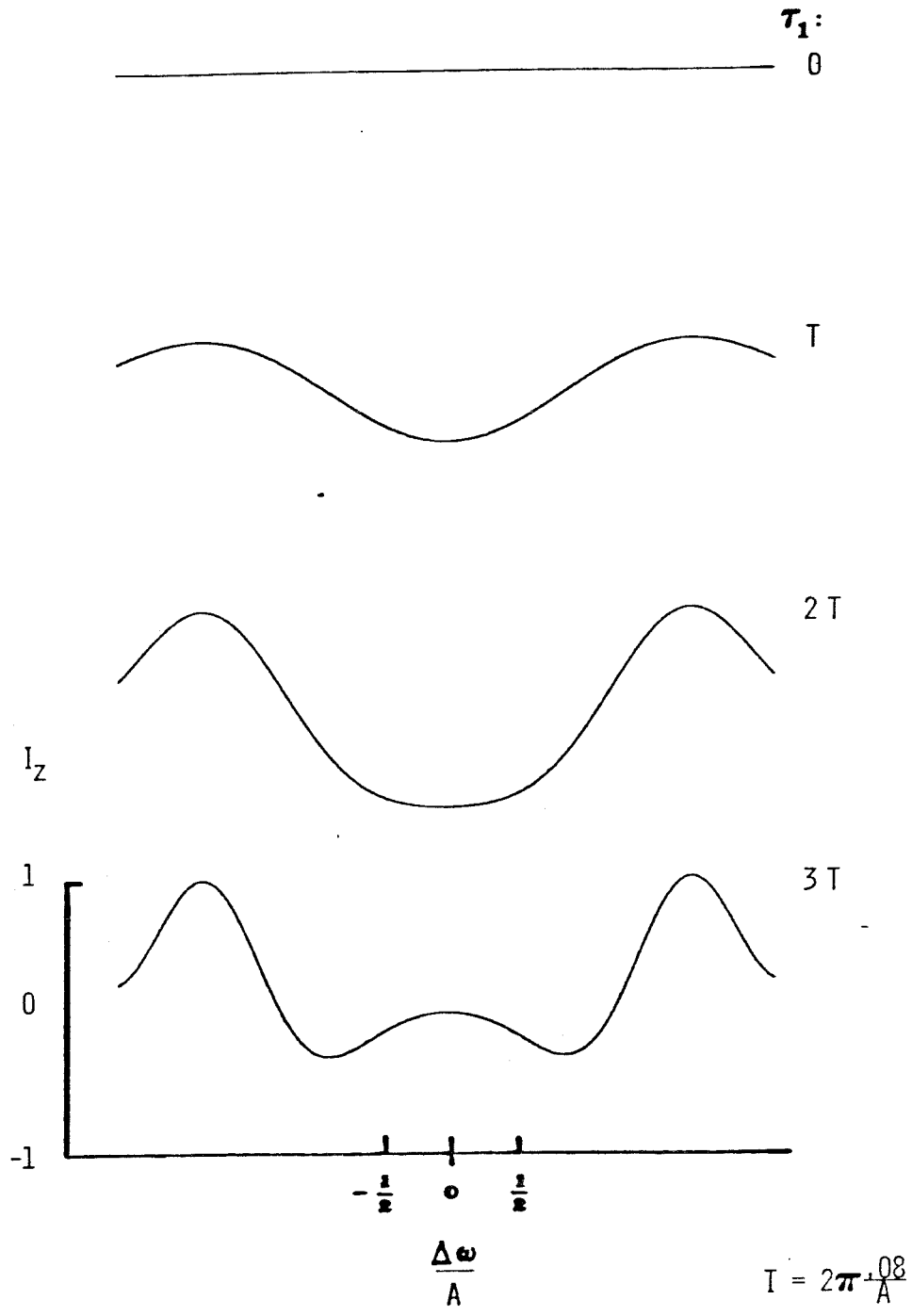
τ_1:
0
T
2 T
3 T
I_z
1
0
-1
$-\frac{1}{2}$
0
$\frac{1}{2}$
$\frac{\Delta\omega}{A}$
$T = 2\pi \frac{08}{A}$

Figure 2c.

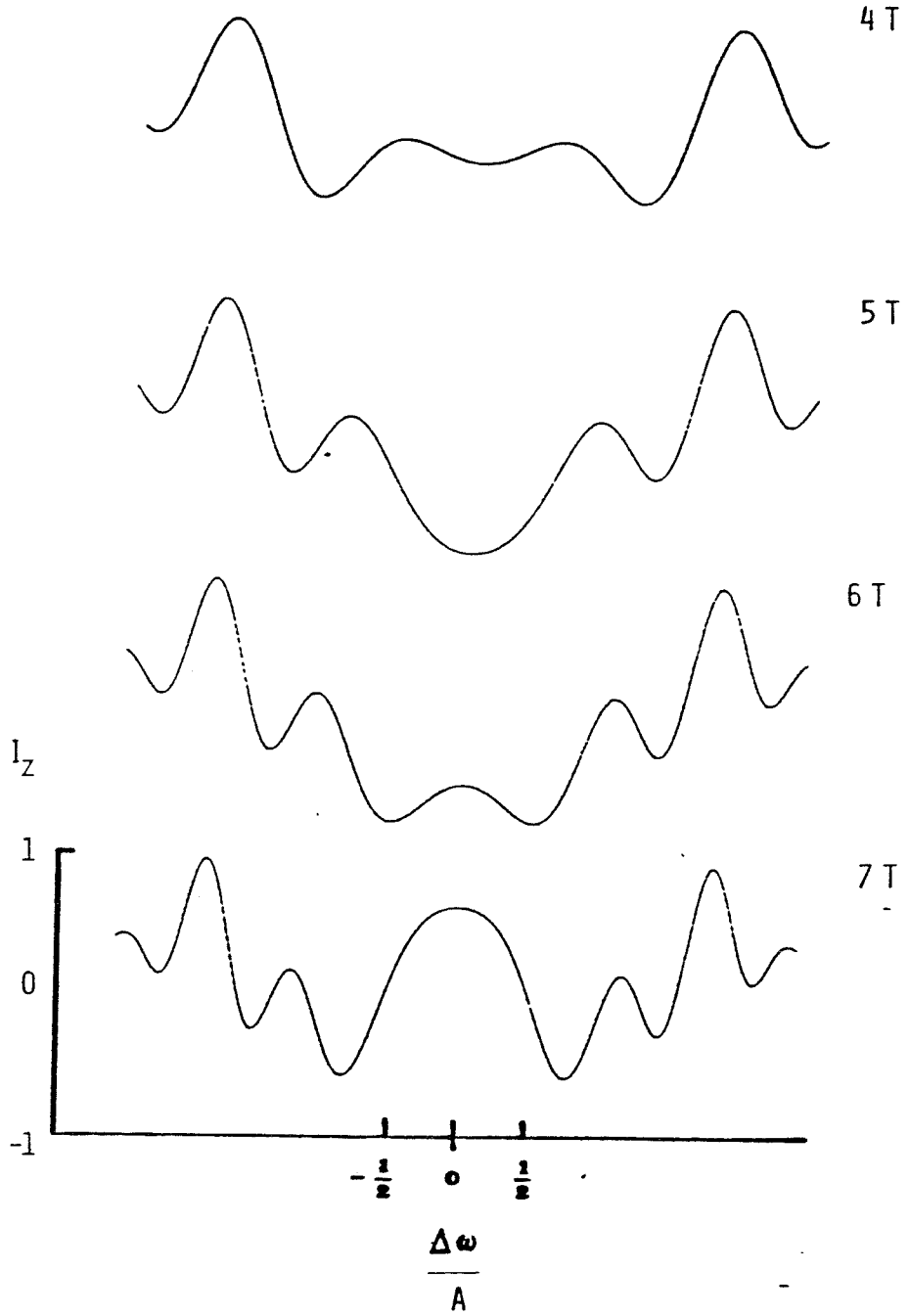
4 T
5 T
6 T
7 T
I_z
1
0
-1
$-\frac{1}{2}$
0
$\frac{1}{2}$
$\frac{\Delta\omega}{A}$

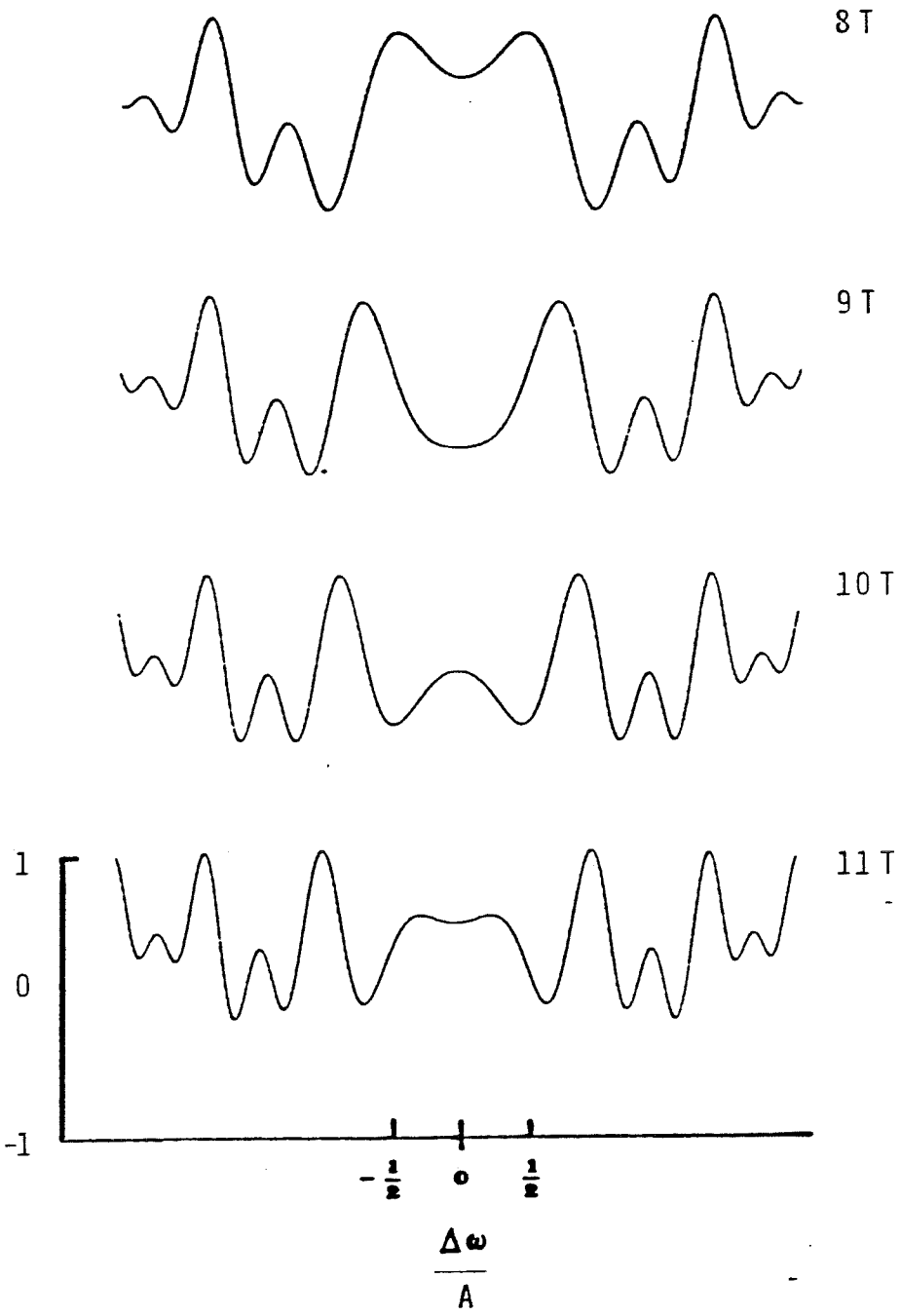
8 T
9 T
10 T
11 T
1
0
-1
$-\frac{1}{2}$
0
$\frac{1}{2}$
$\frac{\Delta\omega}{A}$

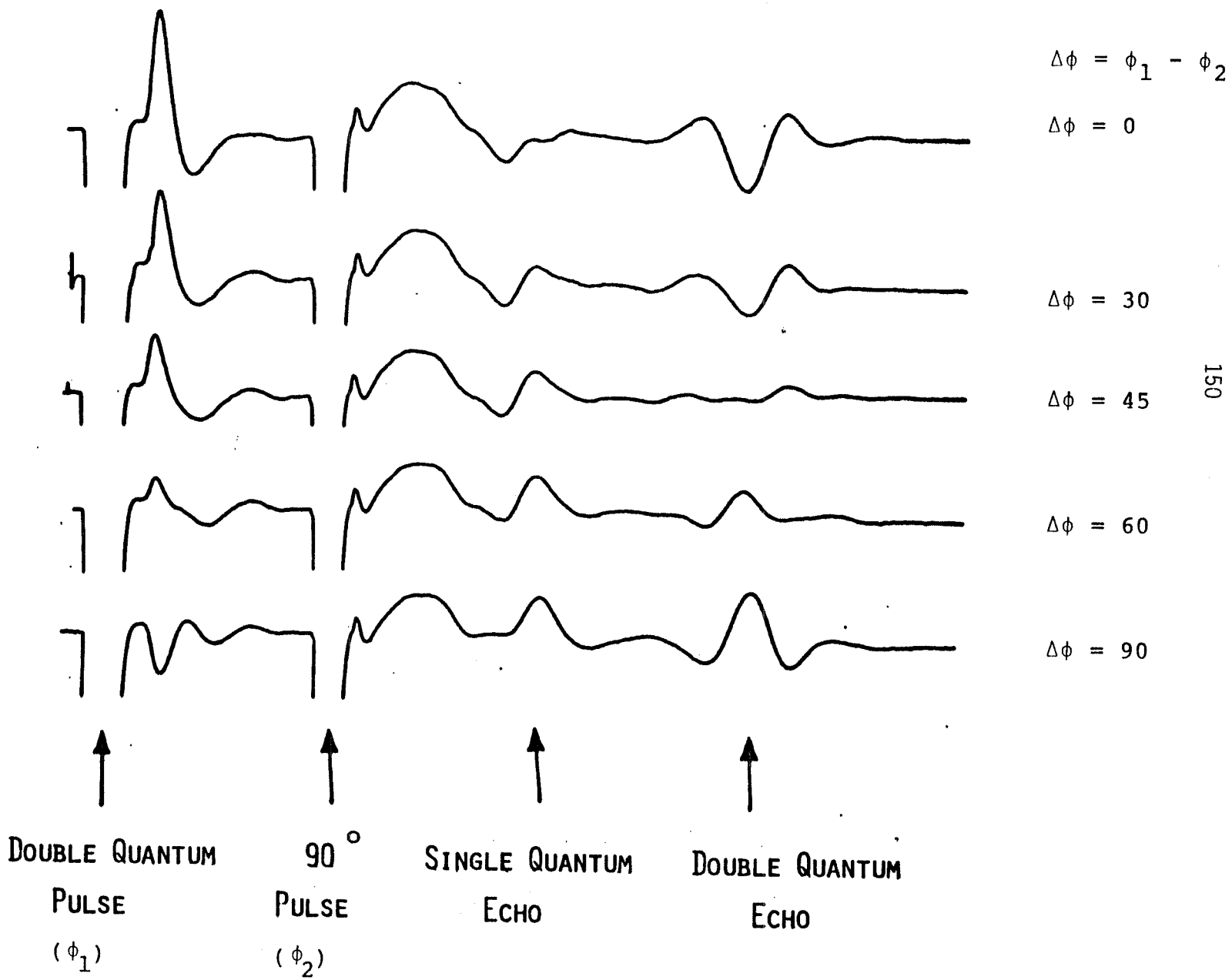
$\Delta\phi = \phi_1 - \phi_2$
$\Delta\phi = 0$
$\Delta\phi = 30$
$\Delta\phi = 45$
$\Delta\phi = 60$
$\Delta\phi = 90$
DOUBLE QUANTUM PULSE (ϕ_1)
90° PULSE (ϕ_2)
SINGLE QUANTUM ECHO
DOUBLE QUANTUM ECHO

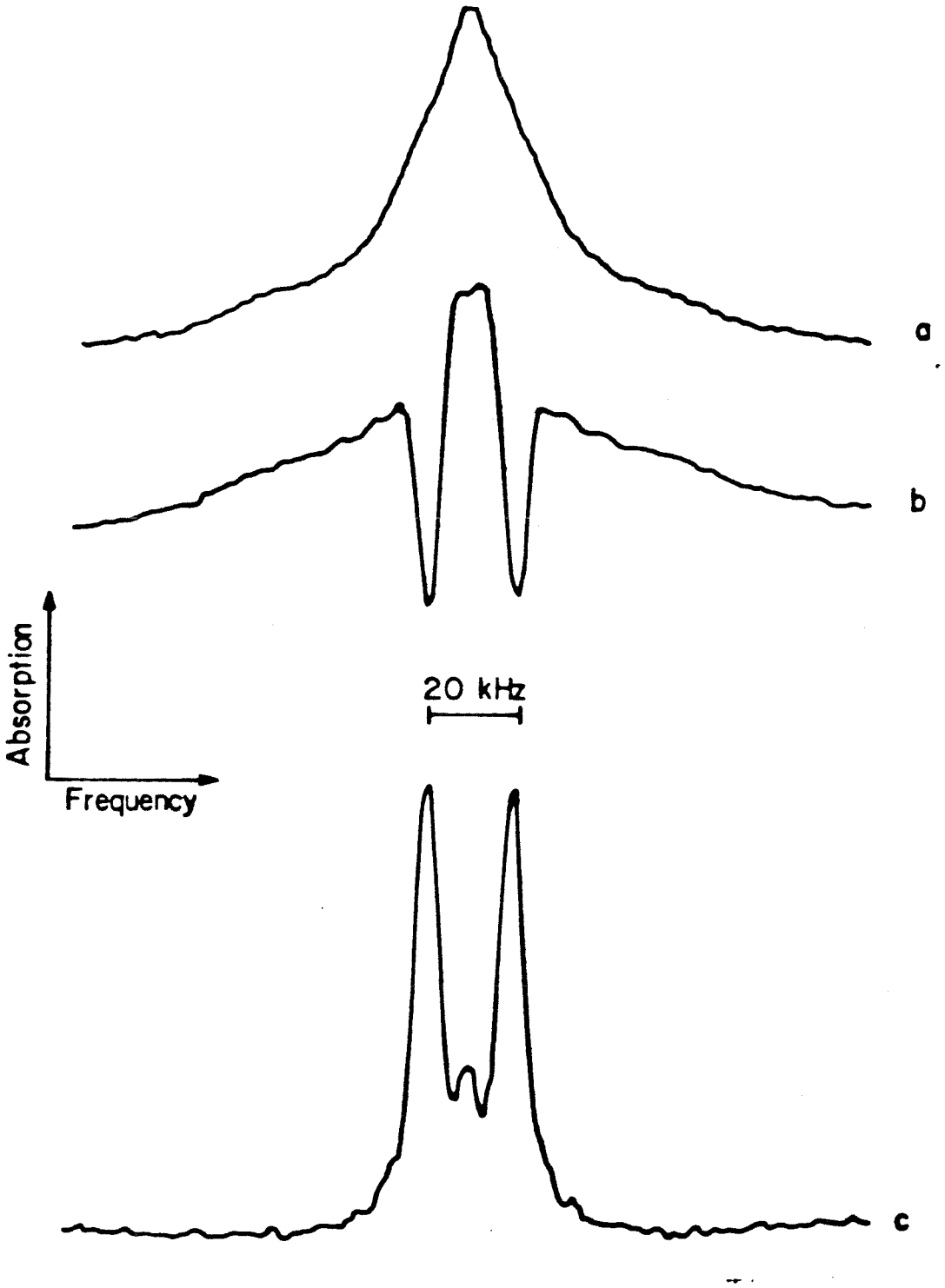

Figure 4.

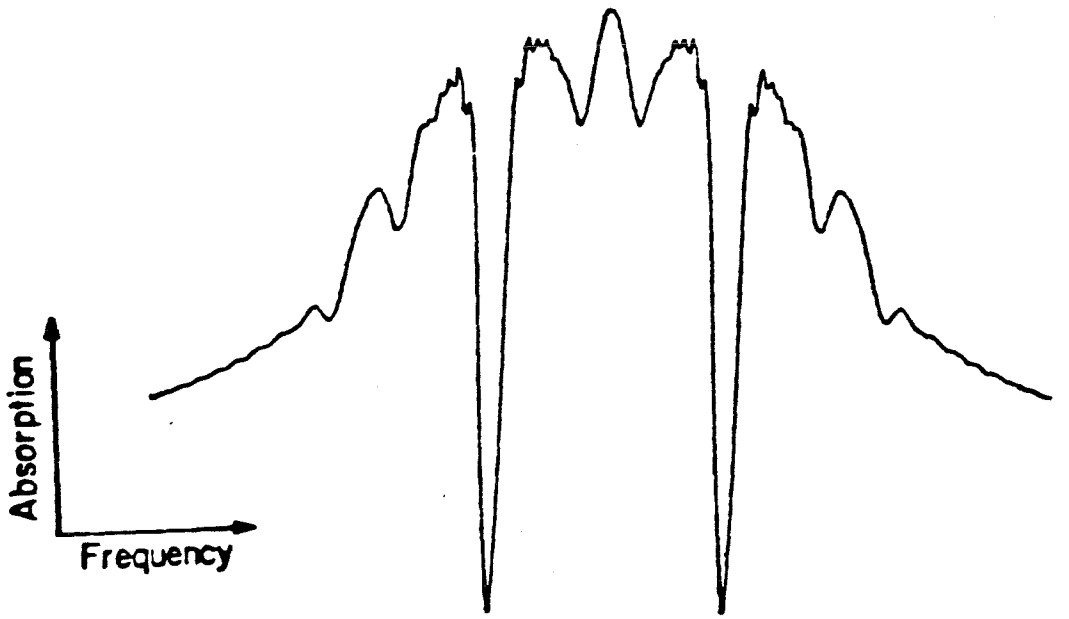

Figure 5.

CHAPTER 8

Orientation and Motion of Water Molecules in Cordierite: A Proton Nuclear Magnetic Resonance Study

(Chapter 8 is an article by D.G. Carson, G.R. Rossman, and R.W. Vaughan which is to be published in the Physics and Chemistry of Minerals.)

INTRODUCTION

The structure of cordierite, $(Mg,Fe)_2 Al_4 Si_5 O_{18}$ has been refined by Gibbs (1), Cohen et al. (2), and more recently by Hochella et al. (3) and Wallace and Wenk (4) among others. The structure of cordierite is a network of aluminosilicate tetrahedra forming six membered rings joined together by four membered rings. The six membered rings are stacked to form continuous channels parallel to [001] with maximum and minimum diameters of 2.2 Å and 1.4 Å respectively. Water molecules reside in the channels of cordierite as do many other molecules and cations (2,5). The effect of the channel water on the crystal structure of cordierite has been discussed (6,7,8), however, the orientation of the water molecules in cordierite has been interpreted differently in a polarized infrared absorption study by Goldman et al. (9), a neutron diffraction study by Hochella et al. (3), and a previous NMR study by Tsang and Ghose (10). The infrared absorption results indicate that there are two types of water in the channels of cordierite; one type oriented with its hydrogen-hydrogen vector parallel to the channels ,[001], and the other type oriented with its hydrogen-hydrogen vector parallel to [010]. The planes of both types of water are in the (100) plane. The neutron

diffraction results indicate that there is only one type of water with its hydrogen-hydrogen vector tipped 19° away from [001] with the plane of the water molecule inclined by 29° from (100). The conclusion of the previous NMR study is that there is only one type of water molecule with its inter-hydrogen vector parallel to [001]. The purpose of the present NMR study was to provide additional data to resolve this discrepancy.

The hydrogen nuclei in water, which behave as an isolated pair of spin 1/2 magnetic dipoles, have an NMR spectrum consisting of a doublet, termed Pake doublet, with a splitting given by

$$\Delta H = \frac{3\mu}{2}\left\langle \frac{1 - 3\cos^2\theta}{r^3} \right\rangle \qquad \#1$$

where μ is the magnetic moment of the nuclei, r is the length of the dipole-dipole vector, and θ is the angle between the dipole-dipole vector, $\vec{r}$, and the magnetic field, $\vec{H}_o$ (11). By measuring the dipolar splitting as a function of θ, it is possible to calculate accurately the orientation of the hydrogen-hydrogen vector with respect to the crystal axis. It is also possible to calculate the NMR averaged hydrogen-hydrogen distance (12). Many studies of solid hydrates have been performed using the Pake doublet

splittings; reviews are given by Chidambaram (13) and El Saffar (14).

EXPERIMENTAL DETAILS

The cordierite used in the NMR study is part of the same sample used in the polarized infrared absorption study of cordierite by Goldman et al. (9), their sample #3 from the Malagasy Republic. Its composition is $Na_{.02}(Mg_{1.86}Fe_{.21})Al_{3.96}Si_{4.97}O_{18}$. Using cleavage and optic figures for orientation, it was fabricated into approximately a 4 mm cube with (100),(010), and (001) faces. Orientations of the fabricated cube were verified by X-ray alignment photographs.

Several NMR techniques were used to measure the nuclear magnetic dipolar interaction given by equation 1. These techniques consisted of conventional free induction decays, solid echoes (15), and double quantum NMR (16). Basically, the Fourier transform of a free induction decay gives the Pake splitting in frequency space, but the loss of the first 5 microseconds of the decay due to receiver recovery

slightly distorts the spectrum. To alleviate this problem, solid echoes were employed to obtain the same information as the free induction decay without distortion, since the echo occurs microseconds after the last radio frequency pulse. For cases where the Pake doublets were broadened due to the paramagnetic iron, double quantum NMR was employed in the 63 kilogauss magnet. Basically, double quantum NMR provides the same information about the dipolar interaction as a free induction decay but it is more selective in that it induces transitions for only a narrow part of the broad line, thus providing the Pake doublet splitting.

The NMR experiments were performed on two conventional, pulsed NMR spectrometers operating at 63 kilogauss (270 MHz proton resonance) and 14 kilogauss (56 MHz) (described by Vaughan et al. (17)). Experiments were performed as a function of temperature and orientation on both spectrometers . The double quantum experiments were performed on the 63 kilogauss spectrometer as a function of orientation. For the low temperature experiments, the sample was cooled by cold, dry, nitrogen flowing through the sample chamber while the temperature was kept constant to within 3° C. The sample was mounted $\pm$ 5° on a NMR goniometer accurate to within 2° .

RESULTS

Figure 1a shows the hydrogen spectrum of cordierite observed in the 63 kilogauss field at room temperature with the channel axis [001] parallel to the external field, H_o. Two sets of doublets are observed, both with the same splitting of 60 kHz, separated by 22 kHz. The ratio of the areas of the two doublets is 3:1. As the crystal is rotated about an axis perpendicular to H_o, either [100] or [010], the doublets become broader and the splitting becomes smaller. Figures 1b and 1c show the spectra when the crystal is rotated 7° and 90° about [010] respectively. In the 14 kilogauss magnet, the doublets were much narrower than those in the 63 kilogauss magnet. The spectrum in figure 1d was observed in the 14 kilogauss field at the same orientation as figure 1a. Only one doublet is observed with a splitting of 60 kHz. The line in the center is due to impurities arising from the sample holder. As the crystal was rotated about an axis perpendicular to H_o, the doublet splitting became smaller and the peaks became broader but not nearly as severely broadened as at 63 kilogauss.

In figure 1a, the shift of the center of gravity of the two doublets is -22 kHz at room temperature in the 63 kilogauss magnet, while at 100 K the shift is -50 kHz as is

shown in figure 1e. The shift is plotted as a function of inverse temperature in figure 2. Comparing figures 1a and 1e, the doublet splitting also increases as the temperature decreases. The doublet splitting observed with [001] parallel to H_o is plotted as a function of temperature in figure 3.

Figure 4 shows typical spectra from the double quantum experiments. Figure 4a is the Fourier transform of a free induction decay and figure 4b is the result of the double quantum experiment at the same orientation as figure 4a. Figure 4c, which is figure 4b subtracted from figure 4a, shows the Pake doublet. The resolution of figure 4c is markedly increased over figure 4a. The doublet splittings were observed as the crystal was rotated about an axis perpendicular to H_o along the [100],[010], and [001] crystal axes and are plotted in figure 5. The maximum splitting was observed when [001] was parallel to H_o while the minimum splitting was observed when [010] was parallel to H_o. The observed splitting when [100] was parallel to H_o was 14 kHz larger than for [010] parallel H_o.

DISCUSSION OF RESULTS

Figure 1a contains two sets of doublets with the same splitting. The shift of the center of gravity of the less intense doublet is due to interaction with paramagnetic ions. In cordierite these would be predominantly Fe^{++} in the octahedral site, replacing Mg. Fe^{++} has 6 valence electrons and in octahedral symmetry Fe^{++} has an electron spin of 2. The shift due to such a paramagnetic center is (18)

$$\Delta H_s = \frac{AH_o}{T} S(S+1) \left\langle \frac{1 - 3\cos^2\theta}{r^3} \right\rangle \qquad \#2$$

where H_o is the Zeeman field, T is the temperature, S is the electronic spin, r is the Fe-hydrogen distance, θ is the angle between the Fe-hydrogen vector and H_o and A=0.83 kHz $\mathring{A}^3$K. The nearest midpoint of the nearest channel to the octahedral site is 6.2$\mathring{A}$. Using this distance with S=2, H_o=63 kilogauss, and $\theta=90^\circ$, which corresponds to the orientation where the channels are parallel to H_o, equation 2 predicts a shift of -23 kHz for room temperature. This is in excellent agreement with the observed splitting of -22 kHz for the same conditions. Also the experimental shift (Figure 2) follows the temperature dependence of equation 2 (Curie law). This is further confirmation that the low intensity doublet arises from the interaction of a paramagnetic ion with the water.

It is interesting to note that there is only one relatively narrow displaced doublet in figure 1a. This means that the water molecule is in a unique site in the channel and is not randomly distributed in the channel. . If the water molecules were randomly distributed, the displaced doublet would be very broad and unresolvable. The next nearest channel to the octahedral site is 15 Å away giving rise to a 2 kHz effect, which is small and can be neglected. The water site one lattice spacing above or below the nearest site is 9 Å away but the geometric factor $\langle 1-3\cos^2\theta \rangle$ is almost 0. However, this site will be broadened as the crystal is rotated away from the orientation [001] parallel to H_o. Because there is no longer a unique orientation for all the water molecules in the channels at orientations other than the channel axis parallel to H_o, these spectra are broadened as in figure 1c. The water molecules are isolated from one another as is demonstrated by figures 1d and 4c. The line width of the doublets in figure 3c is 2 kHz and is due to intermolecular dipolar interactions. Based on a second moment analysis of the line width, the distance between water molecules is approximately 5Å .

Equation 1 gives the Pake doublet splitting for an

isolated pair of hydrogen nuclei such as an isolated water molecule. The doublet splitting is independent of the size of the magnetic field and depends only on the geometric term $\langle 1-3\cos^2\theta\rangle/r^3$ and the gyromagnetic ratio of the hydrogen nucleus, which is an intrinsic property of the hydrogen nucleus. The lack of magnetic field dependence for the water molecules in cordierite is demonstrated in figure 1 where the doublet splitting is the same at 63 kilogauss as it is at 14 kilogauss. The significance of the geometric term is that two geometrically inequivalent rigid water molecules will give rise to a spectrum with two sets of doublets, each with a splitting according to its own geometric term. At some orientations, two geometrically inequivalent water molecules will give rise to the same doublet splitting due to our inabilty to distinguish between positive and negative doublet splittings. However this ambiguity is resolved if the crystal is rotated about the two axis perpendicular to H_o. Also, proton NMR observes all hydrogen nuclei with equal weight, i.e. the area under the absorption curve is directly proportional to the number of hydrogen nuclei in the sample. The consequence of all this and the fact that only one doublet splitting was observed at all orientations, is that there is only one type of water molecule in the channels of this cordierite, within the time scale of the experiment and within the sensitivity of the

spectra, about 5%. In this sense, one type of water means that all the water molecules are indistinguishable with respect to geometry and motion.

According to equation 1, the doublet splitting of a rigid water molecule should conform to the geometric term $\langle 1-3\cos^2\theta \rangle$ as the crystal is rotated in the magnetic field. Figure 5 shows the doublet splitting as the crystal was rotated about three mutually orthogonal axis very close to [100], [010], and [001]. The observed splittings do not conform to the geometric term of equation 1. Of prime importance is the fact that at some point during the rotation of a rigid water molecule by 180° about an axis perpendicular to H_o the minimum doublet splitting must be observed. That is, the hydrogen-hydrogen vector is at some point perpendicular to H_o. This is not observed. Also, just below room temperature (~10°C), the maximum doublet splitting in cordierite is 62 kHz and occurs when [001], the channel axis, is parallel to H_o. A rotation pattern conforming to the $\langle 1-3\cos^2\theta \rangle$ term with a maximum doublet splitting of 62 kHz would result in a measured inter-hydrogen distance of 1.80 Å. Typically, the hydrogen-hydrogen distance in water is about 1.60 Å (14). The maximum splitting for such a rigid water molecule is 88 kHz. This means that the geometric term is being motionally

averaged. Figure 3 supports this contention; the doublet splitting for the orientation [001] parallel H_o increases as the temperature decreases. The exact nature of the motion cannot be determined from the present data alone because it is conceivable that several motional models could explain the data. However, it is possible to rule out some types of motion and it is also possible to give a feeling for the order of magnitude of the motion needed to explain the data.

First of all, since Pake doublets are indeed observed, motion such as random isotropic reorientation can be ruled out; such motion would completely average the geometric term and the doublet would collapse into a single line, as in a liquid. A simple exchange or 180° rotation does not alter the doublet splitting. The NMR data exclude molecular diffusion through the channels since a water molecule exhibiting such motion would average all the magnetic fields acting on it. Thus the paramagnetic effect discussed above would be averaged and it would not be directly observed. A hindered rotation could be responsible for the averaging, however θ would have to change by over 60° to explain the data. The effects due to molecular vibrations and librations as quantified by Pedersen (19) are undoubtedly present in the water molecules of cordierite but these

effects are small. Typically, vibrations and librations can account for a decrease of 5 kHz in the dipole splitting; the decrease in the present case is 20kHz. However, what can be said is that on the basis of the rotation data, the motion must be anisotropic and have mirror planes along (001), (010), and (100) since the minima and maxima in the doublet splittings occur when the magnetic field is parallel to [100],[010], and [001]. Also, since only one set of Pake doublets are observed which are relatively narrow even at 100 K, the motion is fast compared with the total line width; that is, faster than 1 microsecond.

COMPARISON WITH OTHER STUDIES

Recently, the water molecules in the channels of cordierite have been the subject of an NMR study (10), a polarized infrared absorption study (9), and a neutron diffraction study (3). As stated previously, the cordierite used in the present study is from the same sample used in the infrared absorption study, Goldman's sample #3, while the cordierite used in the neutron diffraction study is similar in composition to sample #3. The results of the present study of water molecules in the channels of cordierite appear to contradict both the infrared absorption results and the neutron diffraction results which contradict

each other. The conclusion of the neutron diffraction study is that there is one type of water molecule with its hydrogen-hydrogen vector tilted 19° from [001] . This conclusion cannot be reconciled with the present NMR data, in particular the demand for the symmetry planes. It is possible that the symmetry plane of the motionally averaged geometric factor is not exactly in the [010] plane but the deviation from this position is at most 7°, based on the combined maximum of all potential goniometeric errors. Also, the motion which averages 20 kHz of the NMR doublet splitting is substantial. One would assume that the neutron density would be smeared to give a diffuse density map. It must be pointed out, however, that the sample used in the neutron diffraction study was not the same specimen used in the present study.

On the basis of the observed fundamental stretching and bending modes of water in the infrared region and the combination and overtone modes in the optical region at different polarizations, Goldman et al. (9) conclude that there are two distinct types of water in the channels of cordierite. Type I water is in the (100) plane with its hydrogen-hydrogen vector parallel to [001], and type II water is also in the (100) plane but with its hydrogen-hydrogen vector parallel to [010]. Using the

intensities of the polarized infrared absorption peaks, they report that approximately 77% of the water is type I and 23% is type II for sample #3. These conclusions are consistent with the present NMR results if one assumes that there is only one type of water which is jumping back and forth between type I and type II orientations rapidly compared to the time scale of the NMR experiment (1 microsecond) but slowly compared to the time scale of the infrared experiment (1 picosecond). According to this motional model, the Pake doublet splitting is given by

$$\Delta H = 40\ p1(1-3\cos^2\theta_1) + 40\ p2(1-\cos^2\theta_2) \qquad \#3$$

ΔH has the units of kHz and
where p1 is the fraction of time that the water molecule spends at an orientation corresponding to θ_1 and p2 is the fraction of time that the water molecule spends at an orientation corresponding to θ_2. Equation 3 is plotted in figure 5 as the solid curves, assuming the type I type II hopping model with p1=.85 and p2=.15. The agreement of the distribution of type I and type II sites between IR and NMR is good considering the uncertainty in the infrared determination. Further, assuming the relative populations p1 and p2 follow a Boltzman distribution, the Pake doublet splitting for the orientation [001] parallel to H_o as a function of temperature is given by

$$\Delta H = 40 \text{ kHz}\left(2 - \frac{3}{(1 + \exp(dE/kT))} \right) \qquad \#4$$

where dE is the difference in the standard free energy between the type I and type II water sites. Using the room temperature values of p1 and p2 from above, the temperature dependent data can be best fit with dE = .8 kcal as can be seen in Figure 3, where the solid curve is equation 4. Again, the agreement is excellent. According to this model, the hydrogen-hydrogen distance in the water molecule is 1.64Å . This value is close to the average value of hydrogen-hydrogen distances calculated by NMR (14) for rigid water molecules, which is 1.60Å .

Another conclusion of the study by Goldman et al. (9) is that 95% of the iron occupies the octahedral site and only 5% occupies channel sites. Therefore for Malagasy Republic cordierite, 10% of the Mg is replaced by Fe^{++}. Figure 6 shows a side view of the channel with the lattice vectors shown in the figure. For every octahedral site, there are two channel sites for the water molecule. Site one and the octahedral site are in the same [001] plane while site two is half a unit cell below, about 4.9 Å . A Fe^{++} ion residing in the octahedral site would cause a shift of the doublet of the site one water by -22 kHz while

shifting the doublet of the site two water by only 2 kHz due to the geometric factor in equation 2. Thus, one-half of the water sites produce doublets which are effectively unshifted irrespective of the constituent of the octahedral sites. On the other hand, the other water site may produce doublets which are shifted, depending on the constituents of the nearest octahedral sites. Every channel site one has six octahedral sites 6.2 Å away. Based on a random distribution of the Fe^{++} in the octahedral sites, 53% of the site ones would have no neighboring Fe^{++}, 35% of the site ones would have one neighboring Fe^{++} and 10% would have two neighboring Fe^{++}s. If the water molecules were randomly distributed between site one and site two, one would expect three sets of doublets. 76% of the doublets would not be shifted, 17% of the doublets would be shifted by -22 kHz, and 5% would be shifted by -44 kHz. Based on these numbers, the ratio of the no Fe^{++} to one Fe^{++} intensities is nearly 4.5. Experimentally the ratio is 3.0. The doublets shifted by -44 kHz were not observed but they may have been below the noise level. However, if for some reason two Fe^{++} ions were prohibited from occupying adjacent octahedral sites, 73% of the doublets would not be shifted, 24% would be shifted -22 kHz, and 3% would be shifted -44kHz. The ratio of the no Fe^{++} to one Fe^{++} intensities for this case is 3.09. The agreement with the experimental value is significantly

better. In any event, the NMR results support the conclusion of Goldman et al. (9) that 95% of the iron occupies the octahedral sites as opposed to the conclusion of Duncan and Johnston (20) that only 75% of the iron occupies the octahedral sites because the lower the occupancy rate of the octahedral site by Fe^{++} the higher the non-shifted to -22 kHz shifted ratio would be.

The NMR study by Tsang and Ghose (10) was conducted on a sample from the same region as the sample used in the present study. They report a maximum room temperature doublet splitting of 60 kHz when the channels are parallel to Ho and they conclude that the doublet splittings follow a $1-3\cos^2\theta$ dependence. Within experimental error this is in agreement with the present NMR data. However, based on the room temperature NMR data alone, Tsang and Ghose could only state that the dipolar interaction was somehow motionally averaged . Their final conclusion was that the water molecule was oriented with its motionally averaged hydrogen-hydrogen vector parallel to the channels.

HADDAM CORDIERITE

Most of the cordierites studied by Goldman et al. (9) were found to have roughly the same proportion of

type I water (80%) as the Malagasy Republic cordierite with the exception of their sample #6 from Haddam, Connecticut. According to their polarized infrared absorption results, Haddam cordierite contains only 27% type I water and 73% type II water making it an ideal sample to test our proposed motional model.

We obtained a single crystal of Haddam cordierite from the same speciman as Goldman's sample #6 and conducted the same magnetic resonance experiments discussed previously. However, due to the presence of a large amount of paramagnetic iron (5.7 weight per cent), we were only able to observe well resolved Pake doublets when the [001] direction was parallel or near parallel to the external magnetic field. At this orientation, the Pake doublet splitting is 42 kHz $\pm$ 5 kHz and decreases when the crystal is rotated about either [100] or [010]. Only broad lines were observed at other orientations. If we assume the two site hopping model, then the 42 kHz splitting indicates that there is proportionally less type I water than in the Malagasy Republic sample. The quality of the spectra, however, allow us to neither quantify this nor even to verify the hopping model for the Haddam sample.

CONCLUSIONS:

The most important conclusion that the present study can provide is that there is only one type of water molecule occupying a well defined site in the channels of Malagasy Republic cordierite. Further, this water molecule is undergoing some kind of motion on a time scale faster than 1 microsecond. The exact nature of this motion cannot be determined on the basis of the NMR results alone. However, if the NMR results are combined with the conclusions of the infrared absorption study, a plausible model can be presented. Namely, one water molecule is jumping back and forth between two orientations within the cavity. Orientation I is the type I water and orientation II is the type II water. At room temperature the water occupies orientation I 85% of the time and orientation II 15% of the time. The standard free energy difference between these two orientations is .8 kcal.

ACKNOWLEDGEMENTS

This work was supported by the National Science Foundation (DMR-7721394). We would like to thank Professor S. I. Chan for helpful discussions.

References

1. G.V. Gibbs, Am. Mineral. 51, 1068 (1966).

2. J.P. Cohen, F.K. Ross, and G.V. Gibbs, Am. Mineral. 62, 67 (1977).

3. M.F. Hochella, G.E. Brown, F.K. Ross, and G.V. Gibbs, Am. Mineral. 64 337 (1979).

4. J.H. Wallace and H.R. Wenk, Am. Mineral. 65, 96 (1980).

5. J.V. Smith and W. Schreyer, Mineral. Mag. 33, 226 (1962).

6. J.H. Stout, Am. Mineral. 60, 229 (1975).

7. J.H. Stout, A reply. Am. Mineral. 61, 1041 (1976).

8. K. Langer and W. Schreyer, Am. Mineral. 61, 1036 (1976).

9. D.S. Goldman, G.R. Rossman, and W.A. Dollase, Am. Mineral. 62, 1144 (1977).

10. T. Tsang and S. Ghose, J. Chem. Phys. 56, 3329 (1972).

11. G.E. Pake, J. Chem. Phys. 16, 327 (1948)

12. D.F. Holcomb and B. Pedersen, J. Chem. Phys. 38, 54 (1963).

13. R. Chidambaram, J. Chem. Phys. 36, 2361 (1962).

14. Z.M. El Saffar, J. Chem. Phys. 45, 4643 (1966).

15. N. Boden and M. Mortimer, Chem. Phys. Lett. 21, 538 (1973).

16. D.C. Carson and R.W. Vaughan, (Chapter 7, to be published)

17. R.W. Vaughan, D.D. Elleman, L.M. Stacey, W.K. Rhim, and

J.W. Lee, Rev. Sci. Instrum. 43, 1356 (1972).

18. C.P. Slichter, Principles of Magnetic Resonance (Springer-Verlag, Berlin, Heidelberg, New York 1978)

19. B. Pedersen, J. Chem. Phys. 41, 122 (1964).

20. J.F. Duncan and J.H. Johnston, Austr. J. Chem. 27, 249 (1974).

FIGURES

Figure 1. Typical proton magnetic resonance spectra of water in a single crystal of Malagasy Republic cordierite: a) room temperature spectrum with [001] parallel H_o in the 63 kilogauss field. The two pairs of doublets, labeled D1 and D2, have the same doublet splitting (60 kHz) but are separated by 22 kHz. A small signal is also observed due to an impurity in the sample holder, labeled imp. As the crystal is rotated about [010], the Pake doublets broaden, as shown in b) (7°), and c) (90°). Figure 1d was observed with [001] parallel H_o at room temperature in the 14 kilogauss field. Figure 1e was observed at the same conditions as 1a except at 110 K.

Figure 2. The temperature dependence of the shift of the Pake doublets due to the paramagnetic iron for the orientation [001] parallel to H_o in the 63 kilogauss magnet follows the Curie law ($\Delta H \propto 1/T$, represented by the solid line).

Figure 3. The temperature dependence of the Pake doublet splitting for the orientation [001] parallel H_0 observed in the 63 kilogauss magnet. The points are experimental data and the solid curve is the predicted temperature dependence for a water molecule jumping between two orientations (site I and site II as described by Goldman et al. (9)) faster than 1 microsecond.

Figure 4. Typical double quantum spectra: a) a conventional spectrum broadened by paramagnetic iron, b) a selective inversion of a Pake doublet employing double quantum NMR, c) a difference spectrum, a) minus b).

Figure 5. The doublet splitting as a function of orientation as measured by double quantum NMR. The single crystal was rotated about an axis perpendicular to H_0. Specific orientations are marked in the figure.

Figure 6. A side view of the channel. The circles represent oxygen atoms and the ferrous ion is shown. There are two cavities (a and b) where the water may reside. The cavities are distinguished from each other by their proximity to the ferrous ion in an octohedral site.

Figure 1.

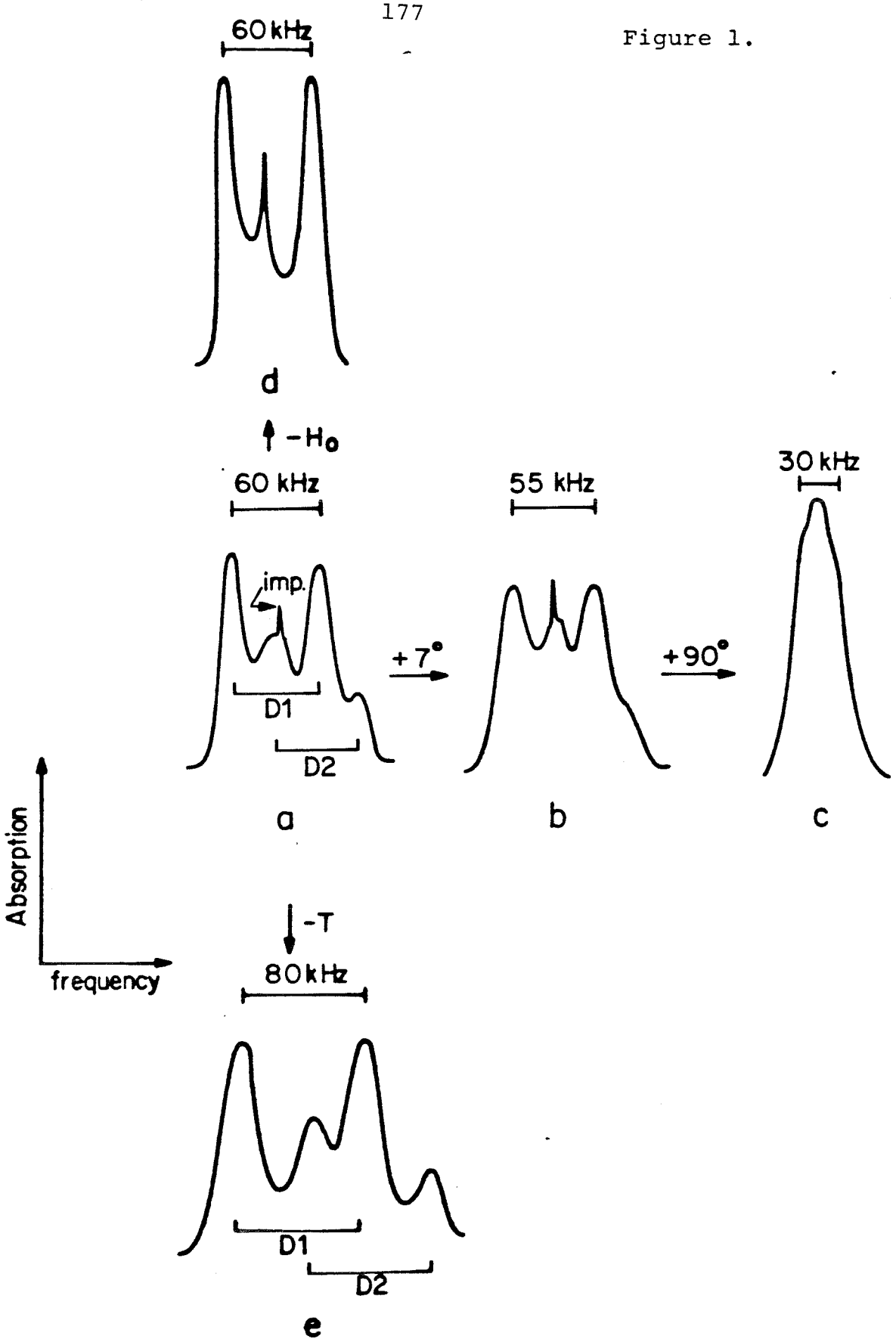
60 kHz
d
-Ho
60 kHz
55 kHz
30 kHz
imp.
+7°
+90°
D1
D2
a
b
c
Absorption
frequency
-T
80 kHz
D1
D2
e

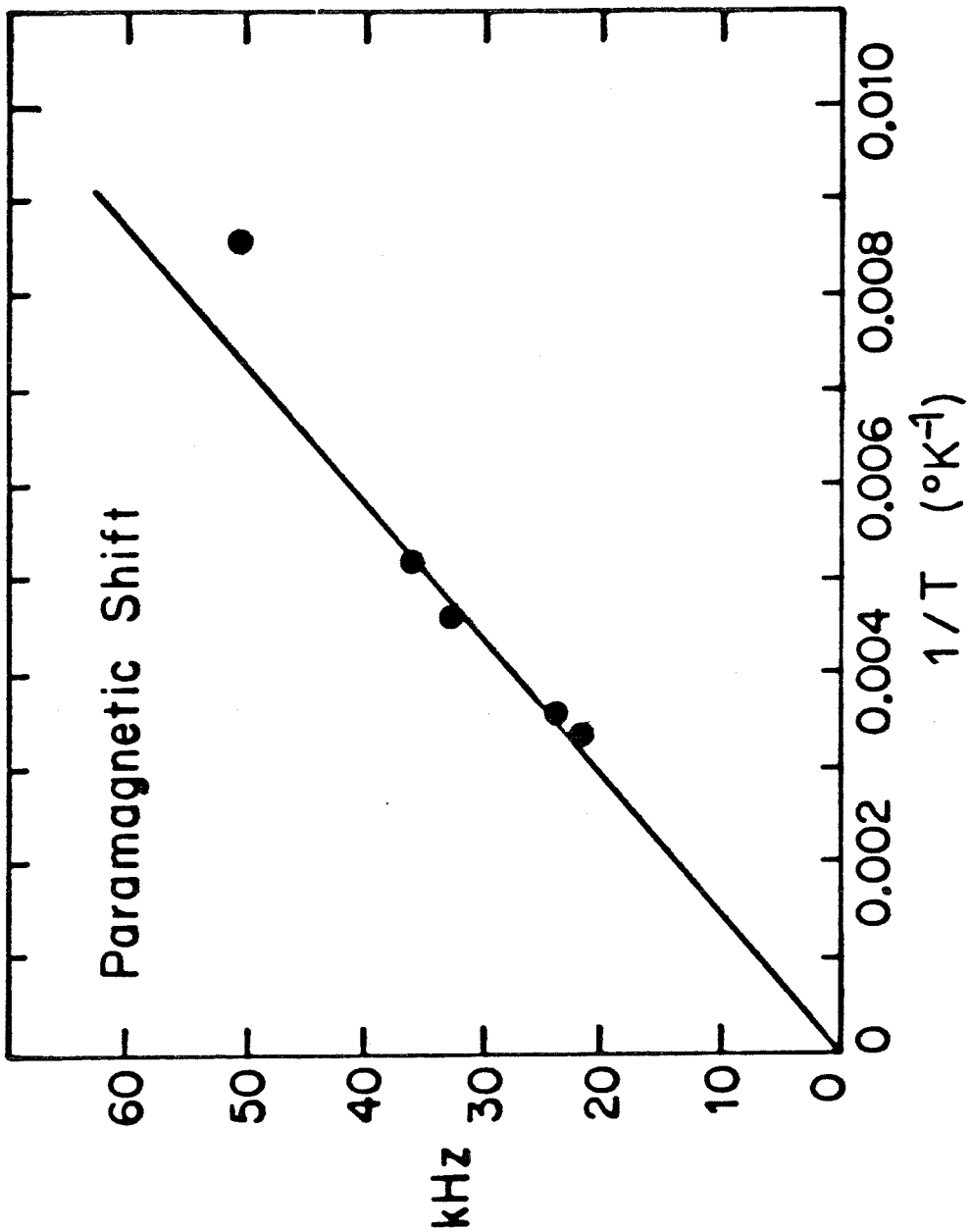
Paramagnetic Shift
kHz
60
50
40
30
20
10
0
0
0.002
0.004
0.006
0.008
0.010
1/T (°K⁻¹)

Figure 2.

Figure 3.

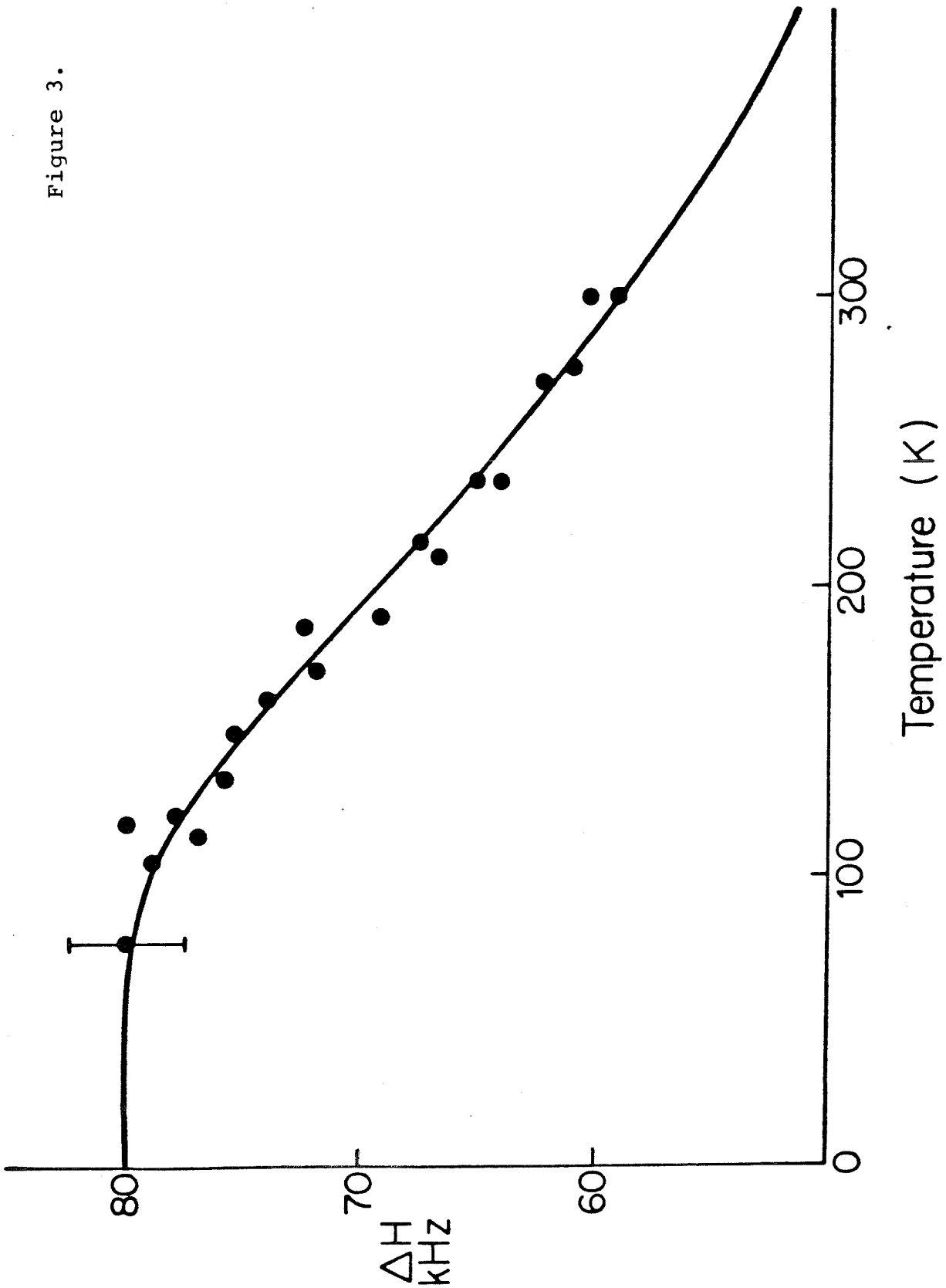

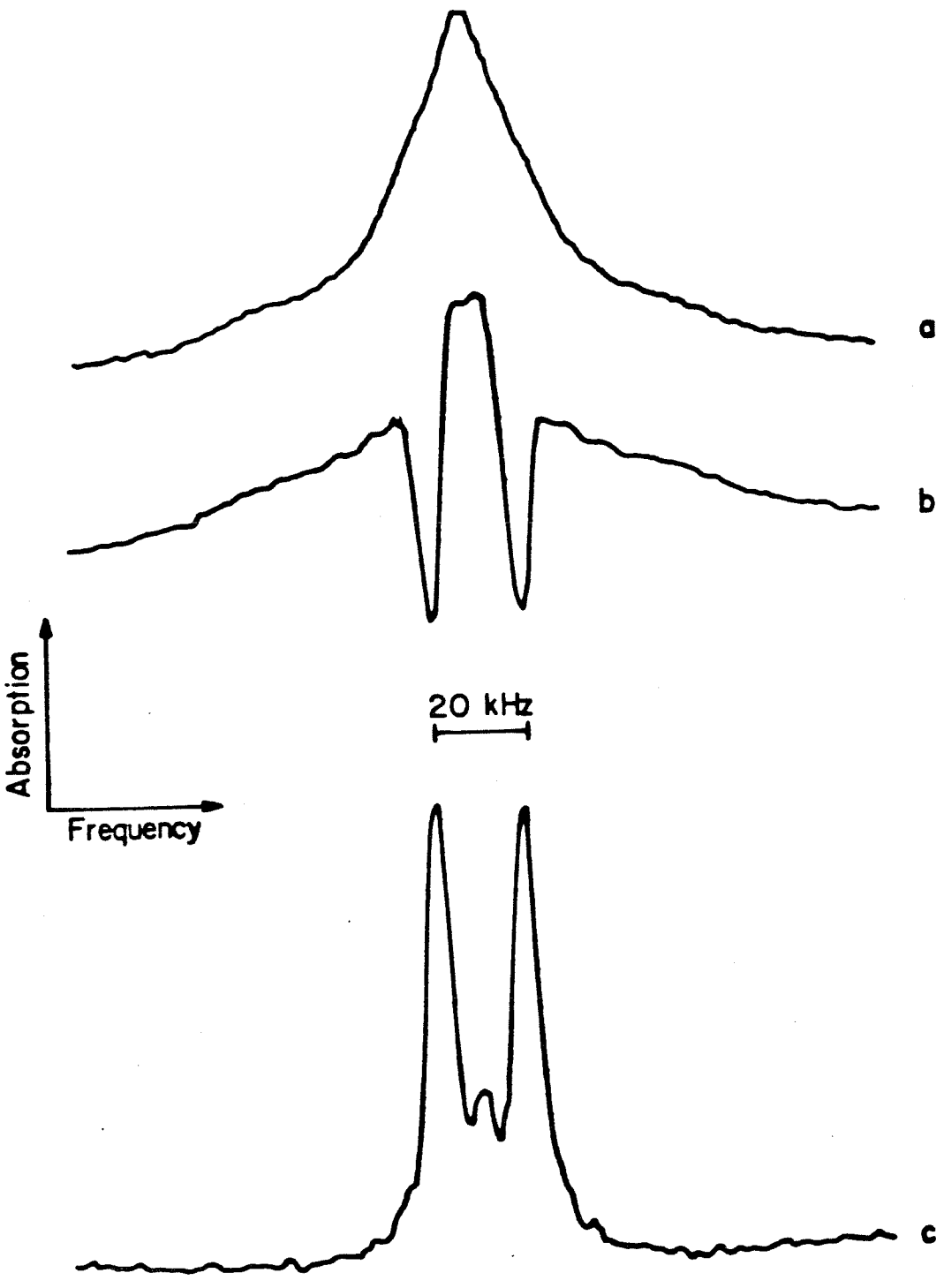

Figure 4.

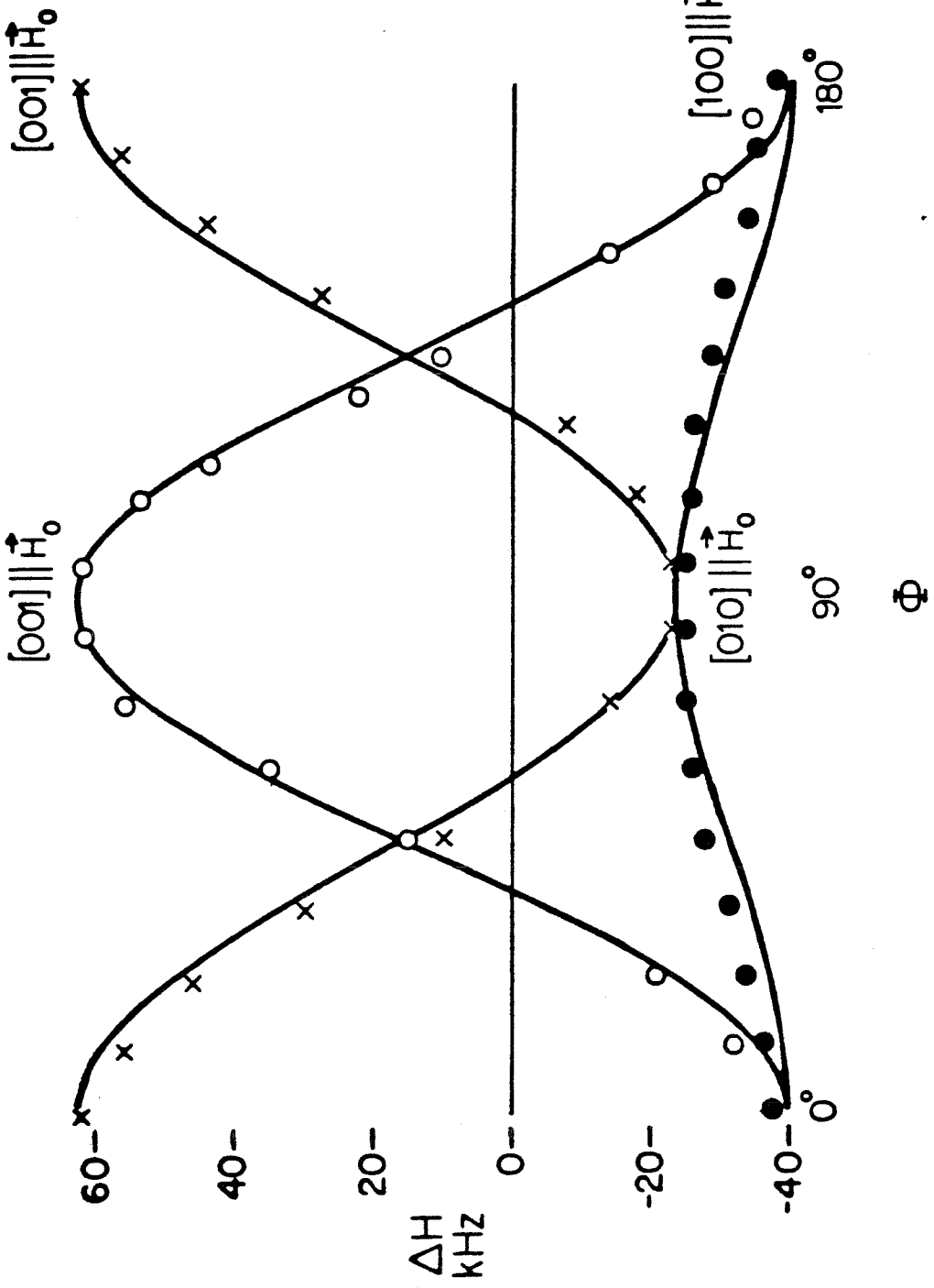
[001]||$\vec{H}_o$
[001]||$\vec{H}_o$
[100]||$\vec{H}_o$
[010]||$\vec{H}_o$
60
40
20
0
-20
-40
ΔH kHz
0°
90°
180°
Φ

Figure 5.

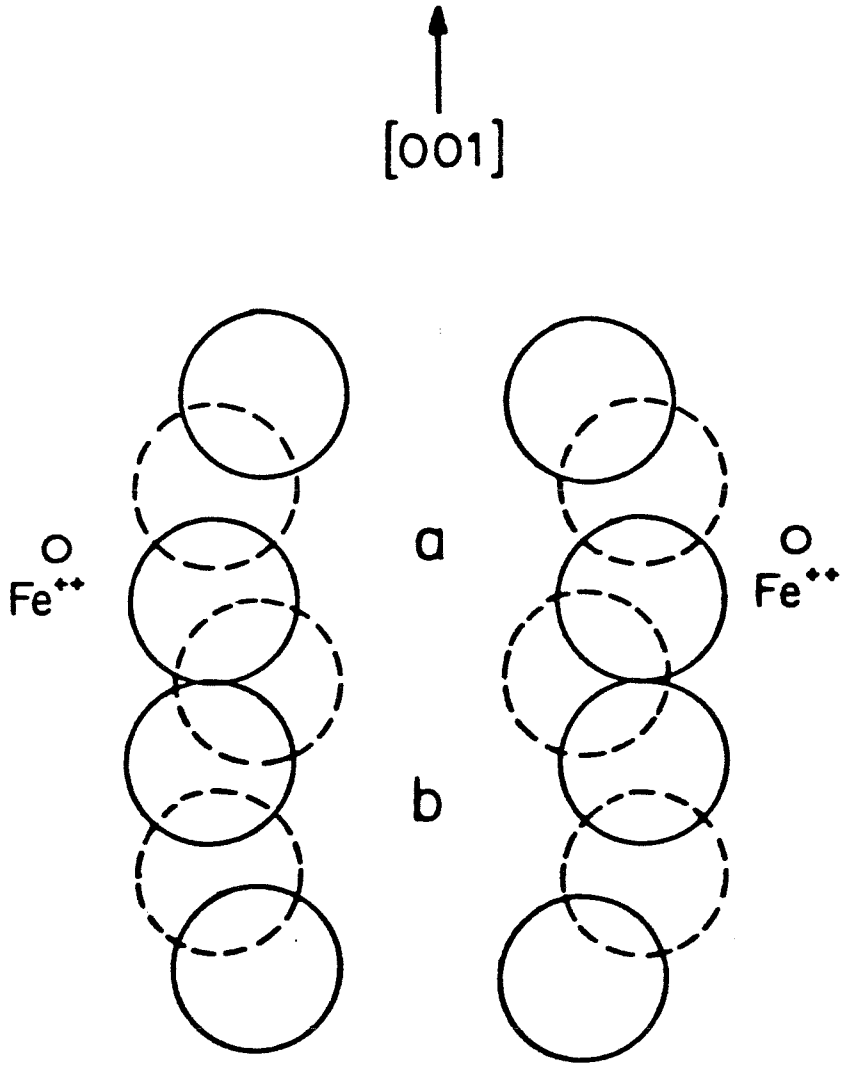

Figure 6.

APPENDIX

A Proton Magnetic Resonance Study of the Water Molecule in Hilgardite

(The Appendix is an article by M.J. Peltre, B. Berglund, D.G. Carson, and R.W. Vaughan which was published under the same title in American Mineralogist, Volume 65, page 346, 1980.)

Abstract

A proton magnetic resonance study, at room temperature, of a single crystal of hilgardite, $Ca_2[B_5O_9]Cl \cdot H_2O$, has been carried out at 270 MHz. The variations of the dipolar splittings in the NMR spectra have been studied as a function of the orientation of the crystal relative to the magnetic field. This provides more accurate information about the orientation of the water molecule than a recently reported x-ray diffraction study of the crystal structure of hilgardite. A length of the proton-proton vector of 1.66 Å is calculated and the vector is found to be fairly close to, but significantly out of the b-c plane. The positions of the hydrogen atoms of the water molecule are estimated from the NMR results by making some assumptions about the hydrogen bond arrangement, giving coordinates rather close to those estimated from the x-ray diffraction experiment.

INTRODUCTION

The mineral hilgardite, $Ca_2B_5O_9Cl \cdot H_2O$, found in the Choctow Salt Dome, Iberville Parish, Louisiana, has recently been studied by x-ray diffraction by Ghose and Wan (1). The crystal structure of hilgardite belongs to the monoclinic space group Aa, and the structure consists of a three-dimensional pattern of pentaborate polyanions $[B_5O_{12}]^{-9}$. The arrangement of the polyanions is such that open channels parallel to the a and c axes are formed, with channel diameters of about 5-6 Å. Within these channels the water molecules and the chlorine atoms form almost linear hydrogen bonded chains parallel to the c-axis. As x-ray diffraction gives poor information about the positions of the hydrogen atoms and since we were kindly provided with a single crystal cut from the same crystal used in the x-ray diffraction experiment, we decided to undertake an NMR experiment in order to get more precise information about the orientation of the water molecules.

According to Pake (2), the dipolar splitting in an NMR

spectrum of a single crystal containing an isolated proton pair can be written as

$$\Delta H = \frac{3\mu}{2r^3}(3\cos^2\theta - 1) \qquad (1)$$

where μ is the magnetic moment of the nuclei, r the length of the proton-proton vector, and θ the angle between r and the magnetic field.

For the purpose of analysing proton spectra, a crystal containing water molecules can be considered, in most cases, to contain isolated proton pairs. This is , of course, an approximation since the water molecules in the structure will couple to each other. It has been shown, however, by Holcomb and Pedersen (3) that even in such cases, equation 1 can be used if ΔH is taken to be the separation between the centers of gravity of the two peaks rather than between their two maxima. A large number of studies of solid hydrates using Pake's technique has been published and reviews are given by Chidambaram (4) and El Saffar (5).

EXPERIMENTAL

NMR spectra were recorded on a pulsed NMR spectrometer operating at 270 MHz. A solid echo technique was used as described by Boden and Mortimer (6), and references therein,

in order to minimize the deadtime problems usually occurring when very broad lines are studied by a pulsed NMR spectrometer.

The size of the single crystal of hilgardite used in the experiment was about 4 mm^3, containing 10^{19} protons. The plate-shaped crystal had well-developed facets, which were used in the orientation of the crystal. In order to protect the crystal, it was embedded in a polymer. To eliminate the narrow line from the polymer, a spectrum from the polymer was recorded and subtracted from the crystal spectra.

The NMR spectra were recorded every 5-10 degrees in an 180° rotation of the crystal about an axis perpendicular to the magnetic field. Three mutually orthogonal rotation axes (a,b,c, $\beta = 90.06^{\circ}$) were used to obtain full information about the orientation of the proton-proton vector. Since the crystal structure belongs to a monoclinic space group, two dipolar splittings are expected for each independent proton-proton vector in the unit cell (except when the magnetic field is parallel or perpendicular to the b-axis, where the two doublets collapse to one), for all angles (see Figure 1).

The proton-proton vector was refined using a least-squares procedure described by Berglund and Tegenfeldt (7). The fit between the experimentally observed splittings and the calculated splittings is illustrated in Figure 1.

RESULTS AND DISCUSSION

The lengths of the proton-proton vector is 1.66 (1) Å and it makes an angle of 24 (1)° with the c-axis and 80 (2) ° with the a-axis, i.e., the vector is tilted by 10° from the b-c plane. The proton-proton distance is slightly longer than found for other hydrates studied by NMR. El Saffar (5) has given a mean value of 1.60 Å taken over a number of different hydrates including lengths up to 1.64 Å (8,9). Therefore the proton-proton distance in hilgardite has to be considered as reasonable. It is known, however, that internuclear distances from an NMR experiment are significantly longer than the equilibrium value, R_e, due to the vibrational averaging. Similarly, the lengths determined from a neutron diffraction experiment are also affected by vibrational motion of the water molecule. In order to obtain a value for R_e from either NMR or neutron diffraction, the vibrational behavior of the molecule has to be known (10,11).

From a proton NMR experiment alone it is impossible to calculate directly the position of the hydrogen atoms. It has been shown, however, by El Saffar (5) that estimates of the positions, agreeing very well with those obtained from neutron diffraction, can be obtained from the NMR data if some assumptions about the hydrogen bond arrangement are made. The procedure is as follows: estimate the two O-H distances in the water molecule and then minimize the sum of the squares of the hydrogen bond distances $H_1 \cdot\cdot A_1$ and $H_2 \ldots A_2$ where A_1 and A_2 are the two hydrogen bond acceptors (assuming that for each hydrogen bond there is only one acceptor). In the case of hilgardite only the chlorine atoms in the quasi-linear chain can act as acceptor since all distances from the proton atoms to all oxygen atoms in the borate arrangement are too long to be within the limit for a hydrogen bond (2.4 Å). Both O-H distances in the water molecule were put equal to 0.965 Å, a mean value calculated by Ferraris and Franchini-Angela (12) from a review of 41 hydrates studied by neutron diffraction. In this average 90 water molecules were involved.

The fractional coordinates of the hydrogen atoms are given in Table 1 together with those determined from the x-ray diffraction experiment. As can be seen the agreement is fairly good.

In order to illustrate the arrangement of the water molecule in hilgardite based on the new hydrogen atom coordinates, a stereographic plot of the water molecule and its hydrogen bond arrangement is given in Figure 2.

Acknowledgements

We would like to thank Professor G.R. Rossman for providing the single crystal of hilgardite and for helpful discussions. This work was supported by the National Science Foundation (DMR-7721394).

References

1. S. Ghose and C. Wan, Am. Mineral. 64, 187 (1979).

2. G.E. Pake, J. Chem. Phys. 16, 327 (1948).

3. D.F. Holcomb and B. Pedersen, J. Chem. Phys. 38, 54 (1963).

4. R. Chidambaram, J. Chem. Phys. 36, 2361 (1962).

5. Z.M. El Saffar, J. Chem. Phys. 45, 4643 (1966).

6. N. Boden and M. Mortimer, Chem. Phys. Lett. 21, 538 (1973).

7. B. Berglund and J. Tegenfeldt, J. Mag. Res. 30, 451 (1978).

8. R.G. Shulman and B.J. Wylude, J. Chem. Phys. 35 1498 (1961).

9. Z.M. El Saffar, J. Chem. Phys. 45, 570 (1966).

10. B. Pedersen, J. Chem. Phys. 41, 122 (1964).

11. A.B. Eriksson, B. Berglund, J. Tegenfeldt and J. Lindgren, J. Mol. Structure 52, 107 (1979).

12. G. Ferraris and M. Franchini-Angela, Acta Crystallogr. B28, 3572 (1972).

Table 1. Fractional coordinates of the hydrogen atoms in hilgardite as determined from the NMR data together with those determined from the X-ray data.

	NMR	X-ray
	0.006	0.034
H(1)	0.039	0.026
	0.759	0.789
	0.030	0.041
H(2)	-0.015	-0.005
	1.000	1.021

Figure 1. Experimental dipolar splittings ($\Delta\upsilon$) for the three axes as a function of the rotation angle Φ together with the calculated splittings (solid lines). The errors in $\Delta\upsilon$ and Φ are about 1 KHz and 2°, respectively. Sym 1 and 2 refer to the two symmetry-related proton-proton vectors in the unit cell.

Figure 2. A steroscopic view of the water molecule in hilgardite based on parameters from the X-ray and NMR data. The hydrogen bond angles O(W)-H(1)·· Cl and O(W)-H(2)·· Cl are 170°and 125°, respectively.

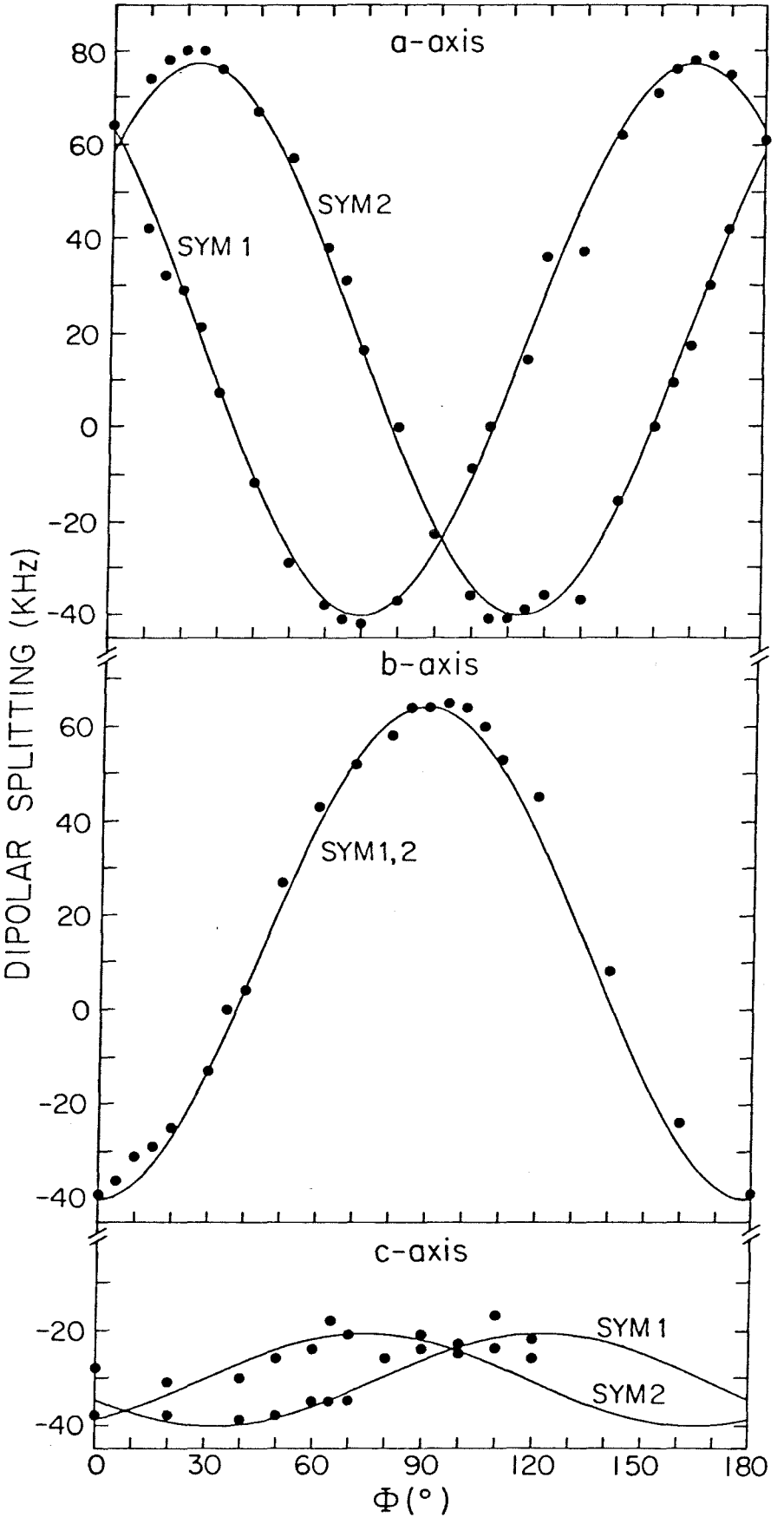
a-axis
SYM2
SYM 1
b-axis
SYM1,2
c-axis
SYM 1
SYM2
DIPOLAR SPLITTING (KHz)
Φ(°)
80
60
40
20
0
-20
-40
30
90
120
150
180

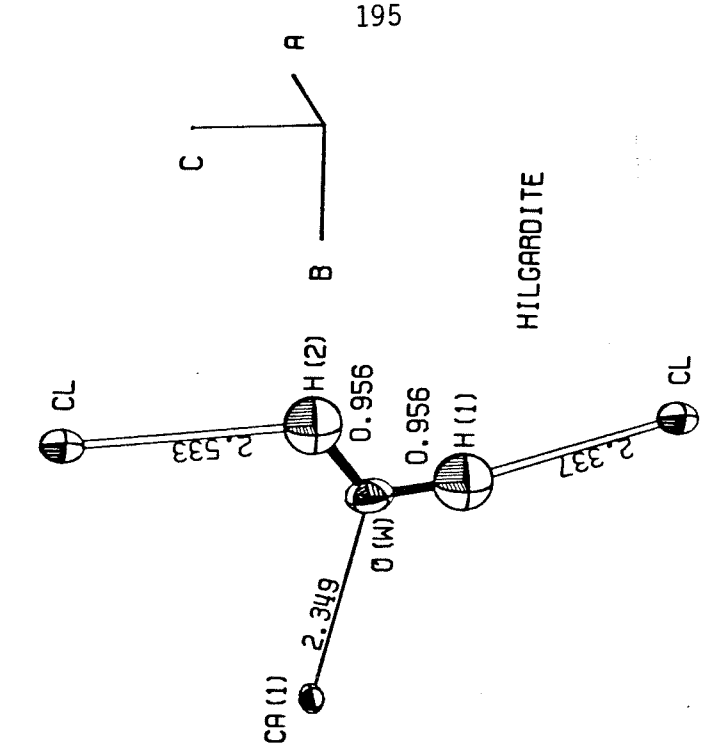
A
C
B
HILGARDITE
CL
H(2)
0.956
0.956
H(1)
CL
2.533
2.337
O(W)
2.349
CA(1)

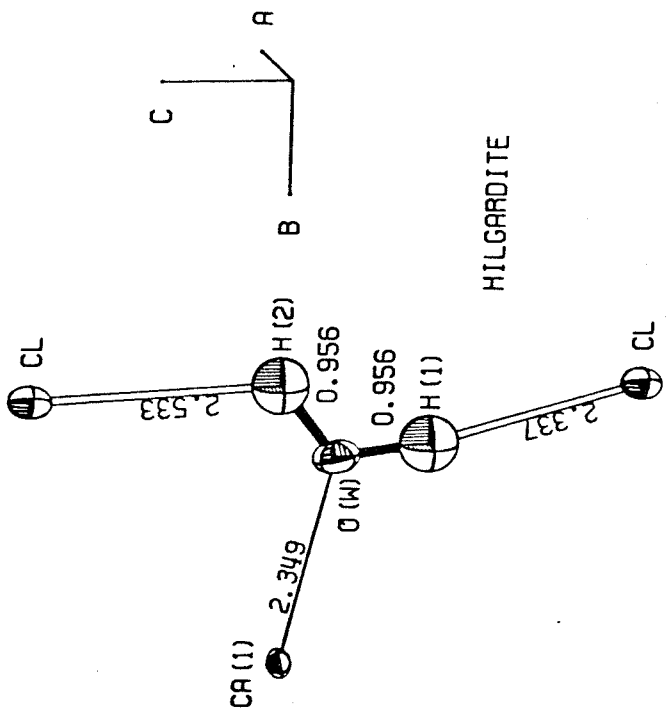
A
C
B
HILGARDITE
CL
H(2)
0.956
0.956
H(1)
CL
2.533
2.337
O(W)
2.349
CA(1)